Nadja Pöcher, B.Sc.

Impact of Perilipin5 overexpression on Triglyceride Homeostasis in Cardiomyocytes and the Consequences of Defective Adipose Lipolysis on Cardiac Energy Metabolism

MASTER`S THESIS

To achieve the university degree of

Master of Science

Master`s degree programme: Biochemistry and Molecular Biomedical Science

Submitted to:

Graz University of Technology

Supervisor

Assoz. Univ.-Prof. Mag. Dr.rer.nat. Günter Hämmerle

Institute of Molecular Bioscience

Graz, February 2015

AFFIDAVIT

I declare that I have authored this thesis independently, that I have not used other than the declared sources/resources, and that I have explicitly indicated all material which has been quoted either literally or by content from the sources used. The text document uploaded to TUGRAZonline is identical to the present master's thesis dissertation.

_____	_____
Date	Signature

ACKNOWLEDGMENT / DANKSAGUNG

Zu aller erst möchte ich Prof. Dr. Günter Hämmerle für seine hochgeschätzte Betreuung während meiner Masterarbeit und für die Möglichkeit an diesem hoch renommierten Institut meine Masterarbeit zu absolvieren danken.

Ich bedanke mich bei Doris, die mich während meiner Masterarbeit unterstützt hat und mir eine sehr große Hilfe war. Außerdem möchte ich mich bei allen Kolleg/innen des Institutes, insbesondere bei Susanne, Kathi und Martina, für ihre wertvollen Ratschläge und das gute Arbeitsklima bedanken.

Liebe Lisa, liebe Pia, ich danke euch für eure Unterstützung während meiner Masterarbeit. Dank euch durfte ich am Institut eine wunderbare Zeit erleben, die ich nie vergessen werde.

Meinen lieben Mitbewohnerinnen danke ich für die zahlreichen schönen Momente, die wir gemeinsam erlebt haben. Ebenso danke ich meiner Freundin Nadja, die mich bereits während meiner Schulzeit begleitet hat und immer einen Rat für mich hat.

Von Herzen danke ich meiner Familie, meinem Bruder Sascha und vor allem meinen Eltern, die mich in jeder Lebenslage unterstützen, immer für mich da sind und mir ermöglichen all meine Ziele zu erreichen.

Einen besonders großen Dank widme ich meinem Freund Josef, der mich bei allem unterstützt und jederzeit für mich da ist.

ABSTRACT

Triglycerides (TGs) are deposited within Lipid droplets (LD) and play an essential protective role in the sequestration of cytotoxic fatty acids (FAs) in non-adipose tissues. The LD is coated by proteins from the PAT-family (designation derived from perilipin, adipophilin and tail-interacting protein of 47kDa). Perilipin5 (Plin5), a member of the PAT family, is highly expressed in oxidative tissues and can interact with central members of the lipolytic machinery including adipose triglyceride lipase (ATGL) and comparative gene identification-58 (CGI-58). Plin5 controls ATGL-mediated lipolysis via binding or releasing CGI-58.

In this study, we investigated the impact of Plin5-overexpression on TG homeostasis in H9C2 cardiomyocytes to establish a cell culture model for studying the functional role of Plin5 in cardiac energy metabolism. Therefore, we generated a Plin5 recombinant adenovirus to transduce and overexpress Plin5 in H9C2 cardiomyocytes. During pulse chase experiments, Plin5 overexpression significantly interferes with TG homeostasis in cells loaded with oleic acid and during serum starvation. In Plin5/ATGL co-transduced cells, Plin5 overexpression impairs ATGL-mediated TG catabolism. Results demonstrate that Plin5-overexpression inhibits ATGL-mediated TG breakdown in H9C2 cardiomyocytes *in vivo* verifying this cell culture approach as a model to further study the functional role of Plin5 in cardiomyocyte energy metabolism.

Furthermore, we examined the impact of exogenous adipose tissue derived FAs in the regulation of cardiac energy metabolism. We compared the expression levels of selected peroxisome proliferator-activated receptor alpha (PPARα) target genes in cardiac muscle of ATGL deficient mice (ATGL-/-), adipose tissue specific ATGL knock out mice (ATGL-ATko) and transgenic mice overexpressing Plin5 exclusively in cardiac muscle (CM-Plin5).

The mRNA expression levels of *Nrf*-1, *Nrf*-2, *Hif*-1α, *Pdk*-4 and *Oxct*-1 were significantly decreased in ATGL-/- mice. Unlike mRNA expression, Nrf2 protein content was significantly increased in these mice, indicating, that Nrf2 may be regulated post-transcriptionally. Contrary, CM-Plin5 mice exhibit significantly increased *Nrf*-1/2 mRNA expression whereas mRNA levels were unchanged in ATGL-ATko mice compared to wild type.

TABLE OF CONTENTS

1 INTRODUCTION

1.1 The myocardium as an energy consuming tissue

Myocardial energy metabolism is an important determinant of cardiac structure and function [1]. The heart is one of the highest adenosine-5`-triphosphate (ATP) consuming organs in mammals. Its metabolic function has evolved a remarkable degree of efficiency to meet high energy demand and plasticity in response to varying changes in energy substrate availability [2].

1.1.1 Energy metabolism in the healthy heart

To constantly pump blood with oxygen and nutrients into the circulation, the mammalian heart must produce vast amounts of ATP under diverse nutritional and physiological conditions. The normal adult heart uses either FAs or glucose as energy substrate. The flexibility to utilize multiple fuels according to availability and physiological demands is important for normal cardiac function [3]. Under physiological conditions, the adult heart derives most of its energy through mitochondrial FA oxidation (FAO) [4]. Although FAs serve as the primary myocardial energy source, the heart has relatively limited lipid storage capacity, thus, cellular FA uptake and oxidation must be tightly coupled [4]. Uptake of long-chain FAs (LCFA) into cells is facilitated by the transporter proteins FA transporter protein 1 (FATP1) and cluster of differentiation 36 / FA translocase (CD36/FAT) [5]. The uptake of LCFA is coupled to esterification by fatty acyl-CoA synthetases (FACS). The resulting long-chain acyl-CoA are converted to their carnitine derivates by carnitine palmitoyltransferase 1 (CPT-1), which are transported into the mitochondria and enter the β-oxidation pathway (Figure 1) [4]–[6]. On the other side, glucose is oxidized to pyruvate in the cytosol which in turn is oxidized within the inner mitochondrial membrane by pyruvate dehydrogenase (PDH) (Figure 1). Acetyl-coenzyme A (CoA) derived from both pathways is oxidized by the tricarboxylic acid cycle (TCA) generating nicotinamide adenine dinucleotide (NADH) and flavin adenine dinucleotide ($FADH_2$), which carry electrons to the electron transport chain. The electron transport chain then produces ATP through the process of oxidative phosphorylation (OXPHOS) (Figure 1) [1], [6].

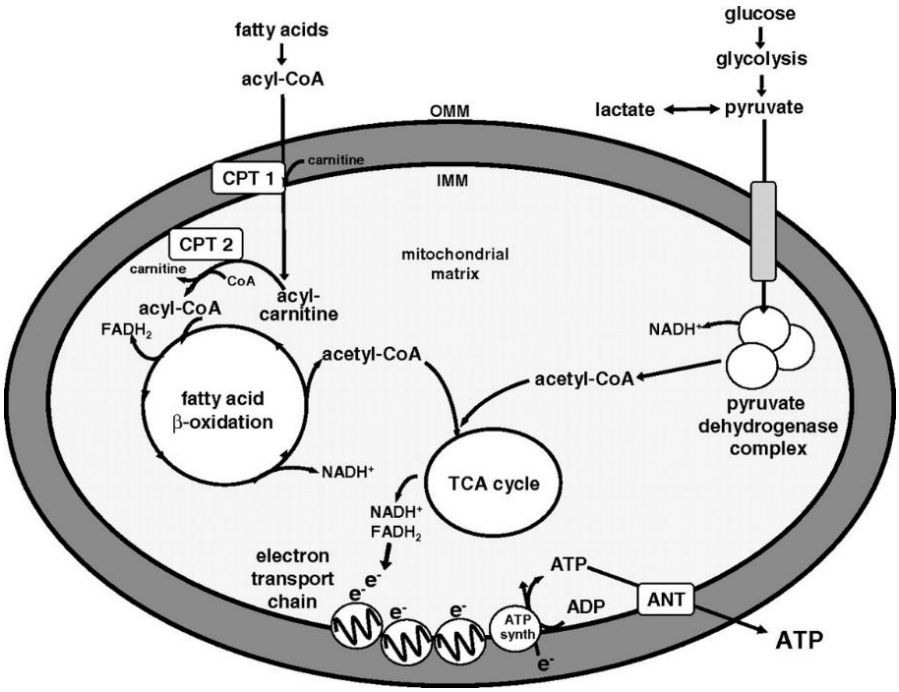

Figure 1: Schematic overview of mitochondria energy transduction and ATP synthesis pathways: The scheme depicts the major pathways of mitochondrial energy metabolism. Both, FAs and glucose are an important fuel for generating ATP. OMM indicates outer mitochondrial membrane; IMM indicates inner mitochondrial membrane; CPT, carnitine palmitoyltransferase; TCA, tricarboxylic acid; ANT, adenine nucleotide.
Image source: Finck et al. 2007 [6]

1.1.2 Energy metabolism in the failing heart

The heart primarily derives its energy form FAO within mitochondria. However, prolonged ingestion of excess calories increases FA flux to oxidative organs including the heart, skeletal muscle and liver which may contribute to the development of metabolic diseases. These responses may contribute to metabolic inflexibility, insulin resistance, cellular damage and contractile dysfunction [7]–[10].

Obesity has been linked to both, structural and functional changes of heart function including left-ventricular hypertrophy, contractile dysfunction, apoptosis, fibrosis, lipid accumulation and metabolic substrate switching [11], [12]. Insulin resistance and obesity are associated with ectopic lipid deposition in multiple tissues, including the heart. Excess lipids are stored as TG in LD, but are also shunted into non-oxidative pathways that disrupt normal cellular signaling, leading to organ dysfunctions. This process is generally termed lipotoxicity [8]. Although the heart is able to oxidize FA or glucose for ATP production, the normal heart

generates ATP mainly from the mitochondrial FAO (60-70% of ATP generated) and to a lesser extent from glucose, lactate and other substrates (30-40%). In contrast, hearts of diabetic and obese animals have an increase in FA utilization to generate ATP while glucose oxidation rates are decreased [13], [14].

1.1.3 Oxidative stress as a potential cause of metabolic disease

Lipid-induced cardiac dysfunction involves disturbances in various cellular pathways such as mitochondrial dysfunction and endoplasmatic reticulum (ER) stress [14], [15]. Mitochondria are the primary source of cellular reactive oxygen species (ROS) production. Under physiological conditions, ROS participate in cellular signaling. Cellular ROS levels are kept low by enzymatic scavengers including dismutases and peroxidases, and redox-sensitive modulators such as vitamin E and glutathione. Under pathophysiological conditions, ROS generation may exceed cellular antioxidant defenses, resulting in oxidative damage of proteins, lipids and DNA. Oxidative stress can impair membrane integrity, organelle function and regulation of gene expression, thereby contributing to cell death [8], [16]. In diabetic and obese mouse models (*db/db* and *ob/ob*, respectively), an increased number of mitochondria paralleled by impaired mitochondrial function was observed [16]–[18]. These mitochondria showed reduced oxidative capacity for glucose but FA utilization was increased despite a reduction in ATP generation [17].

The ER is important in the regulation of both, lipid and protein metabolism. Conditions that disrupt ER homeostasis or misfolded proteins activate the ER stress response which in turn inhibits protein synthesis to prevent further overloading of the ER and induces chaperones to aid in the refolding of misfolded proteins. However, ongoing or extreme ER stress overwhelms cellular integrity, triggering activation of pro-apoptotic genes and inducing oxidative stress [9]. Lipids can also initiate ER stress. Supplementation with saturated free FA (FFA) of cultured fibroblasts, myoblasts and β-cells leads to alteration in ER structure and function that precede activation of the ER stress response, suggesting that lipid incorporation into the ER may contribute to initiation of ER stress [15], [19].

1.2 Lipolysis, the catabolism and mobilization of endogenous TG

Lipolysis describes the hydrolysis of TG and is a branch of the FA cycle that provides FAs in times of energy demand and neutralize and deposit them when they are present in excess. FAs are essential as substrate for energy production and the synthesis of most lipids including membrane lipids and lipids involved in cellular signaling. However, increased concentrations of FFA may lead to lipotoxicity [9]. To prevent lipotoxicity, all cells are able to detoxify FFA by esterification with glycerol to yield inert TG. These TGs are stored in LD, an ubiquitous cytoplasmatic organelle. Additionally, higher organisms store FAs in a adipose tissue, which supplies FAs to other high-demand tissues such as liver and muscle [20].

1.2.1 Lipolysis involves three different steps

Neutral hydrolysis of TGs to FAs and glycerol requires three consecutive steps that involve at least three different lipolytic enzymes. The initial step of lipolysis is catalyzed by adipose triacylglycerol lipase (ATGL) which converts TG to diacylglycerol (DG) and FFA [21], [22]. The second step is the hydrolysis of DG to monoglycerol (MG) and FFA by the action of hormone-sensitive lipase (HSL). The last step involves the hydrolytic activity of monoglycerol lipase (MGL) which converts MG to FFA and glycerol [23].

ATGL belongs to the patatin domain-containing protein family [21], [22]. The regulation of ATGL expression and enzyme activity is complex. ATGL mRNA expression is elevated by the presence of peroxisome proliferator-activated receptor (PPAR) agonist, upon application of glucocorticoids and fasting, whereas insulin and food intake decrease ATGL expression [24]. The abundance of ATGL and HSL mRNA levels does not always correlate with cellular TG-hydrolytic activity. The discrepancy between mRNA levels and enzyme activities is explained by the extensive post-translational regulation of ATGL and HSL enzymatic activities [20].

ATGL exhibit at least two serine residues which can be phosphorylated by adenosine monophosphate activated kinase (AMPK) but not by protein kinase A (PKA) [21]. AMPK phosphorylates ATGL at serine 406 which leads to an increased hydrolytic activity [25]. However, the role of AMPK in the regulation of lipolysis has been controversial, with data

showing that AMPK induces [26], [27], inhibits [28], [29], or has no effect [30] on lipolysis. For efficient and maximum TG hydrolase activity, ATGL requires a co-activator designated as comparative gene identification 58 (CGI-58). However, CGI-58 itself exhibit no intrinsic lipase activity, but when CGI-58 interacts with ATGL, the TG-hydrolytic activity of ATGL is stimulated up to 20-fold [31]. On the other side, Yang *et al.* discovered a specific inhibitor protein for ATGL, G0G1 switch protein 2 (G0S2), which is expressed very low in adipose tissue during fasting but increased after feeding [32].

HSL exhibit both, DG and TG hydrolase activity, however, HSL predominantly hydrolyzes DG. In addition, HSL also hydrolyzes esters bonds of many other lipids including TG, MG, cholesteryl and retinyl esters, and short-chain carbonic acid esters [20]. Like ATGL, HSL enzyme activity strongly increases upon β-adrenergic stimulation, whereas insulin has a strong inhibitory effect. However, the mechanism of enzymatic regulation differs between HSL and ATGL. While β-adrenergic stimulation regulates ATGL primarily by recruitment of its co-activator CGI-58, HSL is a major target for PKA phosphorylation [33]. Other kinases including AMPK, extracellular signal-regulated kinase, glycogen synthase kinase 4 and calcium/calmodulin-dependent kinase, also phosphorylate HSL to modulate its enzyme activity [24]. To achieve full activation, HSL must gain access to LDs, which, in adipose tissue, is mediated by perilipin1. In parallel, PKA phosphorylates perilipin1 which leads to the access of HSL to the LD TG moiety via binding at the NH_2-terminal region of perilipin1 [34]–[36].

Taken together, HSL phosphorylation and translocation to LDs coupled with ATGL activation by CGI-58 results in more than an 100-fold increase in TG hydrolysis in adipocytes [20].

1.2.2 Lipotoxicity as a consequence of increased intracellular FA levels

Elevated serum TGs and FFAs cause lipid accumulation in non-adipose tissues which further may lead to metabolic diseases such as obesity. While FFAs and their metabolites play a central role in membrane structure, intracellular signaling and energy homeostasis,

accumulation of excess FFAs in non-adipose tissues causes cell dysfunction and cell death. This process is generally termed as lipotoxicity [9].

In animals, lipotoxicity describes changes in cellular integrity encompassing ectopic lipid accumulation, cell death and organ dysfunction. Elevated circulating FFA levels may precede the onset of diabetes and heart failure in rodent models with impaired leptin signaling, which are associated with steatosis and subsequent apoptosis of β-cells and cardiomyocytes, respectively [37], [38]. Dietary and pharmacological interventions that decrease lipid accumulation reduce the progression to diabetes and heart failure, suggesting a causal role for lipotoxicity in the pathogenesis of metabolic disease [9]. In murine models with diet induced obesity, lipid accumulation and cell death in non-adipose tissue are consistent with a role for lipid accumulation in the pathogenesis of organ dysfunction [39]. Mice overexpressing lipoprotein lipase or long-chain acyl CoA synthetase exhibit lipid accumulation in the heart which results in heart failure, supporting the hypothesis that excess lipids contribute to cardiac dysfunction and metabolic diseases [40], [41].

1.3 The impact of Plin5 in lipolysis of oxidative tissues

Constantine Londos and colleagues discovered perilipin1 as a LD protein which is phosphorylated in response to signals that stimulate breakdown of TG stored in adipocytes [42]–[44]. The subsequent discovery of perilipin2 (ADRP, ADFP, or adipophilin) and perilipin3 (Tip47, PP17, or M6PRBP) leads to the designation of the so called PAT-family (perilipin, ADRP, Tip47) [45]. Finally, perilipin4 (S3-12) [46] and Plin5 (MLDP, LSDP5) [47]–[49] completed the PAT family of LD-associated proteins in mice and humans. The PAT family members differ from each other in size, tissue expression, affinity for LD, stability when not bound to LD and transcriptional regulation [50].

1.3.1 Sequence homology of the PAT family members

The members of the PAT family exhibit related amino acid sequences, particularly in the amino-terminal region called the PAT1 domain (Figure 2) [50]. Perilipin2 and perilipin3

exhibit the highest amino acid sequence identity (43%). Plin5 is related to perilipin3 (30% identity) and perilipin2 (26% identity) throughout the amino acid sequence [48], [50]. Perilipin1 and perilipin4 have divergent amino acid sequences relative to the other PAT family members and each other (Figure 2). Sequence similarity between perilipin1 and other members of the PAT family is limited. The most highly conserved sequence of perilipins including approximately 100 amino acids is located at the N-terminus of perilipin1, perilipin2, perilipin3 and Plin5, but not perilipin4 (Figure 2) [50]. Sequence analysis shows that perilipin4 is the most divergent member of the PAT family [45].

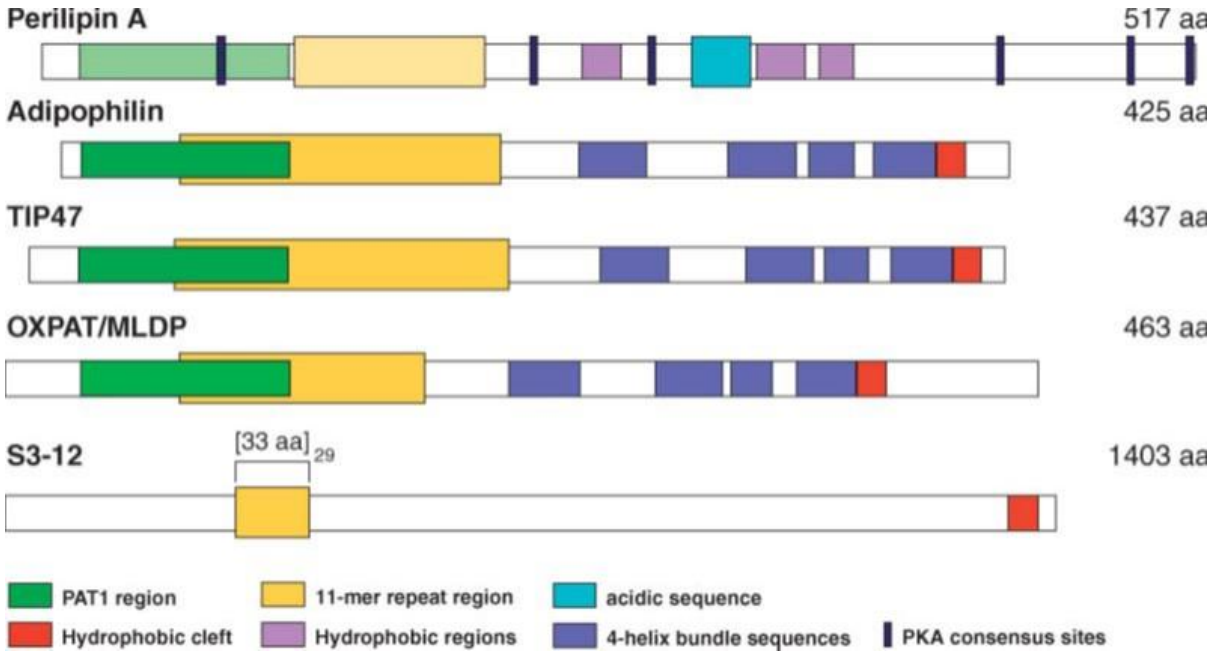

Figure 2: Scheme depicting the structural features of perilipin1 and related proteins: Higher intensity of color represents increased similarity of the sequences between family members, whereas lighter color represents reduced sequence similarity. The N termini of perilipin1 (perilipin A), perilipin2 (adipophilin), perilipin3 (TIP47), and Plin5 (MLDP), but not perilipin4 (S3-12), contain 100 amino acids (aa) that are highly conserved (green). Overlapping with these sequences are stretches of amino acids containing 11-mer repeats that are predicted to fold into amphipathic helices (yellow). Following the putative 11-mer repeats, a sequence stretch of perilipin3 fold into a four helix bundle of amphipathic a-helices (blue). Both, perilipin2 and Plin5 share sequence similarity in this region (blue). In contrast, within this region, perilipin1 has three sequences of moderate hydrophobicity (lilac) and a highly acidic sequence (cyan). The C termini of perilipin2, perilipin3, Plin5, and perilipin4, but not perilipin1, contain a highly conserved sequence of 14 amino acids that folds into a hydrophobic cleft in perilipin3 (red). Perilipin1 is unique among members of the protein family in having six consensus sequences for the phosphorylation of serine residues by protein kinase A (PKA) (charcoal) dispersed throughout its primary amino acid sequence.
Image source: Braseamle et al. 2007 [50]

1.3.2 Expression patterns of the PAT family members

Perilipin1 and perilipin2 are exclusively associated with LDs and are degraded by proteosomal and/or lysosomal pathway when not bound to LDs. Although perilipin2 and perilipin3 exhibit the highest amino acid sequence identity of about 43%, perilipin3 is stable both, as a soluble cytosolic protein and when associated with LD [50]. Perilipin4 and Plin5 exchange on and off LDs depending on the cell metabolic state and are also stable either when associated with LDs or when located in the cytoplasm [46], [51], [52].

The PAT family members exhibit distinct tissue distribution. Perilipin1 is highly abundant in white adipose tissue (WAT) and brown adipose tissue (BAT) whereas perilipin2 and perilipin3 are expressed in many cell types. Further, perilipin2 is the most abundant LD-associated protein of tissues where perilipin1 is not present [51]. Perilipin4 is expressed mostly in WAT, but lower levels are also found in heart and skeletal muscle [53], [51]. The expression of Plin5 is enriched in oxidative tissues, such as the heart, liver and slow-twitch muscles [48]. Moreover, Plin5 is also highly expressed in BAT, but not in WAT [48]. The expression level of Plin5 is induced by fasting in the heart, liver and skeletal muscle [47]–[49].

1.3.3 Plin5 is regulated by peroxisome proliferator-activated receptor

During fasting, FFA are released predominantly from adipose tissue to supply organs with FFA as energy substrate. These organs, including the heart, skeletal muscle and liver, respond to this increased circulation of FFA by inducing gene expression that regulate FA metabolism [54]. The peroxisome proliferator-activated receptors (PPARs) are involved in various aspects of lipid metabolism and consist of three related isotypes namely PPARα, PPARβ/δ and PPARγ [55].

Several of the perilipin genes contain evolutionary conserved cis-regulatory elements occupied by PPARs [56]. As an LD target protein, Plin5 expression is enhanced under physiological or pharmacological conditions that promote systemic FA elevation, for example fasting (heart and liver), enduring exercise (skeletal muscle) and chronic β3-adrenergic

stimulation (liver) [47]–[49], [57]. Exogenous FA can also stimulate Plin5 expression in cell culture, whereas oleate induces Plin5 gene expression to a greater extent than palmitate [58]. Plin5 exhibit a functionally conserved peroxisome proliferator response element (PPRE) site located to the first intron and its expression can be induced in liver, cardiac and skeletal muscle by PPARα, but also in WAT by pioglitazone, a PPARγ agonist [47]–[49], [56].

Although basal Plin5 mRNA levels are severely suppressed in the heart and liver of PPARα deficient mice (PPARα-/-) [59], Plin5 expression responds to fasting, suggesting additional PPARα-dependent regulatory mechanisms. Indeed, PPARβ/δ appears to be the more potent regulator of Plin5 expression than PPARα in skeletal muscle [56].

The different response to PPAR activation are likely important for the distinct perilipin tissue expression profiles [49], [60]. In muscle, enhanced PPARα and PPARβ/δ activation increases Plin5 expression, whereas the adipose tissue-enriched perilipin4 is preferentially induced by enhanced PPARγ activity [56].

1.3.4 Plin5 function in oxidative tissues

Plin5 is a LD binding protein which is highly expressed in oxidative tissues, such as the heart, liver, BAT and skeletal muscle [48]. Plin5 promotes lipid accumulation, enhances FAO through a PPARα-dependent pathway in the liver [61], sequesters FA from excessive oxidation and protects the heart from oxidative stress [53].

In the neutral lipid catabolic pathway of adipocytes, four major proteins have been identified, namely HSL, ATGL, the ATGL co-activator CGI-58 and the ATGL inhibitory factor G0S2 [24], [32]. ATGL, HSL and CGI-58 are also essential regulators of lipid hydrolysis in non-adipose tissue and Plin5 can interact with all of them [36], [62]–[64]. Wang and colleagues showed by energy transfer experiments that ATGL and CGI-58 bind toward the C-terminal half of Plin5, whereas HSL binds to the N-terminal domain, which is common to all perilipins [36]. However, the binding of ATGL and CGI-58 appears to be mutually exclusive [64], [65].

In adipose tissue, perilipin1 is highly expressed and is bound at the LD surface where it constitutes a main regulator in TG mobilization [50]. Upon β-adrenergic stimulation,

perilipin1 is phosphorylated by protein kinase A (PKA) thereby releasing CGI-58 from its binding to perlipin1, which is required for subsequent activation of ATGL TG-hydrolytic activity [35], [66]–[68]. Similar to perilipin1, CGI-58 is also recruited by Plin5 at the LD surface, suggesting that Plin5 may exert a similar role in the regulation of lipolysis in non-adipose tissue [36], [63], [64]. However, the regulation of lipolysis in non-adipose tissue is less understood.

Several independent studies demonstrate that Plin5 is a substrate for PKA, implicating a role for PKA in the regulation of Plin5 function in response to ß-adrenergic stimulation (Figure 3) [63], [69], [70]. The lipolytic barrier of Plin5-enriched LD is reduced upon PKA incubation, suggesting that PKA triggers the release of CGI-58 by phosphorylating Plin5. Accordingly, PKA treatment stimulates FA release from Plin5-enriched LD, indicating that PKA unlocks the Plin5 barrier function (Figure 3) [71].

In silico amino acid sequence analysis revealed a single PKA phosphorylation sequence motif in Plin5 protein, comprising of serine 155. Upon stimulation, for example by fasting, cellular cyclic adenosine monophosphate (cAMP) levels are increased, which further activates adenylate cyclase which in turn stimulates PKA. Plin5 is phosphorylated at serine 155 by PKA, whereby CGI-58 is released from Plin5, which is then available for co-activation of ATGL and stimulation of lipolysis (Figure 3) [71].

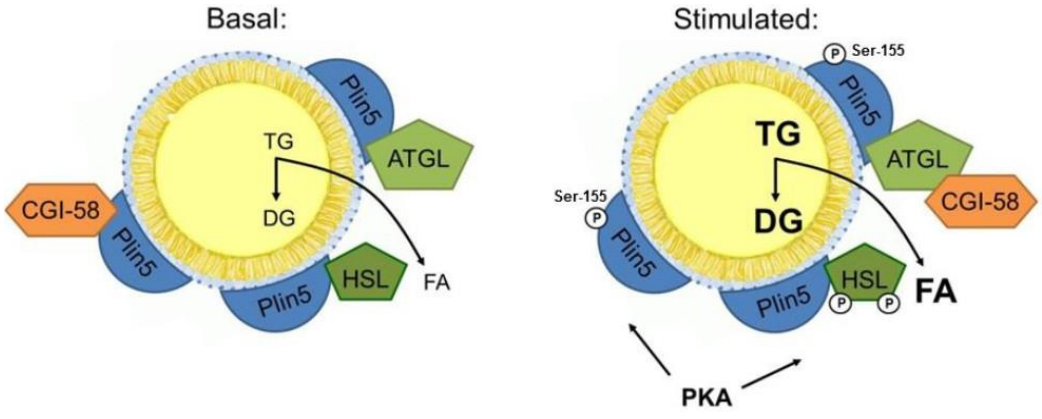

Figure 3: Scheme depicting the functional role of Plin5 and PKA in the regulation of lipolysis: Under basal conditions, Plin5 functions as a lipolytic barrier by binding CGI-58 and counteracting the access of ATGL and HSL to the LD surface. Upon stimulation, for example by fasting, PKA is activated by adenylate cyclase due to the raise in cAMP levels. Active PKA phosphorylates serine 155 of Plin5 which in turn releases CGI-58 required for stimulation of ATGL-mediated TG hydrolysis.
Image source: Pollak et al. 2014 [71]

1.4 The role of peroxisome proliferator-activated receptors in lipid and energy metabolism

The PPARs are involved in various aspects of lipid metabolism and belong to the nuclear receptor superfamily consisting of the isotypes PPARα, PPARβ/δ and PPARγ [55]. All three PPARs are activated by FAs and bind as obligate heterodimers with 9-*cis* retinoid X receptors (RXR) to the consensus response element named PPAR-response elements (PPRE) [54], [55].

PPARs exhibit a broad but isotype-specific tissue expression pattern which can account for the variety of cellular functions they regulate (Figure 4). PPARα is highly expressed in tissues with an elevated capacity of FAO, like the heart, liver, BAT and kidney. PPARγ exhibit two isoforms, γ1 and γ2, whereas γ2 acts in WAT and BAT to promote adipocyte differentiation and lipid storage and γ1 expression is extended to other tissues such as the gut or in immune cells. PPARβ/δ is more widely distributed with relatively high expression levels in skeletal muscle, heart and brain and is implicated in energy metabolism in peripheral tissues by controlling β-oxidation and energy uncoupling [72].

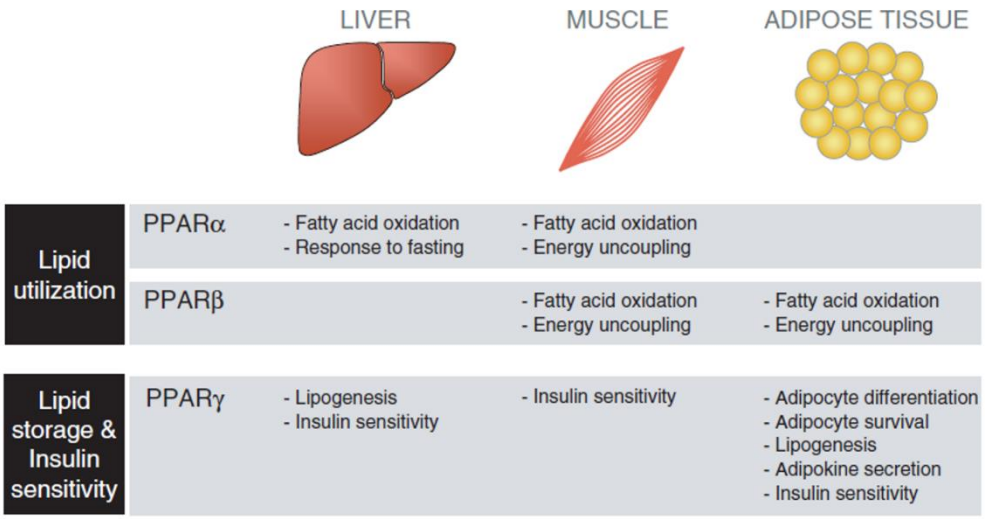

Figure 4: Overview of PPAR expression patterns and functions: Main metabolic functions regulated by PPARs.
Image source: Feige et al. 2006 [72]

2 AIM OF THE STUDY

The aim of my master thesis is to establish a cell culture model for studying the role of Plin5 in cardiac energy metabolism. Therefore, a recombinant adenovirus should be generated to efficiently express Plin5 in H9C2 cardiomyocytes and to study its impact on TG homeostasis. Furthermore, the role of exogenous versus endogenous FAs in the regulation of cardiac energy metabolism will be examined by measuring mRNA expression of PPAR-regulated genes in cardiac muscle of mice globally lacking ATGL or in mice lacking ATGL exclusively in adipose tissue.

3 MATERIAL

3.1 Media

Differentiation medium	DMEM high glucose [4.5g/L] 1% fetal calf serum (FCS) 1% penicillin/streptomycin (P/S)
LB-medium	10g NaCl 5g Yeast Extract 10g Peptone autoclaved
LB-medium agar plates	10g NaCl 5g Yeast Extract 10g Peptone autoclaved 15g Agarose
Full medium	DMEM high glucose [4.5g/L] 10% FCS 1% P/S
NZY^+ Broth	10g Casein Hydrolysate 5g Yeast Extract 5g NaCl Adjust with NaOH to pH 7.5 and fill up to 1L with ddH_2O autoclaved 12.5mL filter-sterilized $MgCl_2$ x 6 H_2O

	[1M] 12.5mL filter-sterilized $MgSO_4$ x 7 H_2O [1M] 20mL filter-sterilized glucose
Plaquing medium	DMEM high glucose [4.5g/L] 2% FCS 1% P/S
SOC medium	1g tryptone 0.3g yeast extract 29.2mg NaCl [10mM] 9.3mg KCl [2,5mM] 101.7mg $MgCl_2$ [10mM] 123.3mg $MgSO_4$ [10mM] 180.3mg glucose [20mM] Fill up to 50mL with ddH_2O Filter-sterilized

3.2 Buffer and Solutions

Agarose gel [1%]	4g Agarose 8mL TAE buffer [50x] 400mL ddH_2O Boil up in microwave oven and equilibrate in incubator at 60°C
CAPS Transfer Buffer	4.4g CAPS [10mM]

	200mL Methanol [100%] Adjust to pH 11 and fill up to 2L with ddH_2O
DEPC-water	800mL ddH_2O 800µL DEPC autoclaved
Destaining Solution	300mL Methanol [100%] 125mL Acetic acid [80%] Fill up to 1L with ddH_2O
Dialyse buffer	40mL $MgCl_2$ [100mM] 400mL Tris pH7.4 [100mM] Fill up to 3600mL with ddH_2O 400mL Glycerin Autoclaved
HSL-Buffer	8.6g Sucrose [250mM] 200µL EDTA [1mM] 100µL DTT [1mM] Adjust with acetic acid to pH 7 and fill up to 100mL with ddH_2O
6x Loading Dye for DNA [Thermo Scientific]	Tris-HCl [10mM, pH 7.6] 60 mM EDTA 60% glycerol [100%] 0.03% bromophenol blue 0.03% xylene cyanol FF

5x Loading Dye for RNA	50% glycerol [100%] 2.5% TAE [40x] 0.03% xylene cyanol FF
4x lower buffer	91g Tris Adjust with HCl to pH 8.8 and fill up to 500mL with ddH_2O
Lysis buffer I	25mL Glucose [5M] 12.5mL Tris [1M, pH 7,05] 10mL EDTA [0,5M] Fill up to 500mL with ddH_2O
Lysis buffer II	200µL NaOH [10M] 0.5mL SDS [20%] Fill up to 10mL with ddH_2O
10x PBS	40g NaCl 1g KCl 5.7g Na_2HPO_4 1g KH_2PO_4 30.1% ddH_2O Fill up to 500mL with ddH_2O autoclaved
Ponceau S	0.5g Ponceau S 1mL glacial acetic acid Fill up to 100mL with ddH_2O
6xSDS	6g glycerin 6mL SDS [20%]

	1.5mL Tris-HCl [2M, pH 6.8] Bromphenolblue 1.5mL β-Mercaptoethanole Fill up to 10mL with ddH_2O
Staining Solution	2.5g Coomassie Blue 93.8mL Acetic acid [80%] 500mL Ethanol [100%] Fill up to 1L with ddH_2O
Stripping Buffer	7.6g Tris 20g SDS 0.7% β-Mercaptoethanol Adjust to pH 6,7 and fill up to 1L with ddH_2O
50x TAE Buffer	242g Tris 57.1mL glacial acetic acid 100mL EDTA [0.5M] pH 8 adjust with acetic acid and fill up to 1L with ddH_2O
1x TAE Running Buffer	20mL TAE Buffer [50x] 980mL ddH_2O
10x Tris-Glycin Buffer	50.4g Tris [0,2M] 241.7g Glycin [1,6M] 16.7g SDS Fill up to 2L with ddH_2O
10x TST	121.1g Tris (HCl)

	175.3g NaCl 20mL Tween20 Adjust to pH 7.4 and fill up to 2L with ddH_2O Storage at 4°C
4x upper buffer	0,5M Tris 60.5g Tris Adjust with HCl to pH 6.8 and fill up to 1L with ddH_2O

3.3 Vectors

The pFLAG-CMV-5.1 vector was used for protein expression in mammalian cells (Figure 5). FLAG sequence is C-terminally linked to the inserted gene of interest and the expression is regulated by CMV promoter. Further, this vector contains an ampicillin resistance gene.

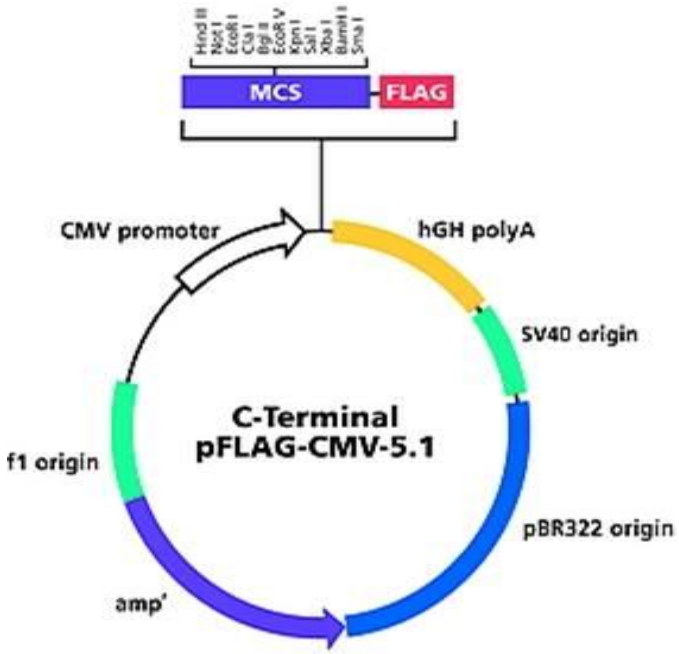

Figure 5: pFLAG-CMV-5.1 expression vector: The inserted gene is regulated by CMV promoter; the FLAG sequence is C-terminally linked. Further, this vector consists of an ampicillin resistance gene.
Image source: http://www.sigmaaldrich.com/catalog/product/sigma/e6908?lang=de&region=AT

The pShuttle vector was used for the prior steps of the generation of a recombinant adenovirus (Figure 6). This vector contains a multiple cloning site which allows inserting of an entire expression cassette. Further, this vector consists of a kanamycin resistance gene. The regions indicated as arms are the stretches of sequence homology with pAdEasy-1 (Figure 6) where the homologous recombination occurs. The R-ITR and L-ITR regions are short inverted terminal repeats (left and right) which are involved in the replication of the viral DNA.

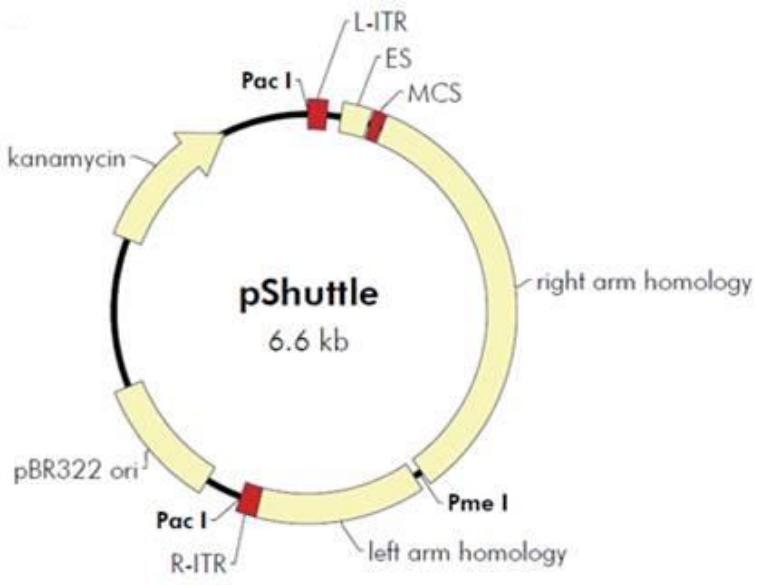

Figure 6: pShuttle expression vector: The inserted gene is regulated by CMV promoter. The regions indicated as arms are relevant for homologous recombination. Further, this vector consist of a kanamycin resistance gene. *Image source*: http://www.chem.agilent.com/library/usermanuals/Public/240010.pdf

The pAdEasy-1 vector was used for homologous recombination (Figure 7) within the competent *E. coli* strain BJ5183-AD-1. The plasmid contains most of the human adenovirus serotype 5 genome, however, the genes E1 and E3 are deleted which creates space for foreign DNA and eliminates self-replication capabilities. The E1 gene which is necessary for production of viral particles, is provided in *trans* by HEK AD293 cells. Further, this vector consists of an ampicillin resistance gene.

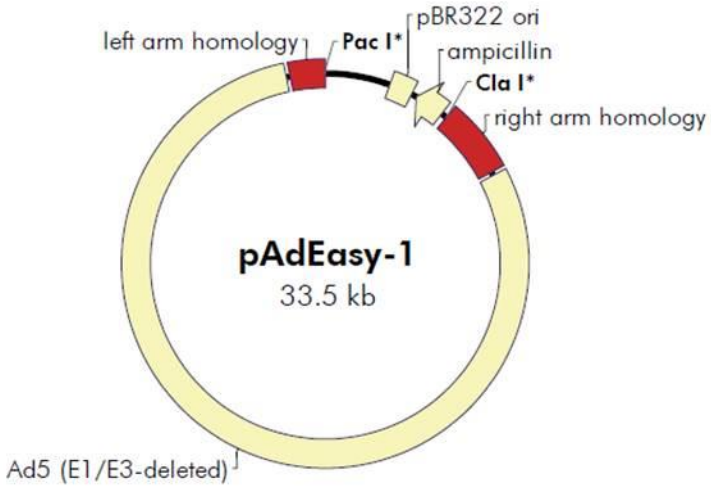

Figure 7: pAdEasy-1 vector: The removal of the genes E1 and E3 creates space for foreign DNA. Further, the vector consists an ampicillin resistance gene.
Image source: http://www.chem.agilent.com/library/usermanuals/Public/240010.pdf

3.4 Primers

Primer pairs used for polymerase chain reaction (PCR) and for quantitative real-time polymerase chain reaction (qRT-PCR) are listed in table 1 and 2.

Table 1: Primer pairs for PCR

Primer	Sequence (5`to 3`)
Plin5 forward *Eco*RIflag [Eurofins Genomic]	CGC GAA TTC ATC CAC CAT GGA CCA GAG AGG TGA A
Plin5 reverse *Sal*Iflag [Eurofins Genomic]	TAG AGT CGA CGA AGT CCA GCT CTG GCA TCA TTG T
*Not*I forward pShuttleP5 [Eurofins Genomic]	CTT GCG GCC GCG AAT TCA TCC ACC ATG GAC CAG A
*Eco*RV reverse pShuttleP5 [Eurofins Genomic]	GGG ATA TCA ACC TAC TTG TCA TCG TCG TCC TTG TA

Table 2: Primer pairs for qRT-PCR

Gene	Primer	Sequence (5`to 3`)
β-*Actin*	forward	AGC CAT GTA CGT AGC CAT CCA
	reverse	TCT CCG GAG TCC ATC ACA ATG
Aox-1	forward	AGA TTG GTA GAA ATT GCT GCA AAA
	reverse	ACG CCA CTT CCT TGC TCT TC
*Cpt*1-β	forward	CGA GGA TTC TCT GGA ACT GC
	reverse	GGT CGC TTC TTC AAG GTC TG
*Hif*1-α	forward	GGG GAG GAC GAT GAA CAT CAA
	reverse	GGG TGG TTT CTT GTA CCC ACA
Lcad	forward	TTT CCG GGA GAG TGT AAG GA
	reverse	ACT TCT CCA GCT TTC TCC CA
Mcad	forward	CAA CAC TCG AAA GCG GCT CA
	reverse	ACT TGC GGG CAG TTG CTT G
Nrf-1	forward	CAA CAG GGA AGA AAC GGA AA
	reverse	GCA CCA CAT TCT CCA AAG GT
Nrf-2	forward	TAG ATG ACC ATG AGT CGC TTG C
	reverse	GCC AAA CTT GCT CCA TGT CC
Osgin-1	forward	CGG TGA CAT CGC CCA CTA C
	reverse	GCT CGG ACT TAG CCC ACT C
Oxct-1	forward	GCC CTG CAT AAG GGG TGT G
	reverse	GCA AGG TTG CAC CAT TAG GAA T
Pdk-4	forward	ATC TAA CAT CGC CAG AAT TAA ACC
	reverse	GGA ACG TAC ACA ATG TGG ATT G
*Pgc*1-α	forward	CCC TGC CAT TGT TAA GAC C
	reverse	TGC TGC TGT TCC TGT TTT C

3.5 Bacterial strains

E. coli BJ5183-AD-1 electroporation competent cells [Agilent Technologies]

E. coli DH5α cells [New England BioLabs®Inc.]

E. coli XL-Gold ultra-competent 1 cells [Agilent Technologies]

3.6 Antibodies

Primary antibodies and their corresponding secondary antibodies are listed in table 3.

Table 3: Antibodies for Western blot analysis

Primary antibody	Secondary antibody
Anti-ATGL 1 :1000 in 5% milk, 1xTST [Cell signaling]	Anti-rabbit HRP conjugated 1 :10000 in 5% milk, 1xTST [Vector Labortories]
Anti-FLAG® M2 Peroxidase (HRP) 1 :5000 in 5% milk, 1xTST [Sigma]	-
Anti-GAPDH 1 :50000 in 5% BSA, 1xTST [Cell signaling]	Anti-rabbit HRP conjugated 1 :10000 in 5% milk, 1xTST [Vector Labortories]
Anti-His N-terminal 1 :5000 in 5% milk, 1xTST [Amersham]	Anti-mouse HRP conjugated 1 :10000 in 5% milk, 1xTST [GE healthcare]
Anti-NRF2 1 :1000 in 5% milk, 1xTST [Proteintech]	Anti-rabbit HRP conjugated 1 :10000 in 5% milk, 1xTST [Vector Labortories]

3.7 Standards

The size of DNA and protein samples were estimated using Gene Ruler1kb DNA Ladder [0.5µg/µL; Thermo Scientific] (Figure 8 A), Gene Ruler 100bp DNA Ladder [0.1µg/µL; Invitrogen] (Figure 8 B) and Precision Plus Protein™ Standards All Blue [BioRad] (Figure 8 C), respectively.

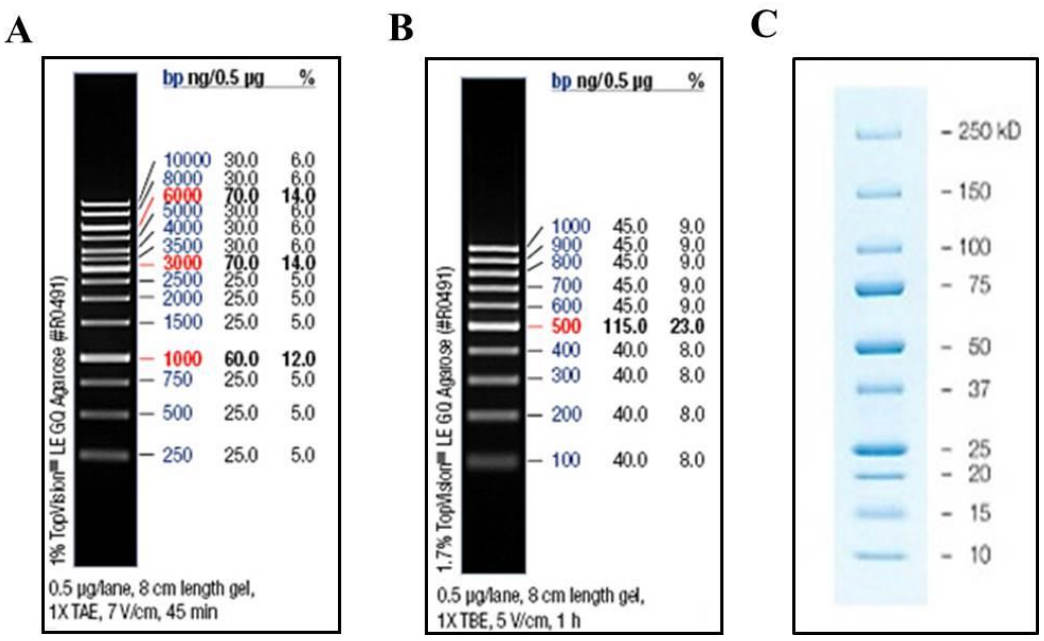

Figure 8: Standards to estimate DNA and protein sizes, respectively: A: Gene Ruler1kb DNA Ladder [0.5µg/µL; Thermo Scientific]; **B:** Gene Ruler 100bp DNA Ladder [0.1µg/µL; Invitrogen]; **C:** Precesion Plus Protien™ Standards All blue [BioRad].

3.8 Kits

AdEasy™ XL Adenoviral Vector System [Agilent Technologies]

BCA Protein Assay Kit [Pierce]

ECL Plus Western Blotting Detection System [GE Healthcare]

NucleoBond® Xtra Plasmid Purification Midi Kit [Quiagen]

Omega® bio-tek Kit [Quiagen]

Infinity triglyceride Kit [Thermo Electron Corporation]

3.9 Cell lines

COS-7

COS-7 (**C**V-1 in **O**rigin carrying **S**V40 genetic material) cells are kidney cells derived from grivet (*Cercopithecus aethiops*) which have a fibroblast like morphology (Figure 9). This cell line was derived from the CV-1 cell line by transformation with an origin defective mutant of SV40, which codes for wild type T antigen. The CV-1 cell line was derived from the kidney of a male adult African green monkey by Fred C. Jensen [73].

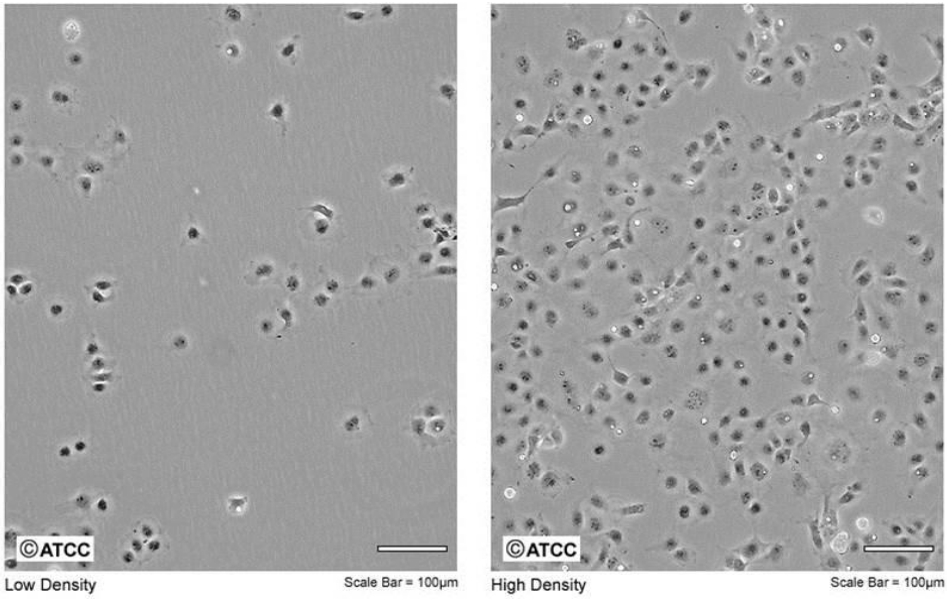

Figure 9: Confocal microscopy image of COS-7 cells: COS-7 cells are kidney cells derived from grivet with a fibroblast like morphology.
Image source: http://www.lgcstandards-atcc.org/~/media/Attachments/5/E/9/D/1824.ashx

HEK AD293

HEK AD293 cells are derived from the commonly used HEK 293 cell line which are human embryonic kidney cells with an epithelial morphology (Figure 10) [74]. HEK AD293 cells have improved cell adherence properties which simplifies the process of producing recombinant adenovirus particles.

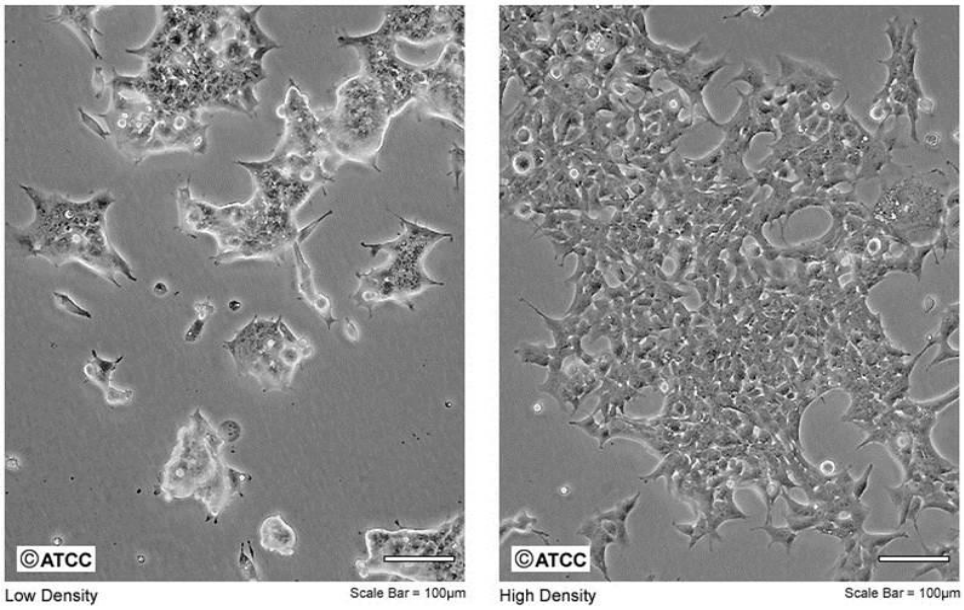

Figure 10: Confocal microscopy image of HEK 293 cells: HEK 293 cells are human embryonic kidney cells with an endothelial morphology.
Image source: http://www.lgcstandards-atcc.org/~/media/Attachments/E/1/4/7/1820.ashx

H9C2

H9C2 is an embryonic ventricular myoblast cell line derived from rat (*Rattus norvegicus*). Chronic culture in low serum media prevents differentiation of embryonic H9C2 myoblast to cardiomyocytes (Figure 11) [75].

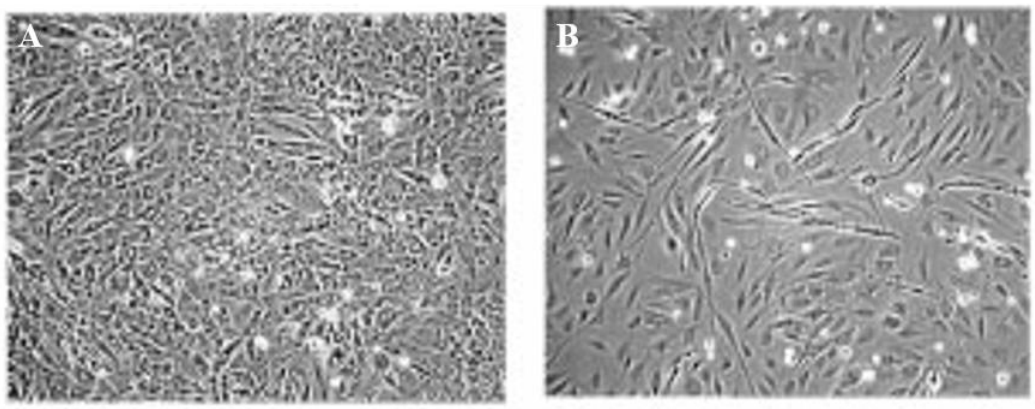

Figure 11: Confocal microscopy image of H9C2 cells: H9C2 is an embryonic ventricular myoblast cell line derived from rat. Chronic culture in low serum media prevents differentiation of H9C2 myoblast to cardiomyocytes. Cells were cultivated for 6 days in either 10% FCS (**A**) or 1% FCS (**B**).
Image source: Pagano et al. 2004 [75]

3.10 Animals

Animals were housed in a pathogen-free facility and maintained on a regular light-dark cycle (14 h light, 10 h dark) with *ad libitum* access to a standard chow diet (4.5% fat) and water.

For overnight fasting experiments, food was withdrawn 16 hours before tissue collection, where the mice were euthanized by cervical dislocation and excised tissues were immediately snap-frozen in liquid nitrogen. Maintenance, handling, and tissue collection from mice was approved by the Austrian Federal Ministry for Science and Research and by the ethics committee of the University of Graz.

In this study, ATGL deficient mice (ATGL-/-), their corresponding A2 wild type control mice, adipose tissue specific ATGL knock out mice (ATGL-ATko), their corresponding flox/flox control mice, and transgenic mice overexpressing Plin5 solely in cardiac muscle, and their corresponding A2 wild type control mice, were used

ATGL-/- mice were generated by inactivating the ATGL gene by replacing the first exon which includes the translational start codon and the lipase consensus sequence motif (GXSXG, where G is glycine, S is serine, and X is any amino acid), with a neomycin expression cassette [76].

ATGL-ATko mice were generated using the loxP-Cre strategy. Therefore, an ATGL targeting vector was constructed to introduce loxP sites upstream and downstream of the first exon which includes its translation start site and catalytic domain. This loxP sites facilitate the removal of the targeted exon1 by the Cre recombinase [25].

CM-Plin5 mice were generated by cloning full-length mouse Plin5 cDNA in the α- myosin heavy chain (MHC) promoter construct [77], kindly provided by J. Robbins as previously described [78].

4 EXPERIMENTAL PRODECURE

4.1 Cell culture

Cell culture studies with recombinant adenovirus were performed in H9C2 cardiomyocytes. Quantification of the recombinant Plin5 adenoviral stock, by testing of applicable multiplicities of infections (MOIs) and plaque assay, H9C2 cardiomyocytes were used. Moreover, *in vivo* TG levels were determined in H9C2 cardiomyocytes. Furthermore, COS-7 cells were used to test proper expression of diverse recombinant adenoviral plasmids and to examine *in vivo* TG levels.

All these cell lines were cultivated in high glucose DMEM medium (containing 4.5g/L glucose) and grown at 37°C, 7% CO_2 and 95% relative humidity.

4.1.1 Passaging of the cells

Cells were cultivated in 175cm^2 cell culture flasks with approximately 20ml full medium (DMEM high glucose medium [4.5g/L glucose] further supplemented with 10% FCS and 1% P/S). For passaging, the medium was aspirated and the cell layer was rinsed with 10ml 1x PBS. After adding 3ml trypsin/EDTA, the cells were incubated at 37 °C, until the cell layer was dispersed (3-5 minutes). The cells were suspended with 10ml full medium, transferred to a 15ml Greiner tube and centrifuged for 3 minutes at room temperature and 1200rpm. The supernatant was discarded and the cells were re-suspended in an appropriate volume of full medium. Desired aliquots were seeded in 175cm^2 culture flasks and cultured with 20ml of full medium.

4.1.2 Differentiation of H9C2 myoblasts

Previous to the experiments, H9C2 myoblasts have to be differentiated to cardiomyocytes. Therefore, the H9C2 myoblasts were seeded in a 175cm^2 cell culture flask with a total cell number of 2x10^5 cells and cultivated with full medium at 37°C, 7% CO_2 and 95% relative humidity. At 95% confluence, the medium was aspirated and the cells were further cultivated

with differentiation medium (DMEM high glucose medium [4.5g/L glucose] further supplemented with 1% FCS and 1% P/S). During consistently medium changing, H9C2 myoblasts differentiated to cardiomyocytes within 10 days.

4.1.3 Transfection of COS-7 cells with recombinant protein DNA

COS-7 cells were seeded in 6-well plates with a total cell number of $1{,}5x10^5$ cells per well. The cells were cultivated with full media and maintained at 37°C, 7% CO_2 and 95% relative humidity.

The plasmid DNA (plasmid DNA preparation produced as described in chapter 4.2.1.5) of respective construct was transfected with Metafectene® [Biontex] in a ratio of 1:5. Therefore, 1µg plasmid DNA and 5µL Metafectene were mixed up with 50µL serum-free media in separate Eppendorf tubes, respectively. These tubes were pooled and incubated for 20 minutes at room temperature. Meanwhile, culture medium of the cells were aspirated and 0.5mL serum-free medium were added. The entire DNA-Metafectene mix was added to the cells. After 4 hour of incubation the medium was aspirated and exchanged to 2mL full medium.

In case of double or triple transfection, the amount of DNA was adjusted with DNA of cloning vector without insert DNA.

To test proper transfection, the protein expression was determined by Western blot analysis as described in chapter 4.7.

4.1.4 Infection of H9C2 cardiomyocytes with recombinant adenovirus

Differentiated H9C2 cardiomyocytes were infected with recombinant adenovirus to test applicable MOIs and to analyze TG levels *in vivo*. Prior to infection, H9C2 myoblast cells were seeded and differentiated as described in chapter 4.1.2.

The volume of viral stock [mL] needed to infect a certain number of cells with a distinct MOI is defined as described in formula 1. For the differentiated H9C2 cardiomyocytes a total cell number of $2x10^5$ cells was assumed.

$$\text{Vol [mL]} = \frac{\text{Number of cells} * \text{MOI}}{\text{pfu/mL}}$$

Formula 1: Calculation of volume of virus stock needed for infection

To infect one well of a 6-well plate, the medium was discarded and 2mL serum-free medium were added to the cells. The calculated volume of viral stock was added to the cells, plates were gently pivoted and incubated at 37°C to allow the infection to occur. After two hours, viral solution containing medium was aspirated and exchanged to 2mL of full medium.

To test proper infection, the protein expression was determined by Western blot analysis as described in chapter 4.7.

4.2 Generation of a recombinant adenovirus overexpressing C-terminal FLAG-tagged Plin5

The generation of a recombinant C-terminal FLAG-tagged Plin5 overexpressing adenovirus included two main cloning steps. The first step was the generation of the C-terminal FLAG-tagged Plin5 construct by cloning Plin5 coding sequence (CDS) into the pFLAG-CMV-5.1 expression vector. The second step was the inserting of FLAG-tagged Plin5 construct into the adenoviral genome by cloning FLAG-tagged Plin5 in the adenoviral pShuttle vector, transfection into *E. coli* cells to let the homologous recombination with the adenoviral genome occur, and amplification of the recombinant adenoviral genome containing FLAG-tagged Plin5.

For generation of a recombinant Plin5 overexpressing adenovirus, the AdEasy™ XL Adenoviral Vector System Kit was used and steps were performed as described in the manufacturer's protocol (a schematic overview of the procedure is shown in figure 12).

In the AdEasy XL system, the gene of interest is cloned into the pShuttle vector. Once constructed, the shuttle vector is linearized with *Pme*I and transformed into BJ5183-AD-1 competent cells. Transformants are selected for kanamycin resistance and subsequently identified by restriction digestion. Once a recombinant is identified, it is amplified using the recombination-deficient XL10-Gold strain. Purified recombinant adenoviral plasmid DNA is digested with *Pac*I to expose its inverted terminal repeats and is then used to transfect HEK AD293 cells where deleted viral assembly genes are complemented *in vivo*.

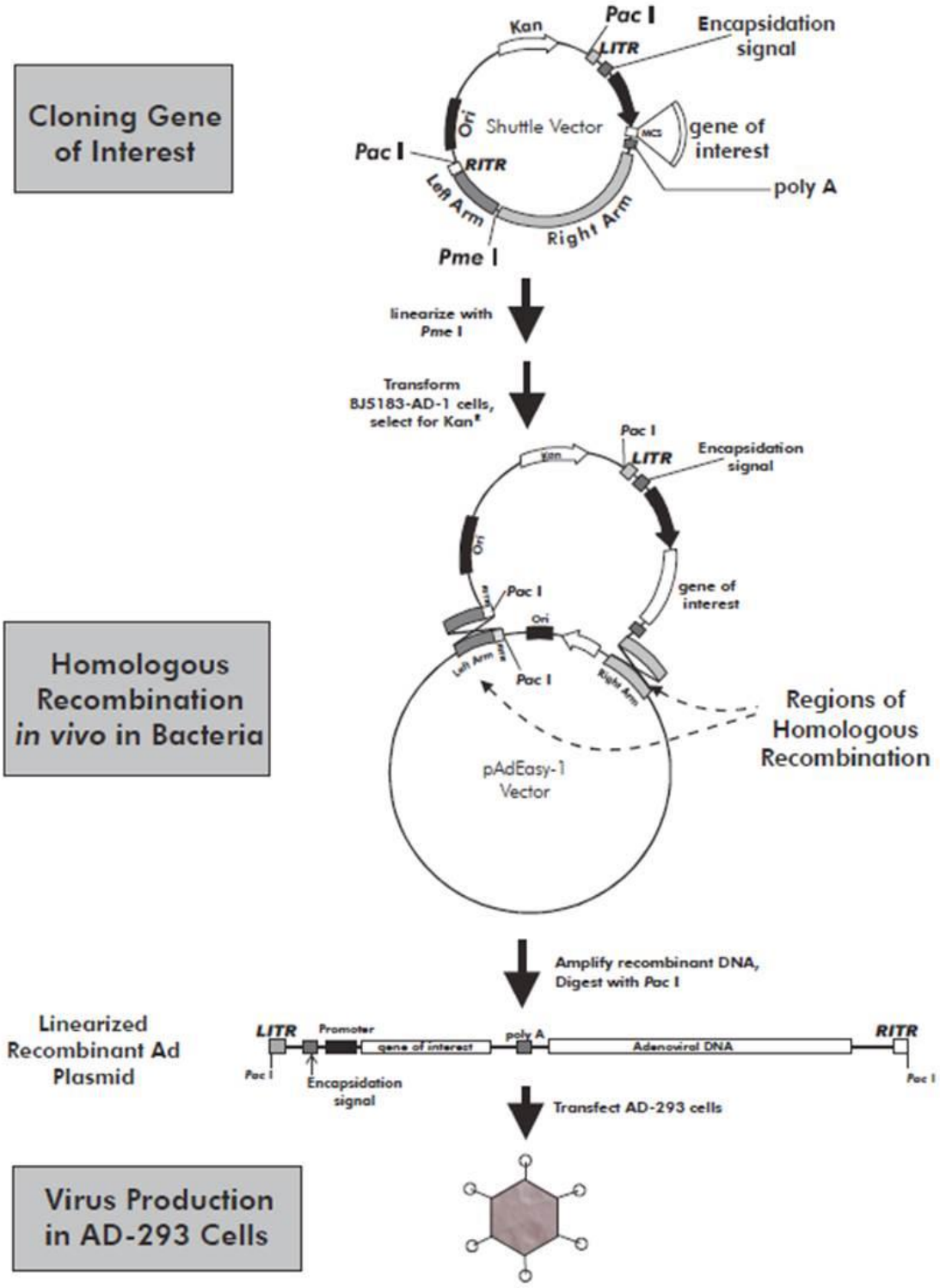

Figure 12: Overview of the generation of recombinant adenovirus: The gene of interest is cloned into the adenoviral shuttle vector. After linearization with *Pme*I, the construct is transformed into competent BJ5183-AD-1 cells. Transformants are selected for kanamycin resistance and recombinant DNA is transfected into ultra-competent XL-Gold cells. After *Pac*I digest, the construct is transfected into HEK AD-293 cells to generate and amplify the adenoviral stock.
Image source: http://www.chem.agilent.com/library/usermanuals/Public/240010.pdf

4.2.1 Cloning of C-terminal FLAG-tagged Plin5

4.2.1.1 Polymerase chain reaction

CDS of Plin5 (1.4kb) was amplified by PCR. Therefore the forward primer Plin5fw*Eco*RIflag (5` - CGC GAA TTC ATC CAC CAT GGA CCA GAG AGG TGA A - 3`) [Eurofins Genomics] and the reverse primer Plin5rev*Sal*Iflag (5` - TAG AGT CGA CGA AGT CCA GCT CTG GCA TCA TTG T - 3`) [Eurofins Genomics] were used.

Each PCR mix contained 1µL cardiac muscle cDNA template, 0.5µL forward and reverse primer [10pmol/µL], respectively, 0.5µL dNTPs Mix [10mM], 5µL High fidelity buffer [5x; Finnzymes] and 0.3µL Phusion® DNA polymerase [2U/µL; Finnzymes] and was filled up with Fresenius water to a final volume of 25µl.

The DNA amplification was set up with following PCR program:

98°C	2 minutes	
98°C	30 seconds	30 cycles
68°C	30 seconds	
72 °C	1 minute	
72 °C	10 minutes	
4°C	forever	

The PCR products were loaded onto a 1% agarose gel and the gel was run at 90 volt for 30 minutes. The respective bands were excised and the DNA was purified with Omega® bio-tek Kit.

4.2.1.2 Restriction Digest

PCR product or prepared plasmid DNA was digested by restriction enzymes, respectively. Amplified Plin5 DNA and the C-terminal pFLAG-CMV-5.1 vector were digested with two restriction enzymes, *Eco*RI high fidelity [20000 U/mL; New England BioLabs] and *Sal*I high fidelity [20000 U/mL; New England BioLabs].

Each restriction mix contained 25µL purified PCR product or 6µg C-terminal pFLAG-CMV-5.1 vector, 1µL of each restriction enzyme and 3µL CutSmart buffer [10x; New England BioLabs] and was filled up with Fresenius water to a final volume of 30µL. The restriction mix was incubated at 37°C, 300rpm for 2 hours.

To prevent religation of the vector, the digested vector DNA was dephosphorylated with alkaline phosphatase (CIP) [10000 U/µL; New England BioLabs]. Therefore 1µL CIP was added to the restriction mix and further incubated at 37°C, 300rpm for 30 minutes.

The digested DNA samples were loaded onto a 1% agarose gel and the gel was run at 90V for 30 minutes. The respective bands were excised and the DNA was purified with Omega® bio-tek Kit.

4.2.1.3 Ligation of plasmid and vector DNA

To estimate required volumes of purified digested Plin5 and vector DNA, 1µL of each DNA sample were loaded onto a 1% agarose gel and run at 90V for 30 minutes.

The Plin5 DNA insert and the C-terminal pFLAG-CMV-5.1 vector were ligated with a ratio of 3:1. Therefore, appropriate volumes of digested Plin5 DNA and digested vector DNA were mixed with 1µL T4 DNA-ligase [400000 U/mL; New England BioLabs] and 1.5µL ligase buffer [10x; New England BioLabs] and filled up with Fresenius water to a final volume of 15µL. After one hour of incubation at 25 °C the reaction was stopped by incubating the samples at 70 °C for 10 minutes.

4.2.1.4 Transformation into competent cells

Transformation of Plin5-pFLAG-CMV-5.1 construct was performed with chemically competent *E. coli* DH5α cells. Therefore, 3µL ligation mix were added to 25µL chemical competent *E. coli* cells on ice and mixed gently. After 10 minutes of incubation on ice, the transformation mix was incubated at 42°C in a water bath for 30 seconds. After 3 minutes incubation on ice, 200µL pre-warmed SOC medium were added and the preparation was mixed by pipetting up and down. The transformation mix was incubated at 37°C and horizontal shaking at 300rpm for 1 hour. Afterwards, cells were plated on LB agar plates supplemented with 100µg/mL of the respective antibiotic and incubated at 37°C overnight.

4.2.1.5 Plasmid DNA preparation

MiniPrep plasmid preparation

At least five colonies of each construct were cultured in 5ml LB medium supplemented with 100µg/ml of the appropriate antibiotic at 37 °C and 180 rpm overnight.

The overnight culture was centrifuged at room temperature and 3000rpm for 10 minutes. The fluid supernatant was discarded and the cell pellet was re-suspended in 250µL lysis buffer I. After adding 250µL lysis buffer II and mixed by inverting. The sample was incubated for 5 minutes at room temperature, then 350µL potassium acetate [3M]/CH_3COOH [5M] were added and mixed by inverting. After 1 minute incubation on ice, the sample was centrifuged at 4°C and 13000rpm for 10 minutes. The supernatant was collected in a fresh Eppendorf tube by inverting and 400µL phenol [Roth] and 250µL sevac (chloroform and isopropyl alcohol in a ratio of 24:1) were added to the supernatant and vortexed briefly. After centrifugation at room temperature and 13000rpm for 1 minute, approximately 700µL of the supernatant were collected in a fresh Eppendorf tube. To precipitate the DNA, 700µL isopropyl alcohol [100%] were added and the sample was centrifuged at room temperature and 13000rpm for 5 minutes. The fluid supernatant was discarded by inverting, the DNA pellet was washed with 500µL ethanol [70% with ddH_2O] and centrifuged at room temperature and 13000rpm for 5 minutes. The fluid supernatant was removed carefully and the DNA pellet was dried at 37°C until the entire ethanol was evaporated. Subsequently, the DNA pellet was diluted in 50µL Fresenius

water further supplemented with 2µL RNase [2.5mg/mL] and the DNA concentration was measured by Nanodrop spectrophotometer ND-1000 [PeqLab Biotechnology GmbH].

Proper cloning was tested by digesting plasmid DNA with the same restriction enzymes used for cloning as described in chapter 4.2.1.2. Moreover, plasmid DNA was sequenced by sequencing analysis (Microsynth AG).

MaxiPrep plasmid preparation

For each DNA construct an overnight culture of one positive clone was produced. A culture flask containing 250mL LB medium supplemented with the appropriate antibiotic was inoculated with the overnight culture and incubated at 37°C and 180rpm overnight. MaxiPrep plasmid preparation was performed according to the manual of NucleoBond® Plasmid Purification Midi Kit. Plasmid DNA pellet was diluted in an appropriate volume of Fresenius water and the DNA concentration was measured by Nanodrop spectrophotometer ND-1000. MaxiPrep plasmid DNA was adjusted to a concentration of 1µg/µL with Fresenius water and stored at -20°C.

Proper cloning was tested by digesting plasmid DNA with the same restriction enzymes used for cloning as described in chapter 4.2.1.2.

4.2.2 Generation of recombinant adenoviral plasmid

4.2.2.1 Cloning of FLAG-tagged Plin5 into pShuttle vector

Amplification of plasmid DNA

FLAG-tagged Plin5 (1.4kb) was amplified by PCR as described in chapter 4.2.1.1 using FLAG-tagged Plin5 plasmid DNA as template (plasmid DNA preparation produced as described in chapter 4.2.1.5). Therefore, forward primer *Not*IfwpShuttleP5 (5` - CTT GCG GCC GCG AAT TCA TCC ACC ATG GAC CAG A - 3`) [Eurofins Genomics] and reverse

primer *Eco*RVrevpShuttle (5` - GGG ATA TCA ACC TAC TTG TCA TCG TCG TCC TTG TA - 3`) were used.

Restriction digest of plasmid and vector DNA

Prior to ligation, PCR product was digested by restriction enzymes as described in chapter 4.2.1.2. Therefore, FLAG-tagged Plin5 DNA (1.4kb) and pShuttle vector DNA (6.6kb) were digested with two restriction enzymes, *Not*I high fidelity [20000 U/mL; New England BioLabs] and *Eco*RV [20000 U/mL; New England BioLabs] high fidelity.

Ligation of plasmid and vector DNA

The ligation of FLAG-tagged Plin5 and pShuttle vector was performed as described in chapter 4.2.1.3.

Transformation into chemical competent *E. coli* cells

Transformation of the FLAG-tagged Plin5 – pShuttle construct (8kb) was performed with chemical competent *E. coli* DH5α cells as described in chapter 4.2.1.4.

Plasmid DNA preparation

MiniPrep plasmid preparation was performed as described in chapter 4.2.1.5.

Proper cloning was tested by digesting plasmid DNA with the same restriction enzymes used for cloning as described in chapter 4.2.1.2. Moreover, the plasmid DNA was sequenced by sequencing analysis (Microsynth AG).

4.2.2.2 Generation of recombinant adenoviral plasmid

Linearization of FLAG-tagged Plin5 – pShuttle construct

Plasmid DNA (MiniPrep plasmid preparation performed as described in chapter 4.2.1.5) of FLAG-tagged Plin5 – pShuttle construct was linearized by *Pme*I restriction enzyme. Prior to linearization, plasmid DNA has to be desalinized.

Each linearization mix contained 7µL desalted plasmid DNA, 1µL *Pme*I [10000 U/mL; New England BioLabs] and 3µL CutSmart buffer [10x; New England BioLabs] and was filled up with Fresenius water to a final volume of 30µL. The sample was incubated at 37°C, 300rpm for 2 hours.

Linearized samples were loaded onto a 1% agarose gel and the gel was run at 90V for 30 minutes. The respective band was excised and the DNA was purified with Omega® bio-tek Kit.

Transformation into electro competent BJ5183-AD-1 *E. coli* cells

Transformation of FLAG-tagged Plin5 – pShuttle construct was performed with electro competent BJ5183-AD-1 *E. coli* cells. Therefore, 5µL linearized plasmid DNA were gently mixed with 40µL BJ5183-AD-1 *E. coli* cells on ice. Transformation mix was transferred into a pre-cooled electroporation cuvette. After drying the surface of the cuvette the electroporation was carried out with 200Ω, 2,5kV and 25µF in the Bio-Rad MicroPulser™ [Bio-Rad Laboratories]. To regenerate the cells, 1mL 37°C pre-warmed LB medium was added and gently mixed by pipetting up and down. Transformation mix was transferred into a fresh Eppendorf tube and incubated at 37°C for 1 hour during horizontal shaking (180rpm). Afterwards, cells were plated on LB agar plates containing 100µg/mL of appropriate antibiotic and incubated at 37°C overnight.

Preparation of the adenoviral plasmid

10 smallest well isolated colonies of each transformant were cultured in 5ml LB medium further supplemented with 100µg/ml of the appropriate antibiotic at 37 °C and 180 rpm overnight. DNA was isolated by MiniPrep plasmid preparation as described in chapter 4.2.1.5. The plasmid DNA pellet was re-suspended in 20µL Fresenius water further supplemented with 0.8µL RNase [2,5mg/mL].

Proper cloning was tested by digesting plasmid DNA with *Pac*I as described in chapter 4.2.1.2. The size of the DNA fragment was estimated by loading the digested sample was onto a 0.8% agarose gel and the gel was run at 90V for 30 minutes.

4.2.2.3 Amplifying recombinant adenoviral plasmid

Transformation into ultra-competent XL-Gold *E. coli* cells

Transformation of the adenoviral plasmid was performed with ultra-competent XL10-Gold *E. coli* cells. Therefore, 50µL XL10-Gold cells were transferred into a pre-cooled Eppendorf tube and 2µL β-mercaptoethanol mix [AdEasy™ XL Adenoviral Vector System Kit] were added. The tube was pivoted gently and incubated on ice for 10 minutes. Afterwards, 2µL of 1:10 diluted adenoviral plasmid DNA were added to the XL10-Gold cells, pivoted gently and incubated on ice for 30 minutes. The sample was incubated at 42°C in a water bath for 30 seconds, then incubated for 2 minutes on ice. The cells were regenerated by adding 0.95mL pre-warmed NZY+ broth medium. The transformation mix was incubated at 37°C and 180rpm for 1 hour. Afterwards, the cells were plated on LB agar plates containing 100µg/mL of appropriate antibiotic and incubated at 37°C overnight.

Preparation of the adenoviral plasmid DNA

DNA was isolated by MaxiPrep plasmid preparation as described in chapter 4.2.1.5.

Proper cloning was tested by digesting plasmid DNA with *Pac*I as described in chapter 4.2.1.2. The size of DNA fragment was estimated by loading the digested sample onto a 0.8% agarose gel and the gel was run at 90V for 30 minutes.

4.2.3 Preparation of adenoviral stock with recombinant adenoviral plasmid

4.2.3.1 Transfection into HEK AD293 cells

Linearization of adenoviral plasmid DNA

Linearization of adenoviral plasmid DNA was performed by *Pac*I restriction enzyme. Therefore, four equal linearization mixes were prepared. Each linearization mix contained 10µL adenoviral plasmid DNA (MaxiPrep) [1µg/µL], 1µL *Pac*I [10000 U/mL; New England BioLabs] and 3µL CutSmart buffer [10x; New England BioLabs] and was filled up with Fresenius water to a final volume of 30µL. The samples were incubated at 37°C, 300rpm for 2 hours.

Purification of linearized plasmid DNA

The four equal linearization mixes were pooled, 120µL phenol [Roth] and 90µL sevac (chloroform and isopropyl alcohol in a ratio of 24:1) were added and vortexed briefly. The sample was centrifuged at 4°C, 14000rpm for 15 minutes, then 200µL ethanol [100%] were added and vortexed briefly. After 2 hours of incubation at -80°C, the sample was centrifuged at 4°C, 14000rpm for 30 minutes. Fluid supernatant was discarded, 800µL ethanol [70%] were added and centrifuged at 4°C, 14000rpm for 5 minutes. Afterwards, supernatant was discarded and DNA pellet was dried at 37°C until the entire ethanol is evaporated. Subsequently, purified plasmid DNA pellet was diluted in 20µL Fresenius water.

Transfection into HEK AD293 cells – Calcium phosphate method

For transfection, the ProFection® Mammalian Transfection System Kit [Promega] was used.

One day prior to transfection, HEK AD293 cells were seeded in a petri culture dish with a total cell number of $7{,}5x10^5$ cells. The cells were cultured with 8mL full medium and maintained at 37°C, 7% CO_2 and 95% relative humidity. The medium was changed 3 hours prior to transfection.

For transfection, 18µg linearized adenoviral plasmid DNA were mixed with 62µL $CaCl_2$ [2M] and filled up with Fresenius water to a final volume of 500µL. Furthermore, 500µL 2x HBS buffer [ProFection® Mammalian Transfection System – Promega] were transferred into a fresh Eppendorf tube. DNA-$CaCl_2$ mix was slowly pipetted into 2x HBS buffer during constant pivoting, then incubated at room temperature for 30 minutes. Meanwhile, the culture medium of the cells was aspirated and exchanged to 6mL serum-free medium. The sample was slowly trickled to the HEK AD293 cells during gently pivoting. After 6 hours, the medium was exchanged to 10 mL full medium.

During consistently adding full medium, holes in the cell layer were visible under the microscope within 7-10 days, indicating the lytic activity of the adenovirus. The cells has to be harvested until the whole cell layer is lysed by the adenovirus.

Harvesting adenoviral plasmid transfected cells

The culture medium of the cells was transferred into a Greiner tube and stored at -20°C and the cell layer was rinsed with 5mL 1x PBS. Cells were abraded and re-suspended in 1mL 1x PBS, and transferred into a 15mL Greiner tube. The remaining cells on the dish were re-suspended in 1mL 1xPBS and also transferred into the tube. The solution was centrifuged at room temperature and 3000g for 3 minutes. Fluid supernatant was aspirated, the cell pellet was overlaid with 1mL 1x PBS and lysed by freeze/thaw. Therefore, cells were shock frozen in liquid nitrogen, thaw in a 37°C pre-warmed water bath and shock frozen again. This cycle was repeated four times. The lysed cells were centrifuged at room temperature and 12000g for 10 minutes and the supernatant was transferred into a fresh Greiner tube.

4.2.3.2 Preparation of the viral stock solution

Preparing primary viral stock

HEK AD293 cells were seeded in a 175cm^2 cell culture flask with a total cell number of 4x10^6 cells. The cells were cultivated with full media and maintained at 37°C, 7% CO_2 and 95% relative humidity until they reach 90% confluence.

The medium was exchanged to 10mL serum-free medium and the supernatant of harvested cells (see chapter 4.2.4.1) was added to the HEK AD293 cells. After 2 hours, 10mL full medium were added.

After 2 days, holes in the cell layer were visible under the microscope, indicating the lytic activity of the adenovirus, hence, the cells were harvested. Therefore, the culture medium of the cells was transferred into a Greiner tube and stored at -20°C and the cell layer was rinsed with 10mL 1x PBS. Cells were abraded and re-suspended in 3mL 1x PBS, and transferred into a Greiner tube. The remaining cells in the flask were re-suspended in 2mL 1x PBS and also transferred into the tube. The cells were centrifuged at room temperature and 3000g for 10 minutes. Fluid supernatant was aspirated and the cell pellet was re-suspended in 3mL 1x PBS and stored at -20°C.

Testing primary viral stock for recombinant adenoviral plasmid

The presence of recombinant adenoviral plasmid was tested in the medium and the re-suspended cell pellet by PCR. Therefore, forward primer *Not*IfwpShuttleP5 (5` - CTT GCG GCC GCG AAT TCA TCC ACC ATG GAC CAG A - 3`) [Eurofins Genomics] and reverse primer *Eco*RVrevpShuttle (5` - GGG ATA TCA ACC TAC TTG TCA TCG TCG TCC TTG TA - 3`) were used.

Each PCR mix contained 2µL or 5µL of culture medium, or re-suspended cells as template, respectively, 1µL forward and reverse primer [10pmol/µL], respectively, 0.5µL dNTPs Mix [10mM], 5µL High fidelity buffer [5x; Finnzymes] and 0.3µL Phusion® DNA polymerase [2U/µL; Finnzymes] and was filled up with Fresenius water to a final volume of 25µl.

The DNA amplification was set up with following PCR program:

98°C	2 minutes	
98°C	30 seconds	30 cycles
68°C	30 seconds	
72 °C	1 minute	
72 °C	10 minutes	
4°C	forever	

The PCR products were loaded onto a 1% agarose gel and the gel was run at 90 volt for 30 minutes.

Preparing secondary viral stock

The collected medium of the primary viral stock was centrifuged at room temperature and 1000g for 10 minutes. Supernatant was transferred into a fresh Greiner tube and the cell pellet was re-suspended in 1mL 1x PBS. Cells were lysed by freeze/thaw. Therefore, cells were shock frozen in liquid nitrogen, thaw in a 37°C pre-warmed water bath and shock frozen again. This cycle was repeated four times. The lysed cells were centrifuged at room

temperature and 12000g for 10 minutes. Supernatant was discarded and the cell pellet was re-suspended with the supernatant of the collected primary stock medium (first centrifugation step). The viral stock was stored at -20°C.

4.2.3.3 Amplification of the viral stock

Fifteen 175cm^2 cell culture flasks were seeded with HEK AD293 cells with a total cell number of 4x10^6 cells. The cells were cultivated with full media and maintained at 37°C, 7% CO_2 and 95% relative humidity until they reach 90% confluence.

The viral stock solution was diluted in a ratio of 1:7.5 with serum-free medium supplemented with 1% P/S. Culture medium of the cells was aspirated and 10mL of diluted viral stock were added. After 2 hours, 10mL full medium were added.

After one day, infected HEK AD293 cells were harvested. Therefore, the medium of one cell culture flask was collected in a Greiner tube and stored at -20°C. The medium of the remaining culture flasks was discarded and the cell layer was rinsed with 10mL 1x PBS. Cells were abraded and re-suspended in 3mL 1x PBS, and transferred into a Greiner tube. Remaining cells in the flask were re-suspended in 2mL 1xPBS and also transferred into the tube. The cells were centrifuged at room temperature and 3000g for 10 minutes. Fluid supernatant was aspirated, the cell pellet was re-suspended in 3mL 1x PBS and lysed by freeze/thaw. Therefore, cells were shock frozen in liquid nitrogen, thaw in a 37°C pre-warmed water bath and shock frozen again. This cycle was repeated four times. The lysed cells were centrifuged twice at room temperature for 10 minutes and 3500g. The supernatant contains infectious recombinant adenovirus. The adenoviral stock was stored at -20°C.

4.2.3.4 Purification of viral stock by density gradient centrifugation and dialysis

Viral stock was purified by CsCl density gradient centrifugation and dialysis.

In an ultracentrifuge tube, 3mL 1.25g/mL CsCl solution were submitted and 3mL 1.40g/mL CsCl solution were added beneath the meniscus. Adenoviral stock solution was added onto

the CsCl density gradient. The ultracentrifuge tube has to be completely filled up, if necessary with 1x PBS. The sample was centrifuged at 22°C and 35000rpm for one hour in the ultracentrifuge. Afterwards, ultracentrifuge tube was fixed and the solution at the opalescent layer, which contained the virus, was aspirated with a needle and transferred into a sterile Greiner tube.

In a fresh ultracentrifuge tube, 8mL of 1.33g/mL CsCl solution were submitted and the collected virus solution was added beneath the meniscus. The ultracentrifuge tube has to be completely filled up, if necessary with 1.33g/mL CsCl solution. The sample was centrifuged at 22°C and 35000rpm for 24 hours in the ultracentrifuge. Afterwards, ultracentrifuge tube was fixed and the solution at the opalescent layer, which contained the virus, was aspirated with a needle and transferred in a sterile Greiner tube.

For dialysis, a dialysis membrane was boiled in water for 10 minutes and fixed in a conical flask filled with 2L ice cold dialysis buffer. The viral solution was filled into the dialysis membrane and was dialyzed with constant stirring at 4°C overnight.

The purified adenoviral stock solution was split into appropriate aliquots and stored at -80°C.

4.2.4 Quantification of infectious viral stock

4.2.4.1 Optical measurement

The concentration of the adenoviral stock was determined by the quotient of optical density (OD) measured at 260nm and 280nm by Nanodrop spectrophotometer ND-1000. Therefore, 10µL adenovirus stock was mixed with 10µL 1x PBS and 20µL SDS [0.2%] and the OD was measured via Nanodrop spectrophotometer at 260nm and 280nm. The concentration is indicated as plaque forming units per milliliter (pfu/mL). The pfu/mL was calculated as described in formula 2.

$$\text{pfu/mL} = \text{OD}_{260/280} * 1*10^{12}$$

Formula 2: Calculation of pfu/mL

4.2.4.2 Testing applicable multiplicities of infections

MOI is the ratio of the number of virus particles to the number of target cells. Appropriate MOIs for recombinant Plin5 overexpressing adenovirus (AdPlin5) and recombinant ATGL overexpressing adenovirus (AdATGL) were tested in differentiated H9C2 cardiomyocytes. Prior, H9C2 myoblasts were cultured and differentiated as described in chapter 4.1.2.

H9C2 cells were infected with several MOIs of AdPlin5 and AdATGL, respectively, as listed in table 4:

Table 4: MOIs for AdPlin5 and AdATGL infection, respectively

MOIs for AdPlin5	MOIs for AdATGL
500	200
800	500
1000	800
2000	1000
5000	

H9C2 cardiomyocytes were infected as describes in chapter 4.1.4.

Cells were harvested after 24 hours or 48 hours, respectively and the protein expression was determined by Western blot analysis as described in chapter 4.7.

4.2.4.3 Plaque assay

Plaque assay is a widely used approach for determining the quantity of infectious virus. Viral plaque assay is indicated as the number of plaque forming units (pfu) per milliliter. Therefore, HEK293 cells were seeded in 6-well plates with a cell number of $2x10^5$ cells per well. The cells were cultivated with 4mL full medium and maintained at 37°C, 7% CO_2 and 95% relative humidity until they reached 90% confluence.

Several AdPlin5 dilutions were prepared in sterile 1x PBS as follows:

10^{-2}: 10µL of purified adenovirus stock + 990µL 1x PBS

10^{-4}: 10µL of 10^{-2} dilution + 990µL 1x PBS

10^{-6}: 10µL of 10^{-4} dilution + 990µL 1x PBS

10^{-8}: 10µL of 10^{-6} dilution + 990µL 1x PBS

From each well, 1 mL full medium was removed and the following volumes of virus dilutions were added in duplicates to get the respective final virus concentration as follows:

10^{-5}: 100µL of 10^{-4} dilution

10^{-6}: 10µL of 10^{-4} dilution

10^{-7}: 100µL of 10^{-6} dilution

10^{-8}: 10µL of 10^{-6} dilution

10^{-9}: 100µL of 10^{-8} dilution

10^{-10}: 10µL of 10^{-8} dilution

Cells were maintained at 37°C, 7% CO_2 and 95% relative humidity overnight.

At the next day, agarose solution [4%] was melt in a microwave oven and equilibrated in a 65°C pre-warmed water bath for about 20 minutes. Meanwhile, the plaquing medium (DMEM high glucose [4.5g/L] supplemented with 2% FCS and 1%P/S) was equilibrated at 37°C. In a 50mL Greiner tube, plaquing medium and agarose solution was mixed by well shaking, that the end concentration of agarose within the medium is 10%. The medium in the 6-well plates was aspirated and 2mL of the plaquing medium/agar mix was added quickly but gently to each well. The agarose was polymerized at room temperature within 15 minutes and the plates were incubated at 37°C.

After two days, this step was repeated, but this time only 1mL plaquing medium/agarose mix was added to each well.

Whitish spots on the cell layer were visible within five days. After further four days, the cells were stained with dimethylthiazol diphenyltetrazolium bromid (MTT) [Sigma]. Therefore,

300µL MTT [5g/L] were added to each well and the plates were incubated at 37°C for 3 hours. Viably cells incorporated MTT, thus, plaques were seen as whitish spots within the blue stained cell layer.

4.3 Analysis of TG levels in cells expressing recombinant proteins

4.3.1 Loading cells with oleic acid

Respective constructs were transfected into COS-7 cells as described in chapter 4.1.3, or H9C2 cardiomyocytes were infected with respective recombinant adenovirus as described in chapter 4.1.4, respectively.

For *in vivo* TG level analysis, COS-7 or H9C2 cells, respectively, were seeded in 6-well plates, whereby the transfection and infection was performed in triplicates. Additionally, one 6-well was transfected or infected for protein expression control, respectively.

The cells were maintained at 37°C overnight. H9C2 cardiomyocytes were incubated with 1mL full medium supplemented with 0,4mM oleic acid and 0,4nM ^{3}H-labeled oleic acid [0,5µCi per well] for 18 hours, whereas transfected COS-7 cells were incubated with 1mL full medium supplemented with 0,4mM non-radioactive oleic acid for 18 hours.

For pulse-chase experiments, cells were either collected for lipid extraction 18 hours after oleic acid loading (pulse/TG accumulation) or were washed triply with 1xPBS and incubated with 1ml of serum-free media supplemented with 2 % of free fatty acid free BSA for 6 hours (chase/TG mobilization).

4.3.2 Lipid extraction

Medium was aspirated and the cells were washed triply with 1x PBS. For lipid extraction, 1 ml of hexane/isopropanol (3:2) was added to each well and plates were pivoted for 10 minutes at room temperature. Extracting solution was transferred into a 2ml Eppendorf tubes. This procedure was repeated once. Extracting solution was evaporated under nitrogen flow.

Further steps to analyze the TG levels *in vivo* depends on whether the cells were loaded with non-radioactive or radioactive labeled oleic acid. The TG levels of cells loaded with non-radioactive oleic acid were measured by infinity TG assay, whereas the TG levels of cells loaded with radioactive oleic acid were measured by liquid scintillation counting in the β-Counter, respectively.

4.3.3 Infinity TG assay

Lipids extracted from non-radioactive oleic acid loaded cells were resolved in 100µL triton [0.1%] and incubated at 37°C during vigorous pivoting for one hour.

To determine the TG level, a glycerin-standard curve have to be made. Therefore, glycerin standard [2.82mM; Sigma] was diluted with trition [0.1%] to appropriate concentrations. In a 96-well microtiter plate, 40µL sample or glycerin standard, respectively, were submitted, and 150µL Infinity TG reagents were added. The plate was incubated at 37°C for 10 minutes and absorbance was measured at 492nm by plate reader.

4.3.4 Thin layer chromatography

Lipids extracted from radioactive oleic acid loaded cells were resolved in 50µl chloroform and loaded onto a silica-gel coated thin layer chromatography (TLC) plate. TLC was performed using hexane/diethyl ether/acetic acid (70:29:1) as solvent. The TLC chamber was filled with the solvent to a depth of approximately 1cm and was saturated for at least one hour. The TLC plates were put into the chamber and incubated until the solvent almost reached the top of the plate. After taking the plates out of the chamber, they were dried for about 5 minutes. Lipids were reversibly colored by iodine vapor and TG were marked by a pencil. After the entire iodine was evaporated, TG-corresponding bands were excised and put into scinti vials containing 8ml of scintillation cocktail. The samples were shaken at room temperature overnight and the amount of tritium (^{3}H) was measured by liquid scintillation counting in the β-Counter.

4.3.5 Determination of protein concentration

Protein concentration of lysed cells was determined by bicinchoninic acid (BCA) protein assay as described in chapter 4.6.2. To lyse the cells, 1mL of SDS/NaOH [0.1%/0.3M] solution was added to each well and the plate was pivoting at room temperature for at least 6 hours.

The amount of glycerin or ^{3}H in TG, respectively, were equalized to the total amount of protein in each well.

4.4 Determination of gene expression on mRNA level

Gene expression on mRNA level was determined by qRT-PCR. Therefore, total RNA was isolated from murine cardiac muscle and a single-strand complementary DNA copy (cDNA) was produced through the action of reverse transcriptase. The principle of qRT-PCR bases on the conventional PCR and is used to amplify and simultaneously detect and quantify cDNA.

4.4.1 Total RNA isolation

Total RNA was isolated from murine cardiac muscle by TRIzol®. Therefore, the half of cardiac muscle was transferred in a RNA tube, 1mL of TRIzol® reagent [Life technologies ™] was added and the tissue was homogenized on ice using Ultra-Turrax. Afterwards, 0.1mL 1-Brom-3-Chloropropan [Merck Schuchardt OHG] was added to the homogenate and mixed immediately. After 2 minutes incubation on ice, the homogenate was centrifuged at 4°C and 12000g for 15 minutes and the aqueous supernatant was transferred into a fresh RNA tube. To precipitate the RNA, 0.5mL isopropyl alcohol [100%] was added and mixed immediately. After 5 minutes incubation on ice, the sample was centrifuged at 4°C and 12000g for 10 minutes. Fluid supernatant was discarded and the RNA pellet was washed with 1mL ethanol [70% in DEPC-water] and centrifuged at 4°C and 7500g for 5 minutes. Afterwards, fluid supernatant was discarded and the RNA pellet was incubated at room temperature until the entire ethanol was evaporated. Subsequently, the RNA pellet was dissolved in an appropriate volume DEPC-water and the concentration was measured by Nanodrop spectrophotometer.

For further cDNA synthesis, 1µg RNA was transferred in a fresh Eppendorf tube and stored at -80°C. As control, 1µL of each RNA sample was pooled in one Eppendorf tube and adjusted to a final concentration of 1µg RNA with DEPC-water. The RNA samples were stored at -80°C.

Prior to cDNA synthesis, RNA integrity was determined. Therefore, 2µg RNA were loaded onto a 1% agarose gel [1% agar dissolved in DEPC-water] and the gel was run at 90V for 30 minutes.

4.4.2 First strand cDNA synthesis

For qRT-PCR, the RNA sample was transcribed into cDNA through the action of Reverse Transcriptase.

To prevent DNA contamination, RNA was digested with DNaseI [Invitrogen]. Therefore, 5µL of DNaseI master mix (Table 5) were added to 1µg RNA on ice. This mixture was incubated at 25°C and 350rpm for 15 minutes.

Table 5: Composition of the DNaseI master mix

Components	Volume [µL]
DNaseI	1
DNase-buffer [10x]	1
DEPC-H_2O	3

DNaseI was inactivated by adding 1µL EDTA [25mM] and incubation at 65°C and 350rpm for 10 minutes. Subsequently, RNA was transcribed into cDNA by the action of Reverse Transcriptase [Applied Biosystems]. Therefore, 10µL of Reverse Transcriptase master mix (Table 6) were mixed carefully with the RNA on ice.

Table 6: Composition of the Reverse Transcriptase master mix

Components	Volume [µL]
Reverse Transcriptase buffer [10x]	2
dNTPs [100mM]	0.8
Random Primer [10x]	2
Reverse Transcriptase	1
RNase Inhibitor	1
ddH_2O	3.2

Transcription of RNA into cDNA was set up by PCR with following program:

25°C	10 minutes
37°C	120 minutes
85°C	5 minutes
4°C	forever

The amplified cDNA was diluted with DEPC-water in a ratio of 1:25 and stored at -20°C.

4.4.3 Quantitative real-time polymerase chain reaction

Every step was performed on ice. In a RT-PCR plate, 16µL SYBR Green master mix (Table 7) were submitted, and 4µL of diluted cDNA were added.

Table 7: Composition of the SYBR Green master mix

Components	Volume [µL]
SYBR Green [2x]	10
forward Primer [10pmol/µL]	1
reverse Primer [10pmol/µL]	1
nuclease free water	4

RT-PCR plate was covered with MicroAmp Optical Adhesive Film and centrifuged shortly at room temperature and 2500rpm.

The qRT-PCR was set up with following program:

50°C	2 minutes	
95°C	10 minutes	
95°C	15 seconds	40 cycles
60 °C	1 minute	

Values were evaluated by unpaired Student´s two-tailed t-test.

4.5 Determination of gene expression on protein level

Gene expression on protein level was determined by Western blot analysis. Therefore, half of murine cardiac muscle was transferred into a sterile Eppendorf tube and 0.3mL HSL buffer further supplemented with protease inhibitor and phosphatase inhibitor was added. The heart was homogenized on ice by Ultra-Turrax and centrifuged at 4°C and 20000g for 30 minutes. Subsequently, infranatant was transferred into a fresh Eppendorf tube and stored at -20°C.

Protein concentration was determined by Bradford protein assay as described in chapter 4.6.1 and Western blot was performed as described in chapter 4.7.

4.6 Protein determination

4.6.1 Bradford protein assay

Bradford protein assay is a colorimetric assay which is based on an absorbance shift of Coomassie Brilliant Blue G-250 dye. After protein binding to Coomassie Brilliant Blue, the red dye is converted into its stable unprotonated blue form.

To determine the protein concentration, a protein-standard curve have to be made. Therefore, albumin protein-standard [2.5mg/mL; Pierce] was diluted with HSL buffer further supplemented with protease inhibitor and phosphatase inhibitor to appropriate concentrations. In a 96-well microtiter plate, 20µL sample or protein standard, respectively, were submitted, and 200µL Bio-Rad Protein Assay dye reagent [diluted with ddH2O in a ratio of 1:5; Bio-Rad Laboratories GmbH] were added. The plate was incubated for approximately 5 minutes at room temperature and absorbance was measured at 595nm by the plate reader.

4.6.2 Bicinchoninic acid protein assay

BCA protein assay was used to examine protein concentration of cell lysates. The protein concentration is exhibited by a color change from green to purple in proportion to protein concentration. The peptide-bonds of the protein reduce Cu^{2+} ions from the cupric sulfate to Cu^{+}. The amount of Cu^{+} is proportional to the amount of protein. Two molecules of bicinchoninic acid chelate a single Cu^{+} ion, forming a purple water-soluble complex that strongly absorbs light at 562 nm.

To determine the protein concentration, a protein-standard curve have to be made. Therefore, albumin protein standard [2.5mg/mL; Pierce] was diluted with 0.3M NaOH /1% SDS solution

to appropriate concentrations. In a 96-well microtiter plate, 20µL sample or protein standard, respectively, were submitted, and 200µL BCA reagent [50 parts of reagents A plus 1 part of reagents B] were added. The plate was incubated for 30 minutes at 37°C and absorbance was measured at 562nm by plate reader.

4.7 Western Blot analysis

Western blot analysis was applied to determine tissue specific protein expression levels in different genotypes as well as under different nutritional states (non-fasted *versus* fasted).

Furthermore, efficient transfection of recombinant plasmid DNA, and infection with recombinant adenovirus, respectively, were determined by Western blot analysis.

4.7.1 SDS-PAGE

Sodium dodecyl sulfate polyacrylamide gel electrophoresis (SDS-PAGE) is a method used for separation of proteins according to their molecular weight. SDS is an anionic surfactant which denaturizes proteins to unfolded individual polypeptides. Movement of proteins through the gel within an electric current is proportional to the length of the polypeptide chains.

Preparation of the polyacrylamide gel

The composition of the separating and stacking gel is shown in table 8.

Table 8: Composition of the SDS-PAGE gels: The separating gel was prepared in a final volume of 40 ml for 5 gels; the stacking gel finally provided 3 ml for one gel.

Components	Separating gel		Stacking gel
	7.5%	10%	4.5%
ddH_2O	19.6mL	16.4mL	1.77mL
4x Lower Tris Buffer	10mL	10mL	-
4x Upper Tris Buffer	-	-	0.75mL
30% acrylamide mix	10mL	16.8mL	0.45mL
10% SDS	400µL	400µL	30µL
TEMED	36µL	36µL	6µL
10% APS	108µL	108µL	18µL
Bromphenol blue	-	-	4.5µL

Separation gel solution was poured between two glass plates and covered with n-butanol. After polymerization of about 1 hour, n-butanol was discarded and the gel was stored in a wet paper towel at 4°C. Stacking gel was poured on top of the separating gel freshly before use, after removing water via filter paper. Finally, a comb was placed in the stacking gel.

4.7.2 Preparation of protein samples for SDS-PAGE

To prepare tissue lysates for Western Blot analysis, an appropriate protein concentration was calculated and filled up with sterile ddH_2O to a final volume of 15µL. Subsequently, 3µL 6x SDS loading buffer were added to the sample and denaturized at 99°C for 10 minutes. After short centrifugation, the samples were ready for loading onto the gel.

To prepare cell lysates for Western Bot analysis, cells were harvested by adding 200µl 1xSDS loading buffer onto the cell layer. The cells were abraded and denaturized at 99°C for 10

minutes. For SDS-PAGE, 20µL cell lysates were directly loaded onto the gel, without prior determination of protein concentration.

4.7.3 Protein separation by SDS-PAGE

The gel was clamped into the running tank which was filled up with 1x Tris-Glycin buffer. After removing the combs, slots were sluiced out with 1x Tris-Glycin buffer andsamples were loaded onto the gel. Additionally, 8µL protein standard [Precision Plus Protein All Blue Standard; BioRad] were loaded on the gel. The remaining slots were loaded with 20µL 1x SDS loading buffer.

The gel was run with 25 mA per gel until the migration front reached the bottom of the gel.

4.7.4 Transfer of the proteins

The gel was detached of the glass plates. Stacking gel was removed and separating gel was transferred onto a filter paper. The gel was covered with the PVDF membrane [Roth] and sandwiched between sponge and filter paper in the following order: sponge/ filter paper/ gel/ membrane/ filter paper/ sponge. After removing air bubbles between gel and membrane, the sandwich was clamped tightly together and put into the blot chamber, which was filled with CAPS transfer buffer. Transfer was performed during water cooling at 200mA for 1 hour and 15 minutes.

4.7.5 Detection of the proteins

The membrane was blocked with 10% milk (dissolved in 1x TST buffer) [Roth] at room temperature with moderate pivoting for 2 hours or at 4°C overnight, respectively. Milk was discarded and the membrane was incubated with primary antibody at room temperature with moderate pivoting for 1 hour or at 4°C overnight, respectively. Afterwards, the membrane was washed three times with 1x TST buffer for 10 minutes at room temperature with

moderate pivoting. Subsequently, secondary horseradish peroxidase conjugated antibody was added to the membrane and incubated for 1 hour. After washing the membrane three times for 10 minutes with 1x TST buffer, proteins were detected using ECL Plus Western Blotting Detection System [Thermo Scientific].

The Western blot was evaluated with ImageJ software.

4.7.6 Staining the proteins

After detection, the membrane was stained to proof an effective transfer of the proteins from the gel to the PDVF membrane. Therefore, Coomassie Brilliant Blue or Ponceau S was used. Coomassie Brilliant Blue is a triphenylmethane dye which forms a complex with the anionic detergent SDS, thus stain the protein. Ponceau S is a sodium salt of a diazo dye, which stains protein rapidly and reversible. Coomassie Brilliant Blue staining is more sensitive than Ponceau S staining, however, the proteins are irreversible stained by Coomassie Brilliant Blue.

To stain the proteins, the membrane was incubated with staining solution for approximately 2 minutes with constant pivoting. Subsequently, the membrane was incubated with destaining solution until the protein bands are clearly visible.

4.8 Statistical analysis

All results are presented as means ± standard derivation ($n \geq 3$). Statistical significance levels were determined by the unpaired Student´s two-tailed t-test (* $p < 0.05$; ** $p < 0.01$; *** $p < 0.001$).

5 RESULTS

5.1 Generation of a Plin5-recombinant adenovirus

Generation of recombinant Plin5 overexpressing adenovirus was performed in two discrete steps. First, a C-terminal FLAG-tagged Plin5 was generated, then the cDNA of this FLAG-tagged Plin5 was inserted into the adenoviral genome.

5.1.1 Cloning of FLAG-tagged Plin5

The CDS of Plin5 was amplified by PCR and the PCR product was analyzed by agarose gel electrophoresis (Figure 13). The PCR product showed a distinct band at about 1400bp, which is consistent with the size of the Plin5 CDS (1.4kb).

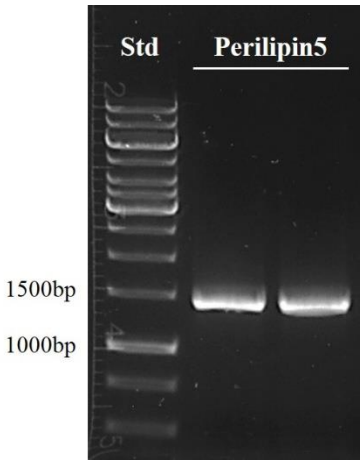

Figure 13: Agarose gel electrophoresis of DNA derived from the amplification of Plin5 CDS by PCR: Amplification was performed with two equal PCR reactions. The size of the PCR product was estimated by 1% agarose gel electrophoresis. The amplified Plin5 PCR product exhibits a distinct band at about 1400bp.

After DNA purification, Plin5 plasmid and pFLAG-CMV-5.1 vector DNA were double digested with *Eco*RI high fidelity and *Sal*I high fidelity restriction enzymes and the restriction digest reaction products were analyzed by agarose gel electrophoresis (Figure 14). The gel showed distinct bands at 1400bp and 4700bp, which is consistent with the size of Plin5 and pFLAG-CMV-5.1 vector, respectively. After ligation of Plin5 and pFLAG-CMV-5.1 vector,

the construct was transformed into competent *E. coli* DH5α cells and plasmid DNA was isolated by MiniPrep plasmid preparation. Afterwards, a MaxiPrep plasmid preparation was performed of *E. coli* colonies identified as carrying the construct of interest.

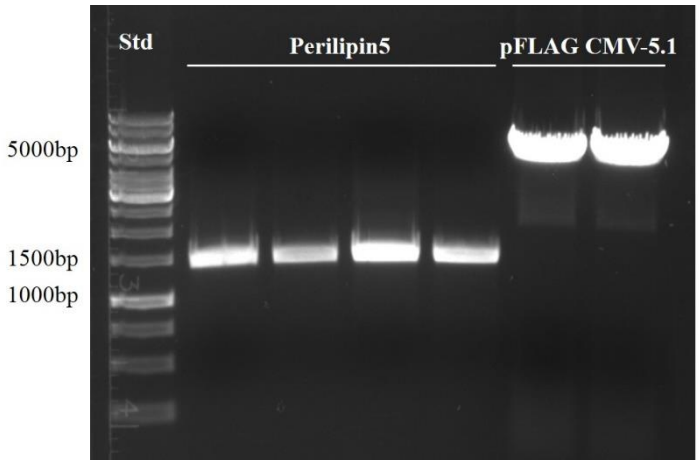

Figure 14: Agarose gel electrophoresis after restriction digest of amplified Plin5 CDS and pFLAG CMV-5.1 vector: Prior to ligation, Plin5 and pFLAG CMV-5.1 vector DNA were double digested with *Eco*RI high fidelity and *Sal*I high fidelity restriction enzymes. The size of the DNA fragments was estimated by agarose gel electrophoresis. The first four lanes show the *Eco*RI-*Sal*I-digested Plin5 with a size of approximately 1400bp and the last two lanes show the digested pFLAG CMV-5.1 vector with a size of about 4700bp.

To verify proper cloning, the plasmid DNA samples were double digested with *Eco*RI high fidelity and *Sal*I high fidelity restriction enzymes and agarose gel electrophoresis was performed. The agarose gel with *Eco*RI-*Sal*I-digested MiniPrep plasmid DNA (Figure 15 A) and MaxiPrep plasmid DNA (Figure 15 B) showed distinct bands at 1400bp, corresponding to Plin5 and at 4700bp, corresponding to the pFLAG CMV-5.1 vector, respectively, indicating correct cloning of Plin5 CDS into the pFLAG CMV-5.1 vector.

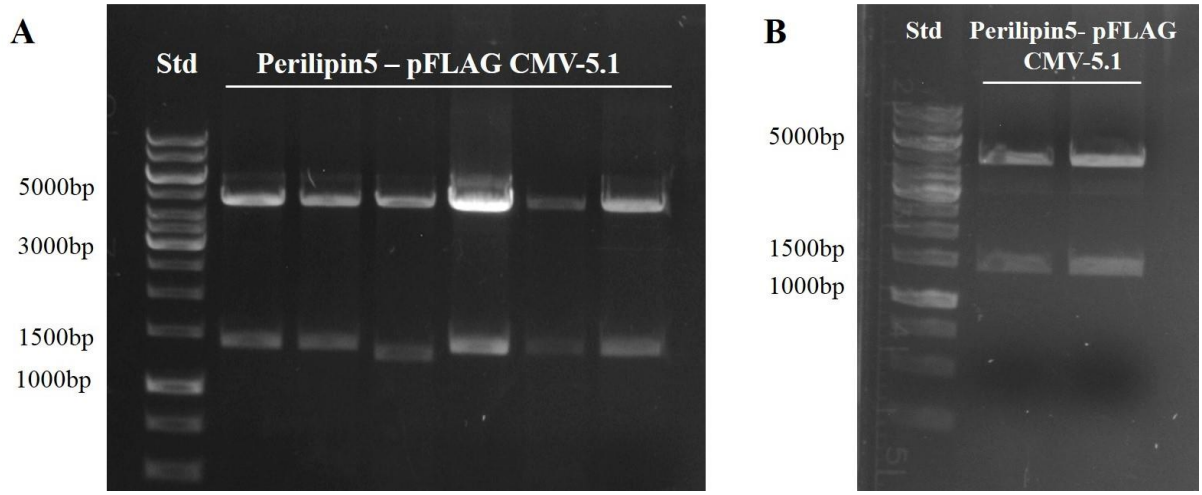

Figure 15: Agarose gel electrophoresis after restriction digest of Plin5-pFLAG CMV-5.1 construct: To verify proper cloning, Plin5-pFLAG CMV-5.1 construct DNA was double digested with *Eco*RI high fidelity and *Sal*I high fidelity restriction enzymes. The size of the DNA fragments was estimated by 1% agarose gel electrophoresis. **A**) Six MiniPrep plasmid DNA samples were analyzed by restriction digest. All lanes, except lane number 3, show two bands, at 4700bp and at 1400bp, representing the size of pFLAG CMv-5.1 vector and Plin5 CDS, respectively. **B**) MaxiPrep plasmid DNA was prepared of two *E. coli* colonies identified as carrying the construct of interest. The plasmid DNA samples were analyzed by restriction digest. Both lanes show two bands, at 4700bp and at 1400bp, corresponding to the size of pFLAG CMV-5.1 vector and Plin5 CDS, respectively.

5.1.2 Generation of recombinant adenoviral plasmid

Plasmid DNA of the Plin5-pFLAG CMV-5.1 construct was amplified by PCR using appropriate primers to insert restriction sites for *Not*I and *Eco*RV flanking FLAG-tagged Plin5 construct. The PCR product was analyzed by agarose gel electrophoresis (Figure 16). The PCR product showed a sharp band at 1400bp, which is consistent with the size of Plin5 CDS (1.4kb).

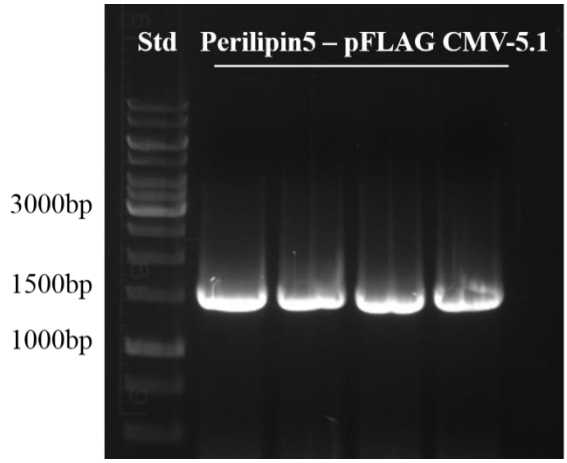

Figure 16: Agarose gel electrophoresis after Plin5-pFLAG CMV-5.1 amplification by PCR: Amplification was performed with four equal PCR reactions. The size of the PCR product was estimated by 1% agarose gel electrophoresis. Sites for the restriction enzymes *Not*I and *Eco*RV flanking the FLAG-tagged Plin5 CDS were introduced using respective PCR primers. The amplified Plin5 construct exhibits a sharp band at 1400bp.

After DNA purification, FLAG-tagged Plin5 and pShuttle vector DNA were double digested with *Not*I high fidelity and *Eco*RV high fidelity restriction enzymes and restriction products were analyzed by agarose gel electrophoresis (Figure 17). The gel showed distinct bands at 1400bp and 6600bp, which is consistent with the size of FLAG-tagged Plin5 and pShuttle vector, respectively. After ligation of FLAG-tagged Plin5 and pShuttle vector, the construct was transformed into competent *E. coli* DH5α cells and the plasmid DNA was isolated by MiniPrep plasmid preparation.

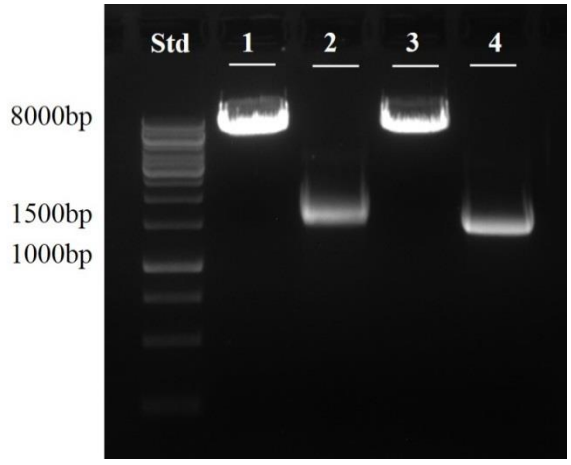

Figure 17: Agarose gel electrophoresis after restriction digest of FLAG-tagged Plin5 and pShuttle vector: Prior to ligation, FLAG-tagged Plin5 and pShuttle vector DNA were double digested with *Not*I high fidelity and *Eco*RV high fidelity. The size of the DNA fragments was estimated by 1% agarose gel electrophoresis. Lane 1 and 3 consists of the digested pShutte vector with a size of about 6600bp. Lane 2 and 4 show the digested FLAG-tagged Plin5 construct with a size of about 1400bp.

To verify proper cloning, the plasmid DNA samples were double digested with *Not*I high fidelity and *Eco*RV high fidelity restriction enzymes and agarose gel electrophoresis of reaction products was performed (Figure 18). The gel showed distinct bands at 1400bp and 6600bp, which is consistent with the size of FLAG-tagged Plin5 and pShuttle vector, respectively, indicating correct cloning of FLAG-tagged Plin5 into the pShuttle vector.

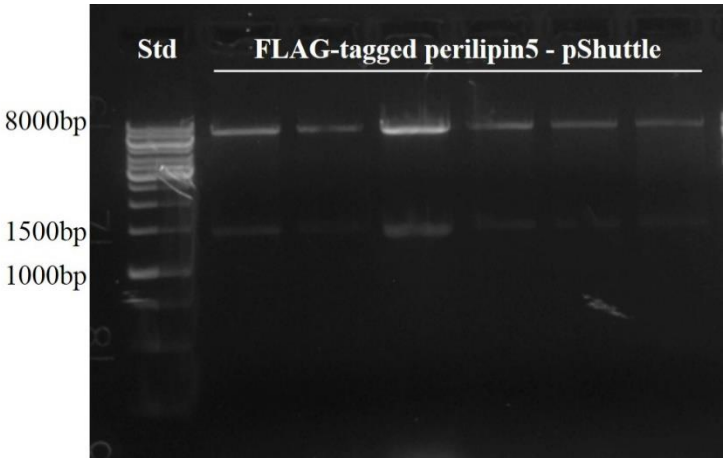

Figure 18: Agarose gel electrophoresis after restriction digest of FLAG-tagged Plin5-pShuttle plasmid DNA: To verify proper cloning, six plasmid DNA samples of FLAG-tagged Plin5 - pShuttle construct were double digested with *Not*I high fidelity and *Eco*RV high fidelity restriction enzymes. The size of the DNA fragments was estimated by 1% agarose gel electrophoresis. All lanes show two bands, at 6600bp and at 14000bp, corresponding to the size of pShuttle vector and FLAG-tagged Plin5, respectively.

Plasmid DNA was linearized with *Pme*I restriction enzyme and the DNA was transformed into electro competent BJ5183-AD-1 *E. coli* cells, where *in vivo* homologous recombination happens. The recombinant adenoviral plasmids were isolated by MiniPrep plasmid preparation and the smallest well isolated colonies were used (Figure 19).

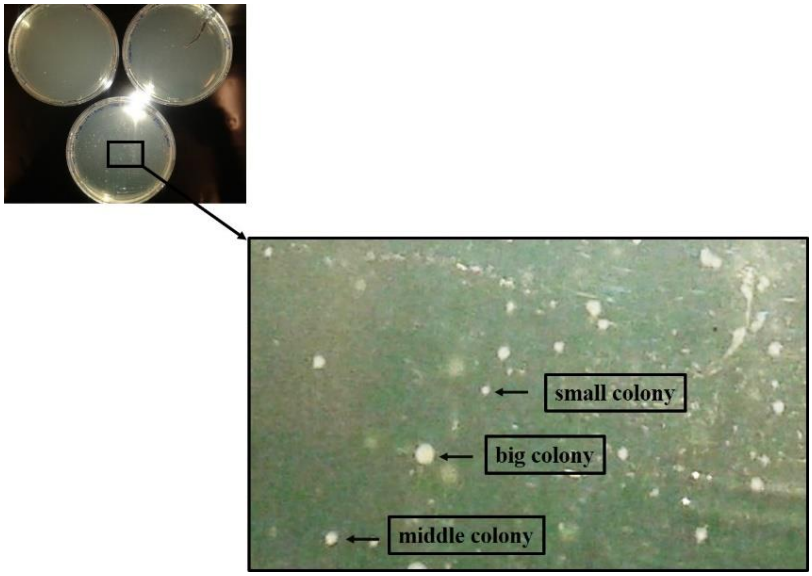

Figure 19: Transformation of FLAG-tagged Plin5-pShuttle construct into electro competent BJ5183-AD *E. coli* cells results in different colony sizes: FLAG-tagged Plin5-pShuttle construct was transformed into electro competent BJ5183-AD *E. coli* cells, which were plated on LB-agar plates containing kanamycin [100µg/mL] and incubated at 37°C. After a couple hours, colonies with different sizes were visible. The smallest colonies possess the recombinant adenoviral plasmid [Instruction AdEasy™ Adenoviral system Kit: http://www.chem.agilent.com/library/usermanuals/Public/240010.pdf].

To test successful insertion of FLAG-tagged Plin5 into the adenoviral genome, plasmid DNA of eight colonies were digested with *Pac*I restriction enzyme and agarose gel electrophoresis of digested products was performed (Figure 20). Except for sample 4, the agarose gel showed a distinct band at the size of approximately 10000bp in all analyzed samples which corresponds to the size of the recombinant adenoviral plasmid.

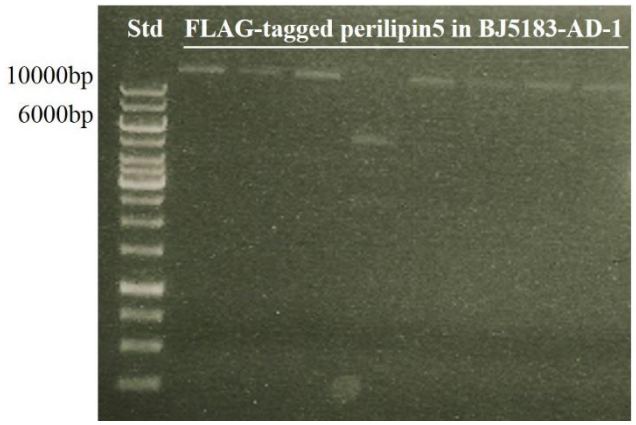

Figure 20: Agarose gel electrophoresis after restriction digest of recombinant adenoviral plasmid DNA: To test successful insertion of FLAG-tagged Plin5 into the adenoviral genome, DNA samples derived from eight clones were digested with *Pac*I restriction enzyme. The size of the DNA fragments were estimated by 0.8% agarose gel electrophoresis. Except lane 4, all lanes show a sharp band at more than 10000bp, consistent with the size of the adenoviral plasmid.

To amplify the recombinant DNA, adenoviral plasmid DNA derived from two clones was transformed into ultra-competent XL10-Gold *E. coli* cells. The recombinant adenoviral plasmid was isolated by MaxiPrep plasmid preparation. To test proper cloning, plasmid DNA was digested with *Pac*I restriction enzyme and agarose gel electrophoresis was performed (Figure 21).

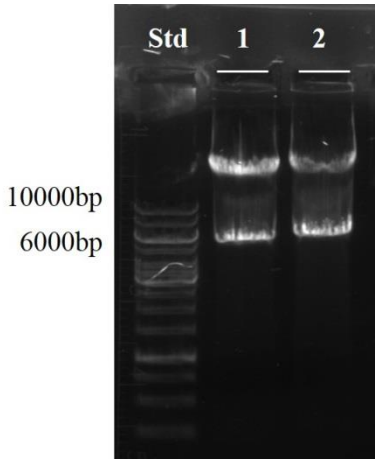

Figure 21: Agarose gel electrophoresis after restriction digest of adenoviral plasmid DNA after transformation into *E. coli* XL-Gold cells: The adenoviral plasmid DNA was transformed into XL-Gold *E. coli* cells and plasmids were isolated by MaxiPrep plasmid preparation. To test successful transformation, plasmid DNA of two clones were digested with *Pac*I restriction enzyme. The size of the DNA fragments was estimated by 0.8% agarose gel electrophoresis. All lanes show two sharp bands, at about 10000bp and about 6000bp, corresponding to the size of the adenoviral plasmid and the inserted Plin5 construct, respectively.

For preparing the adenoviral stock solution, the adenoviral plasmid was transfected into HEK AD293 cells. Therefore, the adenoviral plasmid DNA was linearized with *Pac*I restriction enzyme and transfected into HEK AD293 cells. After eight days, the cells were harvested, lysed and the primary viral stock was prepared.

The presence of the recombinant adenoviral plasmid was tested in the media and in the re-suspended cell pellet by PCR and the PCR product was analyzed by agarose gel electrophoresis (Figure 22). The PCR products derived from the medium samples exhibit a sharp band at 1400bp, which is consistent with the size of Plin5 CDS, indicating that the recombinant adenoviral plasmid was present in the media of the primary adenoviral stock.

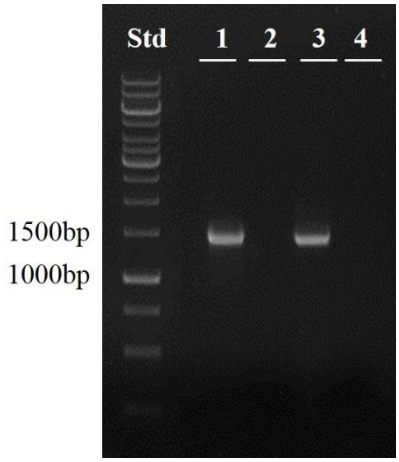

Figure 22: Agarose gel after PCR to test the presence of the recombinant adenoviral plasmid within the primary viral stock: The presence of the recombinant adenoviral plasmid was tested in the medium and the re-suspended cell pellet by PCR. The size of the PCR product was estimated by 1% agarose gel electrophoresis. Lane 1 and 3 are from the PCR products applying 2µL or 5µL medium as template, respectively. Lane 2 and 4 are from the PCR products applying 2µL or 5µL from the re-suspended cell pellet as template, respectively. The PCR products derived from the medium samples exhibit a sharp band at about 1400bp, indicating, that Plin5 was successfully inserted into the adenoviral genome.

For preparation and amplification of the secondary adenoviral stock, HEK AD293 cells were infected with primary viral stock and harvested after two days. The adenoviral stock solution was purified by CsCl density gradient centrifugation and dialysis.

5.1.3 Quantification of the adenoviral stock

The adenoviral stock was quantified by three different methods, optical measurement, testing of applicable MOIs and plaque assay.

5.1.3.1 Optical measurement

The concentration of the adenoviral stock was determined by the quotient of optical density measured at 260nm and 280nm by Nanodrop spectrophotometer. The results of the optical measurements of the respective recombinant adenoviral stocks are summarized in table 9. The formula to calculate pfu/mL is described in the experimental methods.

Table 9: Concentrations of recombinant adenoviral stocks indicated as pfu/mL

Recombinant adenoviral stock	pfu/mL
AdATGL	$1{,}8x10^{12}$
AdLacZ	$1x10^{12}$
AdPlin5	$1{,}79x10^{11}$

AdATGL and AdLacZ were generated similarly to AdPlin5, except that HIS-tagged ATGL DNA and lacZ CDS were inserted into the adenoviral genome, respectively.

5.1.3.2 Testing applicable multiplicities of infections

Appropriate MOIs for AdPlin5 and AdATGL were tested by infecting differentiated H9C2 cardiomyocytes. The infected cells were harvested after 24 hours or 48 hours, respectively and the protein expression was determined by Western blot analysis.

H9C2 cardiomyocytes infected with 500 and 800 MOI, respectively, exhibit low Plin5 protein expression (Figure 23 A). In contrast, cells infected with 1000 MOI for 48 hours showed a strong signal corresponding to high Plin5 protein expression. Furthermore, Plin5 protein

expression was increased in H9C2 cells infected with 2000 and 5000 MOI for 24 hours compared to cells infected for 48 hours. After Western Blot detection, the membrane was stained with Coomassie Brilliant blue to confirm proper loading of protein samples (Figure 23 B). This result indicates that at least 1000 MOI of AdPlin5 is required to achieve a high Plin5 expression level in H9C2 cardiomyocytes.

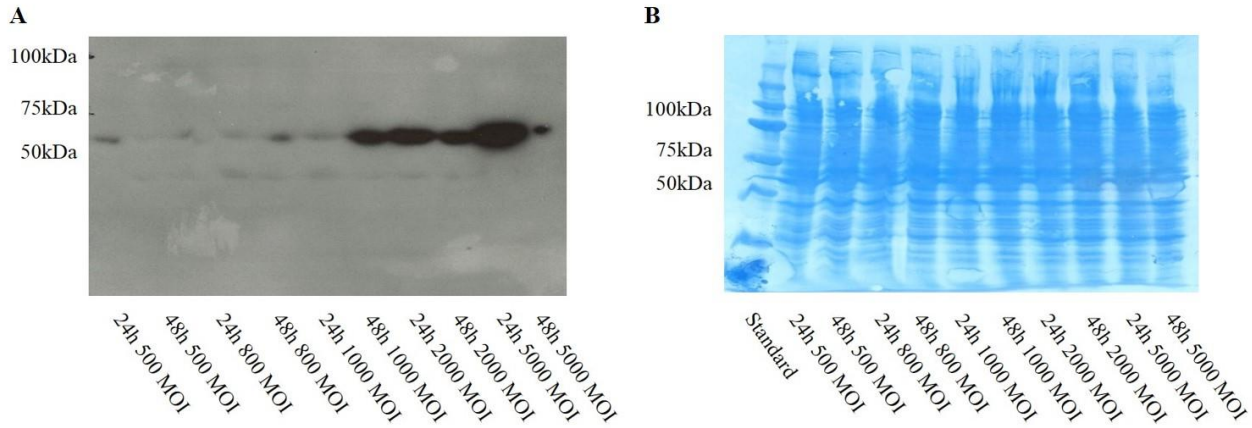

Figure 23: Western Blot analysis of cell lysates derived from differentiated H9C2 cardiomyocytes after infection with AdPlin5: Differentiated H9C2 cardiomyocytes were infected with respective MOIs and harvested after 24 hours and 48 hours, respectively. The protein expression was determined by Western blot analysis using 20µL cell lysate and 10% SDS-gel. Plin5 was detected with anti-FLAG antibody. **A**) Cells infected with 500, 800 and 1000 MOI show a modest expression of FLAG-tagged Plin5 with a size of 50kDa, respectively. In contrast, cells infected with 1000 MOI for 48 hours, 2000 and 5000 MOI show a high Plin5 expression level compared to cells infected with less MOIs. **B**) After detection, the membrane was stained with Coomassie Brilliant blue to confirm proper loading of protein samples.

H9C2 cells infected with AdATGL exhibit modest ATGL expression when infected with 200 MOI (Figure 24). In contrast, cells infected with 500 MOI for 48 hours showed high ATGL expression. The ATGL expression level of cells infected with 800 MOI for 24 hours was equal to cells infected for 48 hours. Cells infected with 1000 MOI exhibit increased ATGL expression after 24 hours compared to cells infected for 48 hours. After detection, the membrane was stained with Coomassie Brilliant blue to confirm proper protein loading (Figure 24 B). Western blot analysis indicates that at least 500 MOI of AdATGL are required to achieve high ATGL expression levels in differentiated H9C2 cardiomyocytes (Figure 24 B).

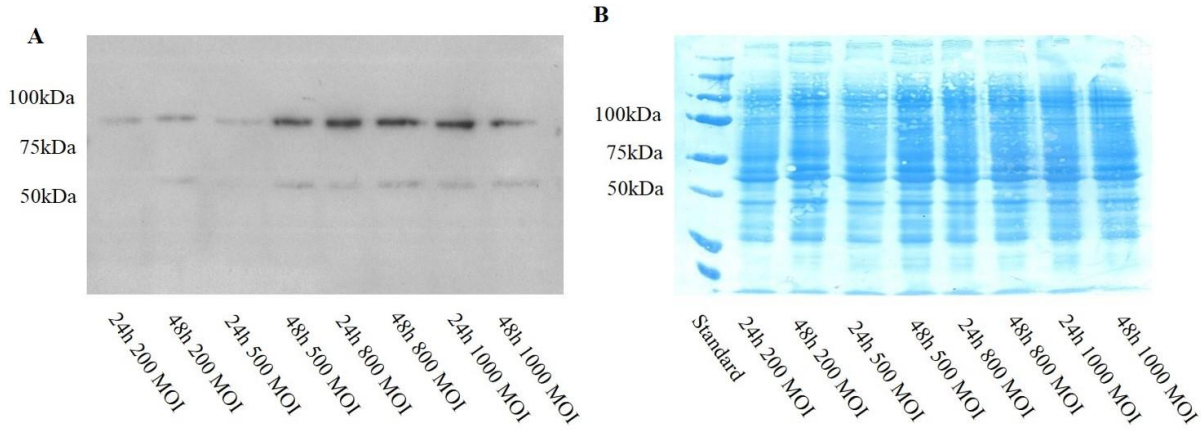

Figure 24: Western Blot analysis of cell lysates derived from differentiated H9C2 cardiomyocytes after infection with AdATGL: Differentiated H9C2 cardiomyocytes were infected with different MOIs and harvested after 24 hours and 48 hours, respectively. Protein expression was determined by Western blot analysis using 20µL cell lysate and 10% SDS-gel. ATGL was detected with anti-HIS antibody as primary antibody and anti-mouse HRP conjugated antibody as secondary antibody. **A**) Cells infected with 200 MOI showed modest ATGL expression compared to the cells infected with higher MOIs. **B**) After detection, the membrane was stained with Coomassie Brilliant Blue to confirm proper protein loading.

5.1.3.3 Plaque assay

Plaque assay is a widely used approach for determining the quantity of infectious virus. Equal to the optical measurement, the viral plaque assay determines the number of plaque forming units (pfu) per milliliter. However, the plaque assay is more sensitive and precise compared to the optical measurement.

Three whitish spots were visible in the HEK293 cell layer infected with the 10^{-10} viral stock dilution, within 14 days. This result indicates that the concentration of AdPlin5 stock is approximately $3x10^{10}$ pfu/mL. The concentration of AdPlin5 determined by plaque assay is less than the concentration measured by optical measurement. The optical measurement determines the amount of total cells within the sample, including viably and death cells, whereas the plaque assay determines the pfu by staining solely viably cells.

5.2 Investigating the impact of Plin5-overexpression on TG homeostasis of infected H9C2 cardiomyocytes

5.2.1 Examination of proper protein expression

To initially test proper protein expression, FLAG-tagged Plin5, HIS-tagged lacZ and HIS-tagged ATGL plasmid DNA were transfected into COS-7 cells, with different combinations. Successful protein expression was determined by Western Blot analysis (Figure 25). The Western Blot showed a sharp band at 120kDa and 55kDa, indicating overexpression of lacZ and ATGL, respectively (Figure 25 A). Furthermore, Plin5 overexpression was indicated by a distinct signal at 55kDa (Figure 25 B). After detection, the membrane was stained with Coomassie Brilliant blue to confirm equal protein loading. Results indicate, that the plasmid DNA of Plin5, lacZ and ATGL were successfully transfected and expressed in COS-7 cells.

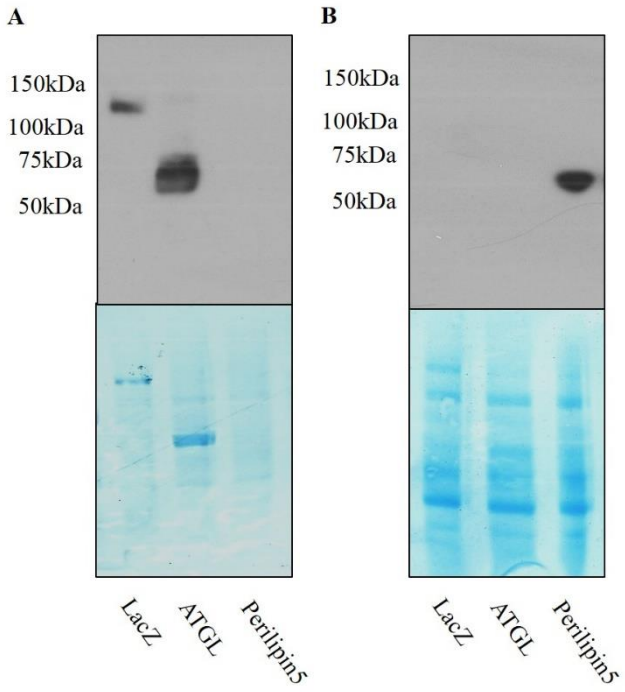

Figure 25: Western blot analysis after plasmid transfection into COS-7 cells: Cells were transfected with lacZ, Plin5 and ATGL, with different combinations. Western Blot analysis was performed to quantify lacZ, ATGL and Plin5 in cell lysates of transfected COS-7 cells. The cells were harvested using 200µL 1xSDS. Analysis was performed using 20µL of each cell lysate and 10% SDS-gel. After detection, the membranes were stained with Coomassie Brilliant Blue to confirm equal protein loading. **A)** Western Blot of membrane incubated with anti-HIS primary antibody and anti-mouse HRP conjugated secondary antibody to detect HIS-tagged lacZ and HIS-tagged ATGL. The blot shows a band at 120kDa in the first lane and a band at 55kDa in the second lane indicating overexpression of lacZ and ATGL, respectively. **B)** Western Blot of the membrane incubated with anti-FLAG antibody to detect FLAG-tagged Plin5. The blot exhibits a band at 55kDa in the third lane corresponding to Plin5.

5.2.2 Determination of the impact of Plin5 and ATGL overexpression on in vivo TG – homeostasis of transfected COS-7 cells

To verify the experimental strategy with respect to determine the impact of Plin5 and ATGL overexpression on cellular TG homeostasis, FLAG-tagged Plin5, HIS-tagged lacZ, HIS-tagged ATGL plasmid DNA were transfected into COS-7 cells with varying combinations. The cells were loaded with non-radioactive oleic acid [0.4mM] for 18 hours and *in vivo* TG levels were determined by pulse-chase experiments. To test successful transfection, expression of the respective recombinant protein was determined by Western Blot analysis (Figure 26).

The pulse-chase experiment was performed in triplicates and lacZ overexpressing cells were used as control (Figure 26 A). The TG content was significantly increased in cells overexpressing ATGL (+20%) and Plin5 (+40%) compared to control cells. Interestingly, cells co-expressing ATGL and Plin5 showed a modest decrease in TG accumulation compared to control cells (Figure 26 A). In control cells and cells co-expressing ATGL and Plin5, TG levels after oleic acid loading and serum starvation were equal, indicating, that TG mobilization was inhibited. In contrast, cells overexpressing ATGL exhibit a significant decrease in the TG level (-40%) after serum starvation compared to the TG level after oleic acid loading. Plin5 overexpression leads to a decrease in the TG level (-23%) after serum starvation, compared to the TG level after oleic acid loading. Comparing TG levels of cells overexpression Plin5 or ATGL and cells co-expressing these plasmids may lead to the assumption that Plin5 overexpression counteracts ATGL-mediated TG breakdown (Figure 26 A).

To test proper protein expression, Western Blot analysis was performed (Figure 26 B and C). The Western Blot showed a distinct band at 55kDa and 120kDa, indicating overexpression of ATGL and lacZ, respectively (Figure 26 B). Furthermore, Plin5 overexpression was indicated by a distinct band at 55kDa (Figure 26 C). After detection, the membrane was stained with Coomassie Brilliant blue to confirm equal protein loading. Taken together, Plin5 overexpression counteracts ATGL-mediated TG breakdown in COS-7 cells.

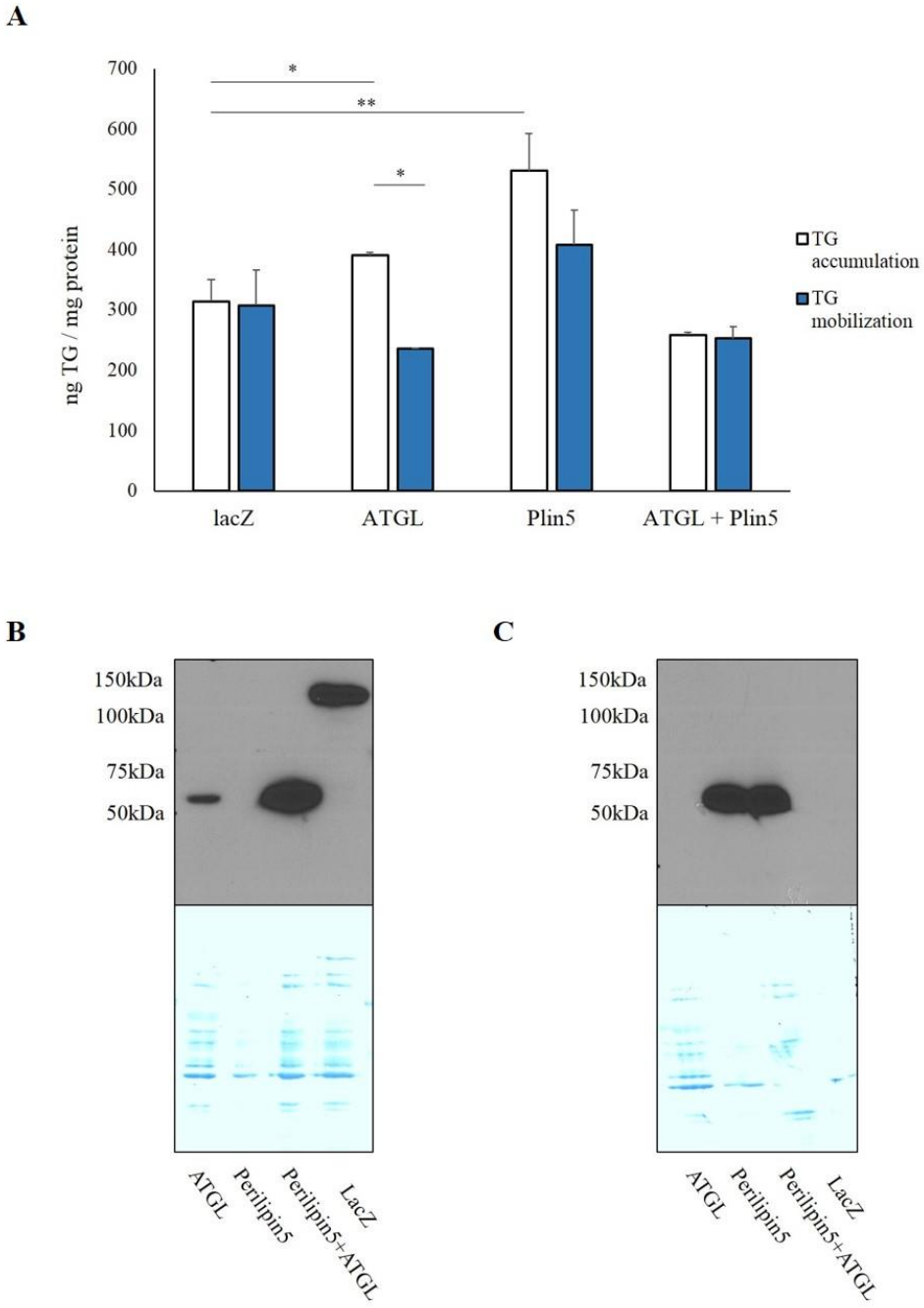

Figure 26: TG homeostasis in transfected COS-7 cells expressing recombinant Plin5 and ATGL: A) COS-7 cells were transfected with ATGL, Plin5 or lacZ expression plasmids and loaded with oleic acid. Lipids were extracted after 18 hours oleic acid loading or after serum starvation for 6 hours. **B)** Protein expression was determined by Western Blot analysis. The cells were harvested using 200µL 1xSDS. Analysis was performed using 20µL of each cell lysate and 10% SDS-gel. After detection, the membranes were stained with Coomassie Brilliant Blue. Western Blot of the membrane incubated with anti-HIS primary antibody and anti-mouse HRP conjugated secondary antibody to detect HIS-tagged lacZ and HIS-tagged ATGL. Lane 1 and 3 show a distinct band at 55kDa, indicating overexpression of ATGL. Lane 4 shows a band at 120kDa, which corresponds to the size of lacZ. **C)** Western Blot of the membrane incubated with anti-FLAG antibody to detect FLAG-tagged Plin5. Lane 2 and 3 show a band at 55kDa, indicating overexpression of Plin5. Data are shown as means ± standard deviation of n = 3. Statistical significance was determined by unpaired Student`s t-test (*** $p < 0.001$, ** $p < 0.01$, * $p < 0.05$).

5.2.3 Plin5 overexpression counteracts ATGL-mediated TG breakdown in cardiomyocytes

Differentiated H9C2 cardiomyocytes were infected either with AdPlin5, AdATGL, AdLacZ, or with different combinations. The infected cells were loaded with radioactively labeled oleic acid for 18 hours and the impact on *in vivo* TG homeostasis was determined after serum starvation. To test proper protein expression, Western Blot analysis was performed (Figure 27).

The pulse-chase experiment was performed in triplicates and AdLacZ infected cells were used as control (Figure 27 A). Overexpression of Plin5 showed increased TG accumulation compared to cells overexpressing recombinant ATGL (+66.4%) and control cells (+57.9%). Furthermore, TG mobilization was inhibited in cells overexpressing Plin5 upon serum starvation. Similarly, TG levels were unchanged in AdATGL and AdPlin5 co-transduced cells after serum starvation indicating that Plin5 inhibits ATGL-mediated TG catabolism. In contrast, cells exclusively overexpressing ATGL exhibit a significant decrease in the TG level (-28.5%) after serum starvation. Taken together, results suggest that Plin5 inhibits ATGL-mediated TG breakdown in differentiated H9C2 cardiomyocytes (Figure 27 A).

Proper expression of recombinant proteins was determined by Western Blot analysis (Figure 27 B and C). The Western Blot showed a distinct band at 55kDa, indicating overexpression of Plin5 (Figure 27 B). Furthermore, ATGL overexpression was indicated by a distinct band at 55kDa (Figure 27 C). After detection, the membrane was stained with Coomassie Brilliant blue to confirm equal protein loading.

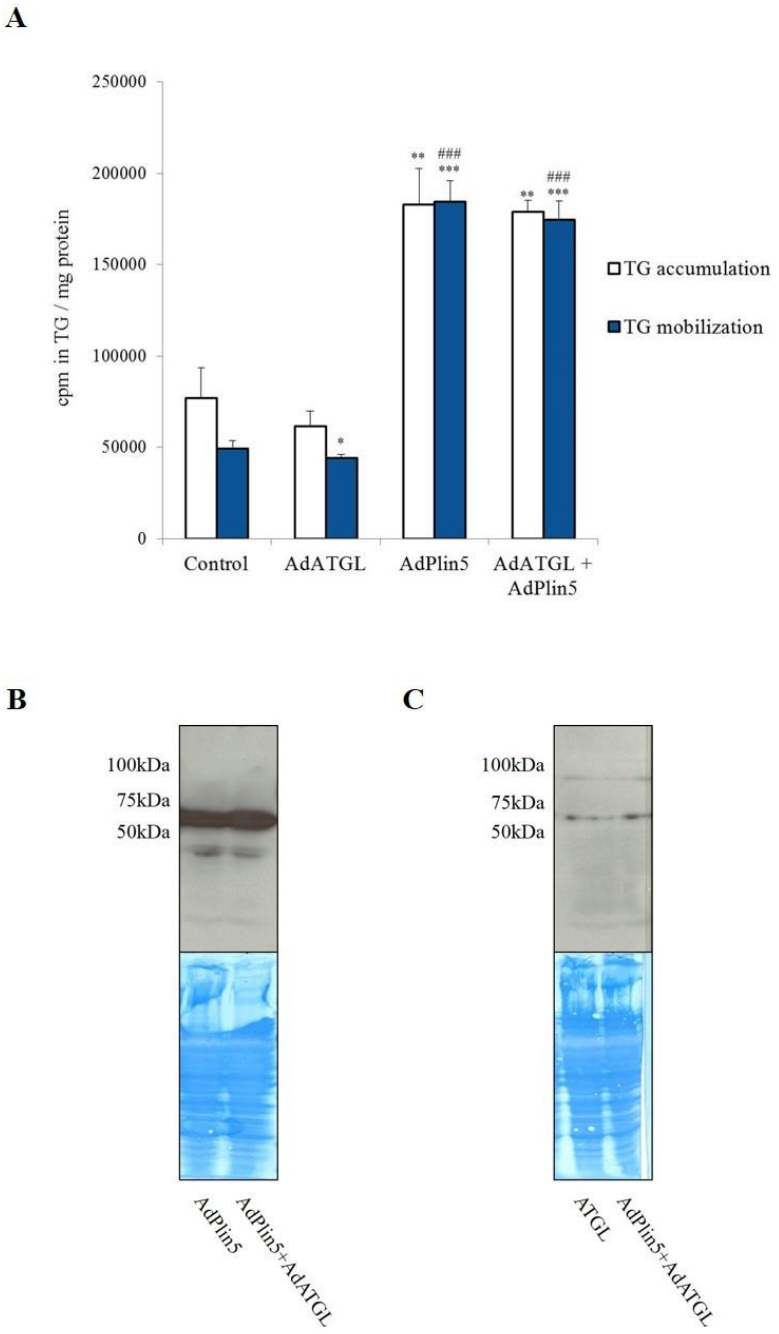

Figure 27: Impact of Plin5 and ATGL overexpression on TG homeostasis of infected H9C2 cardiomyocytes: A) Differentiated H9C2 cardiomyocytes were infected with AdLacZ as control, AdATGL, and AdPlin5, and with different combinations and loaded with oleic acid. Lipids were extracted after 18 hours oleic acid loading or after serum starvation for 6 hours. Incorporation of radioactivity into TG was determined by lipid extraction and separation of lipids by TLC. TG corresponding bands were excised and radioactivity was determined by scintillation counting. **B)** Protein expression was analyzed by Western Blot analysis. The cells were harvested using 100µL 1x SDS. Analysis was performed using 20µL of each cell lysate and 10% SDS-gel. After detection, the membranes were stained with Coomassie Brilliant Blue. Western Blot of membrane incubated with anti-FLAG antibody to detect FLAG-tagged Plin5. Both lanes show a band at 55kDa, indicating Plin5 overexpression. **C)** Western Blot analysis of the membrane incubated with anti-HIS primary antibody and anti-mouse HRP conjugated secondary antibody to detect HIS-tagged ATGL. Both lanes show a distinct band at 55kDa, indicating overexpression of ATGL. Data are shown as means ± standard deviation of n = 3. Statistical significance was determined by unpaired Student`s t-test (*** $p < 0.001$, ** $p < 0.01$, * $p < 0.05$).

5.2.4 Investigating the impact of Plin5 overexpression on TG homeostasis in the presence of a synthetic ATGL inhibitor

Cells overexpressing lacZ showed a modest decrease in the TG level after serum starvation (-36.1%) (Figure 27 A). Cardiomyocytes overexpressing lacZ are expected to moderately increase TG mobilization upon serum starvation. The marked increase in TG mobilization of lacZ-expressing H9C2 cardiomyocytes implicates that this cell line may exhibit intrinsic basal ATGL expression leading to increased TG catabolism upon serum starvation. To further study the impact of Plin5 overexpression on TG homeostasis a pulse-chase experiment was performed in cells incubated with a potent specific ATGL inhibitor designated as Atglistatin [79]. Differentiated H9C2 cardiomyocytes were infected with AdLacZ and AdPlin5 and incubated in the presence or absence of Atglistatin during oleic acid loading and/or serum starvation. Proper expression of recombinant proteins was determined by Western Blot analysis (Figure 28).

The pulse-chase experiment was performed in triplicates and lacZ infected cells were used as control (Figure 28 A). Control cells treated with Atglistatin exhibit significantly increased incorporation of radioactively labeled oleic acid into cellular TG (+52.7%) after oleic acid incubation for 18 hours compared to non-treated cells. Furthermore, TG levels were unchanged in control cells treated with Atglistatin after serum starvation most likely via inhibition of ATGL-mediated TG-breakdown. Contrary, non-treated control cells exhibit a significant decrease in TG level after serum starvation (-58.6%), compared to the TG level after oleic acid loading (Figure 28 A). In contrast, Plin5 overexpression did not significantly increase cellular TG levels after loading with oleic acid but levels stayed constant after serum starvation. Notably, the presence of Atglistatin during serum starvation did not further increase cellular TG levels in Plin5 overexpressing cells strongly implicating the Plin5 overexpression impairs ATGL-mediated TG catabolism during serum starvation (Figure 28 A). Western blot analysis confirmed Plin5 overexpression in H9C2 cardiomyocytes (Figure 28 B).

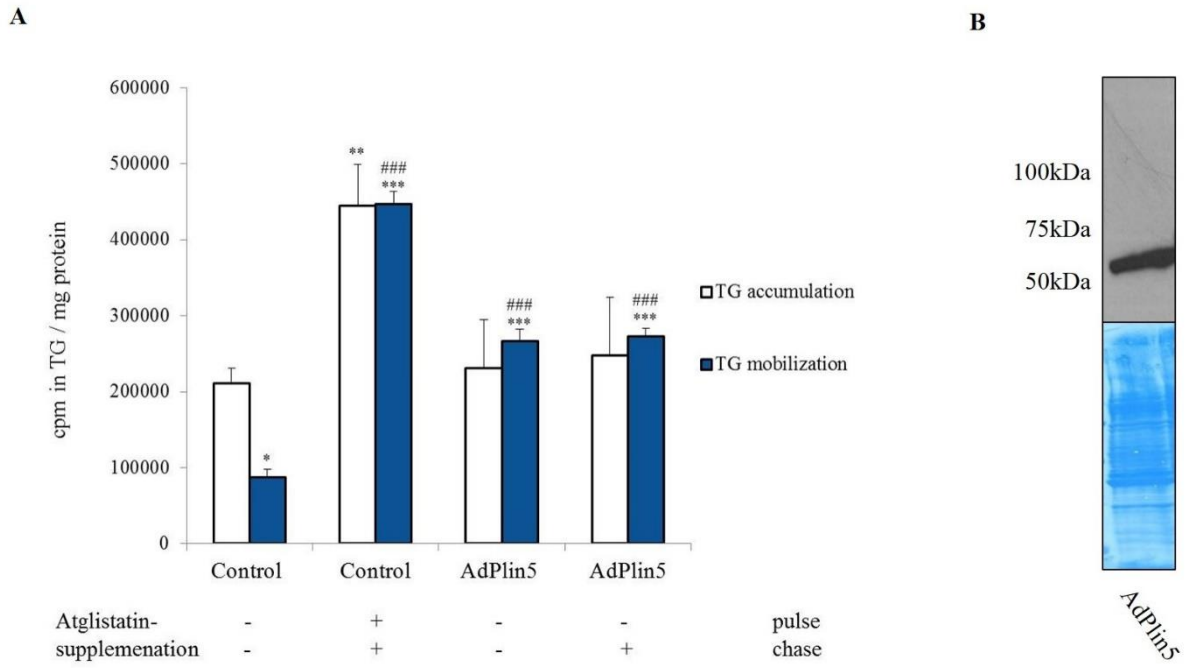

Figure 28: Inhibition of ATGL-mediated TG catabolism via Atglistatin interferes with TG homeostasis in differentiated H9C2 cardiomyocytes after oleic acid loading and serum starvation: A) Differentiated H9C2 cardiomyocytes were infected with AdLacZ or AdPlin5 and loaded with oleic acid. Lipids were extracted after 18 hours oleic acid loading or after an additional serum starvation for 6 hours. **B)** Protein expression in transfected cells was determined by Western Blot analysis. The cells were harvested using 100µL 1x SDS. Analysis was performed using 20µL of each cell lysate and 10% SDS-gel. After detection, the membranes were stained with Coomassie Brilliant Blue to confirm equal protein loading. Data are shown as means ± standard deviation of n = 3. Statistical significance was determined by unpaired Student`s t-test (*** $p < 0.001$, ** $p < 0.01$, * $p < 0.05$).

5.3 Impact of exogenous and endogenous FA supply on PPARα target gene expression in cardiac muscle

The role of adipose tissue derived FA in cardiac energy metabolism was determined by quantitation of mRNA expression levels of selected PPARα target genes in cardiac muscle of mice globally lacking ATGL (exogenous and endogenous defect in FA generation and supply), mice lacking ATGL solely in adipose tissue (impaired delivery of FA from adipose tissue to the periphery including the heart) and in mice overexpressing Plin5 selectively in cardiac muscle (impaired endogenous TG catabolism and FA generation in cardiomyocytes). Mouse genotypes and their corresponding control mice are listed in table 10.

Table 10: Mouse models and their corresponding wild types

Mouse model	Control
Global ATGL knock out (ATGL-/-)	A2 wild type
Adipose tissue specific ATG knock out (ATGL-ATko)	Flox/flox wild type
Cardiac muscle specific Plin5 overexpressing mice (CM-Plin5)	A2 wild type

5.3.1 Confirmation of RNA quality

Prior to transcription of total RNA into cDNA, the quality of the RNA samples was examined by agarose gel electrophoresis. Each RNA sample showed three bands characteristic for 28S, 18S and 5S rRNA (Figure 29) which indicates the mRNA is not degraded by RNAses and can be applied for qRT-PCR analysis.

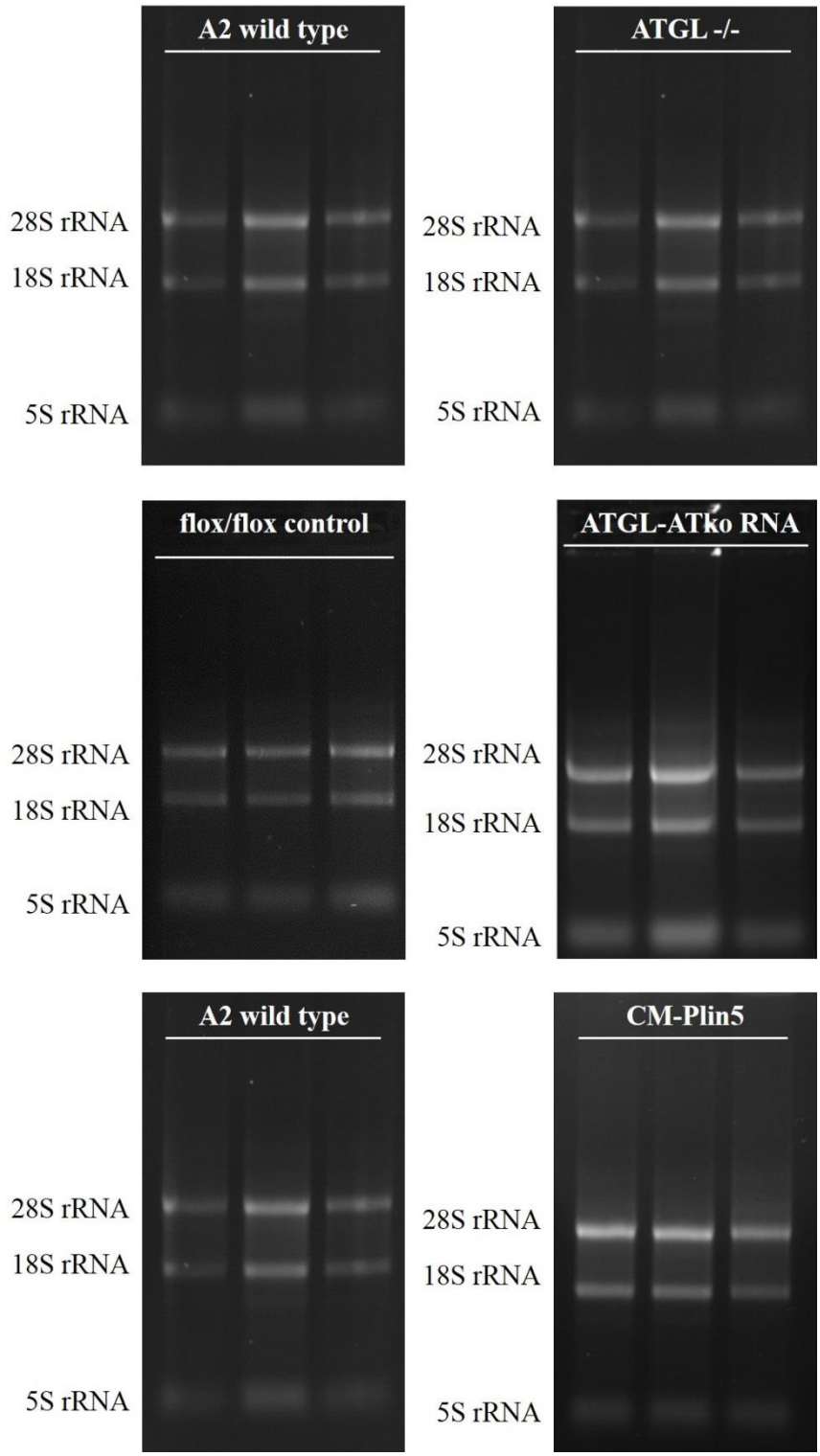

Figure 29: Agarose gel to examine RNA quality: Total RNA was isolated from cardiac muscle of A2 wild type mice, ATGL -/- mice, flox/flox control mice, ATGL-ATko mice and CM-Plin5 mice. The RNA quality was examined by 1% agarose gel electrophoresis. In each samples of the respective genotype, three bands are visible, which are consistent to the 28S, 18S and the 5S rRNA, indicating that RNA samples are not degraded.

5.3.2 The global or adipose tissue-specific lack of ATGL divergently interferes with PPARα target gene expression

The mRNA expression level of selected PPARα target genes, including *Nrf*-1, *Nrf*-2, *Hif*-1α, *Pdk*-4, *Oxct*-1 and *Osgin*-1 were determined by qRT-PCR. Therefore, total RNA was isolated from the cardiac muscle of overnight-fasted (ON-fasted) ATGL-ATko and ON-fasted ATGL-/- mice and transcribed into cDNA by the action of Reverse Transcriptase. The mRNA expression levels of ATGL-/- and ATGL-ATko mice, respectively, were compared with the mRNA expression levels of the corresponding controls (Figure 30).

ATGL-/- mice showed decreased mRNA expression of examined PPARα target genes compared to the corresponding controls (Figure 30 A) encompassing decreased mRNA level of *Nrf*-1 (-42.9%) and *Nrf*-2 (-44.9%) compared to the mRNA expression levels of control mice. Furthermore, mRNA expression of *Hif*-1α (-31.3%), *Pdk*-4 (-56.7%) and *Oxct*-1 (52.8%) were significantly decreased in ATGL-/- mice compared to control mice whereas *Osgin*-1 mRNA expression level was unchanged (Figure 30 A).

Next we examined mRNA expression of selected PPARα-regulated genes in ATGL-ATko mice (Figure 30 B) where exogenous FA supply to the heart is markedly reduced. The mRNA expression of *Nrf*-1, *Nrf*-2 and *Hif*-1α was similar in ATGL-ATko mice compared to controls. In contrast, *Pdk*-4 mRNA expression was significantly decreased (-72.9%) in ATGL-ATko mice compared to controls. Interestingly, *Osgin*-1 mRNA expression was increased (+51.9%) in ATGL-ATko mice compared to control mice (Figure 30 B).

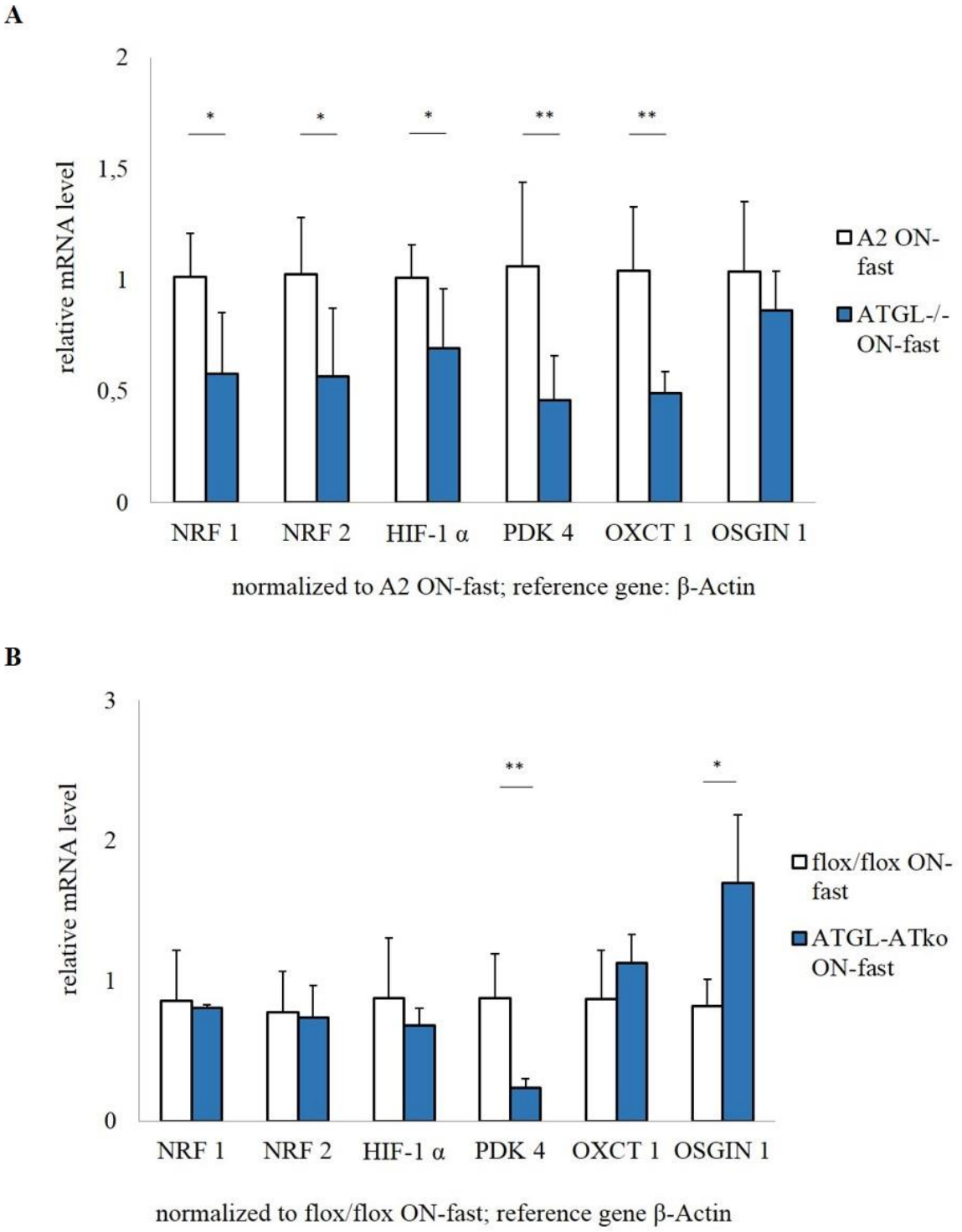

Figure 30: mRNA expression levels of selected PPARα target genes differ between ATGL-/- and ATGL-ATko mice: The mRNA expression level was determined by qRT-PCR. The values were normalized to the corresponding wild type and flox/flox control and β-Actin was used as housekeeping gene. **A)** Relative mRNA expression levels of PPARα target genes in cardiac muscle of ATGL-/- mice. **B)** Relative mRNA expression levels of PPARα target genes in cardiac muscle of ATGL-ATko mice. Data are shown as means ± standard deviation of $n \geq 3$. Statistical significance was determined by unpaired Student`s t-test (*** $p < 0.001$, ** $p < 0.01$, * $p < 0.05$).

5.3.3 Nrf-2 protein expression is increased in cardiac muscle of fasted ATGL knock out mice

The protein expression level of Nrf-2 and ATGL was determined by Western Blot analysis. For the Western Blot tissue lysates from cardiac muscle of ON-fasted ATGL-/- mice, ATGL-ATko mice and their corresponding controls were used (Figure 31).The Western Blot of cardiac muscle lysates of ATGL-ATko mice and flox/flox wild type mice exhibits distinct bands at 50kDa and a faint band at 100kDa corresponding to the size of Nrf-2 (Figure 31 A). The quantitation by ImageJ software showed a significant increase in Nrf-2 (+76.9%) protein expression in ATGL-/- mice compared to controls (Figure 31 B). In contrast, ATGL-ATko mice exhibit a modest decrease in Nrf-2 (-5%) protein expression level compared to flox/flox control mice. The Nrf-2 protein expression level in ATGL-/- mice was significantly increased in ATGL-ATko mice (+77.6%).

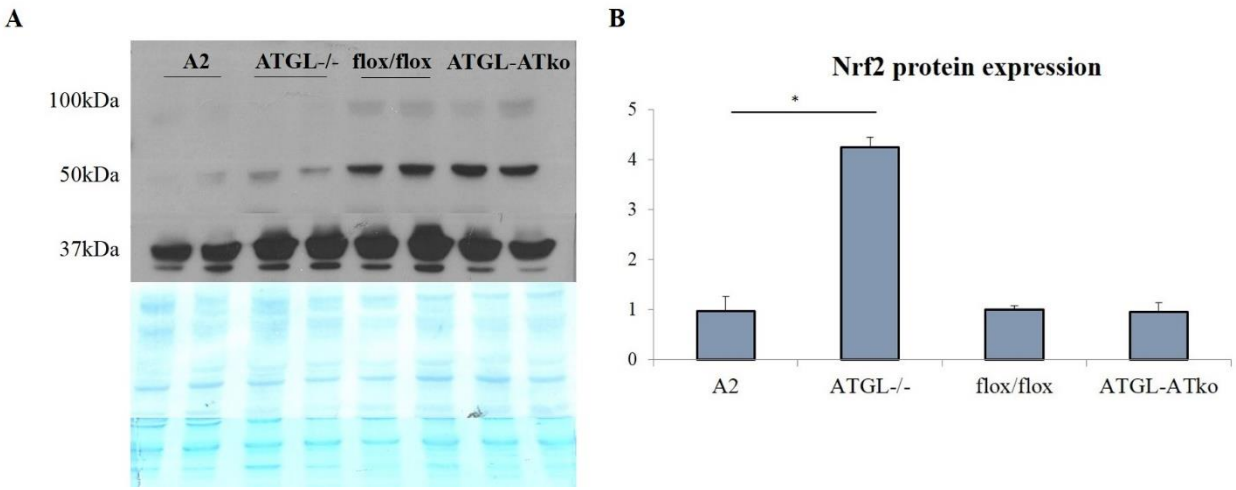

Figure 31: Nrf-2 protein expression differs between ATGL-/- and ATGL-ATko mice: A) Western Blot analysis was performed using 20µg protein of each cardiac muscle lysate and 10% SDS-gel. GAPDH was used as loading control. The blot shows a distinct band at 50kDa and a weak band at 100kDa in the lanes containing flox/flox and ATGL-ATko cardiac lysates, indicating high Nrf-2 expression. Lane containing cardiac lysates of A2 wild type and ATGL-/- mice exhibits merely a faint band at 50kDa and 100kDa. After detection, the membrane was stained with Coomassie Brilliant Blue to confirm equal protein loading. **B)** The Western Blot was quantified by ImageJ software. The Nrf-2 protein expression is significantly increased in ATGL-/- mice compared to wild type mice. Data are shown as means ± standard deviation of n =2. Statistical significance was determined by unpaired Student`s t-test (*** $p < 0.001$, ** $p < 0.01$, * $p < 0.05$).

Next we measured ATGL protein (55kDa) expression levels in ATGL-mutant mice compared to controls (Figure 32 A). As expected, ATGL protein was not detected in global ATGL

knock out mice whereas protein levels were unchanged in ATGL-ATko mice compared to controls.

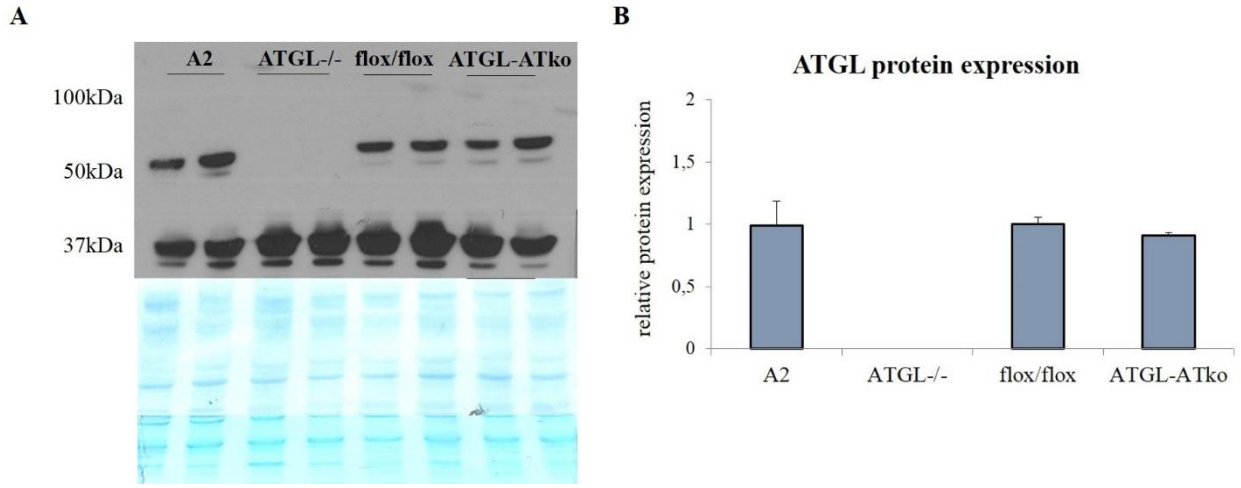

Figure 32: ATGL protein expression differs between ATGL-/- and ATGL-ATko mice: A) Western Blot analysis was performed using 20µg protein of each cardiac muscle lysate and 10% SDS-gel. GAPDH was used as loading control. The blot shows a sharp band at 55kDa which can be assigned to ATGL. After detection, the membrane was stained with Coomassie Brilliant Blue to confirm equal protein loading. **B)** The Western Blot was quantified by ImageJ software. Data are shown as means ± standard deviation of n =2. Statistical significance was determined by unpaired Student`s t-test (*** $p < 0.001$, ** $p < 0.01$, * $p < 0.05$).

5.3.4 Divergent mRNA expression of PPARα target genes in cardiac muscle of mice with impaired adipose lipolysis compared to mice with impaired cardiac lipolysis

Cardiac muscle-specific overexpression of Plin5 provokes severe cardiac steatosis similar to mice globally lacking ATGL. Interestingly, ATGL-/- mice develop lethal cardiac dysfunction within 12 to 16 weeks whereas cardiac steatosis of CM-Plin5 is compatible with normal heart function and life span suggesting metabolic divergences in both mutant mouse models. This phenomenom prompted us to measure mRNA expression levels of PPARα target genes an genes implicated in elimination of reactive oxygen species (Figure 33).

CM-Plin5 mice showed significantly increased mRNA expression levels of *Nrf*-1 (+33.6%), *Nrf*-2 (+19.8%) and *Mcad* (+39.4%) compared to wild type (Figure 33 A) whereas *Aox*-1 mRNA levels were also markedly increased (+50.7%) albeit level did not reach statistical significance. The mRNA expression levels of *Pdk*-4, *Lcad* and *Cpt*-1β were similar in CM-

Plin5 compared to wild type mice. *Pgc*-1α mRNA expression was non-significantly reduced (-31.6%) in CM-Plin5 mice compared to wild type (Figure 33 A).

Unlike CM-Plin5 mice, ATGL-ATko mice showed a significant decrease in the *Pdk*-4 (-57.3%) mRNA expression level compared to flox/flox controls (Figure 33 B). In contrast, mRNA expression level of *Pgc*-1α was markedly increased (+68.2%) in ATGL-ATko compared to controls whereas mRNA expression of *Nrf*-1, *Nrf*-2, *Aox*-1, *Mcad* and *Lcad* was unchanged (Figure 33 B).

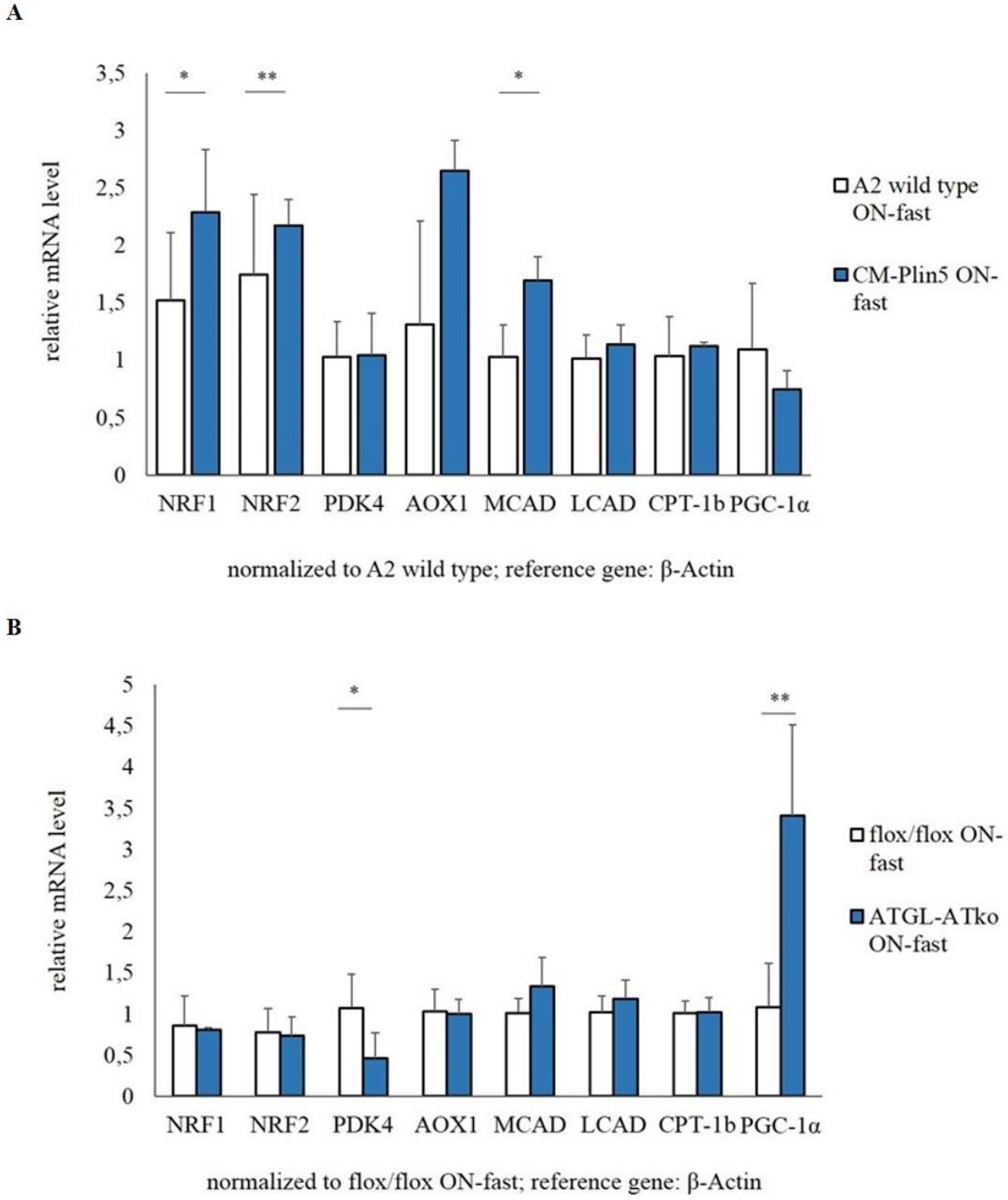

Figure 33: mRNA expression levels of selected PPARα target genes in CM-Plin5 and ATGL-ATko mice: The mRNA expression level was determined by qRT-PCR. The values were normalized to the corresponding wild type or flox/flox control and β-Actin was used as housekeeping gene. **A)** Relative mRNA expression levels of PPARα target genes in cardiac muscle of CM-Plin5 mice. **B)** Relative mRNA expression levels of PPARα target genes in cardiac muscle of ATGL-ATko mice. Data are shown as means ± standard deviation of $n \geq 3$. Statistical significance was determined by unpaired Student`s t-test (*** $p < 0.001$, ** $p < 0.01$, * $p < 0.05$).

6 DISCUSSION

The regulation of TG storage and mobilization determines cellular TG homeostasis and is critical to avoid increased accumulation of lipids which may lead to lipotoxicity. Intracellular lipolysis is regulated by lipases and cofactors including ATGL, CGI-58, HSL and the members of the PAT family which are located on LDs [50]. Plin5, a member of the PAT family, is highly expressed in oxidative tissues, such as the heart, and plays an important role in the regulation of FFA uptake and mobilization [47]–[49]. Recent studies demonstrated that Plin5 plays an important role in the regulation of TG homeostasis *in vivo* as demonstrated in Plin5 deficient mice and in mice with cardiac muscle-specific Plin5 overexpression. Plin5-deficient mice are almost devoid of cardiac LD, whereas cardiac muscle-specific overexpression of Plin5 provokes massive TG accumulation [53], [62], [80]. These results suggest, that Plin5 functions as a lipolytic barrier to protect the cardiac TG pool from uncontrolled TG mobilization and the excessive release of FFA [62], [80] which can damage the cell. ATGL-mediated FA-release is significantly impaired from Plin5-enriched coated LD Plin5 suggesting that Plin5 acts as a lipolytic barrier may counteracting uncontrolled FA release and cell damage [62], [80].

This study aims to elucidate the impact of Plin5 overexpression on TG homeostasis in H9C2 cardiomyocytes which then can be used as a cell culture model to study the functional role of Plin5 in lipid and energy metabolism. For that purpose, a recombinant Plin5 overexpressing adenovirus was generated and *in vivo* TG levels of differentiated H9C2 cardiomyocytes infected with AdPlin5 were measured. Plin5 overexpression promotes TG accumulation up to 66% in cardiomyocytes compared to cardiomyocytes overexpressing ATGL. During serum starvation, Plin5 overexpressing cells show impaired TG mobilization in contrast to cardiomyocytes overexpressing ATGL which leads to increased TG mobilization. Furthermore, Plin5 overexpression impairs ATGL-mediated TG mobilization in cardiomyocytes expressing recombinant Plin5 and ATGL which is in accordance with the proposed role of Plin5 acting as a lipolytic barrier.

Increased adipose tissue TG mobilization and consequently FFA supply to the heart, liver and skeletal muscle stimulates the expression of PPARα-regulated genes of the FA oxidative

machinery to generate energy and to counteract the potentially harmful increase of FFA also known as lipotoxicity [54]. However, the role of exogenous adipose tissue-derived FA versus endogenously generated FA in PPARα-regulated gene expression in cardiac muscle is less established. Therefore, cardiac mRNA expression of PPARα-regulated genes and genes implicated in the detoxification of reactive oxygen species (ROS) was examined in fasted mice either harboring a defect in exogenous FA supply (ATGL-ATko mice) compared to mice with a systemic defect in TG catabolism (ATGL-/- mice) and mice exhibiting impaired endogenous TG catabolism in the heart (CM-Plin5 mice).

Expression of genes encoding antioxidant enzymes is regulated at the transcriptional level through cis-active sequence known as the antioxidant response element (ARE).

One of the selected PPARα target and ROS regulated genes includes the nuclear respiratory factors (Nrf), which regulate target gene expression at the transcriptional level through cis-active sequence known as the antioxidant response element (ARE). Nrf-1 [81] and Nrf-2 [82] target genes are involved in mitochondrial respiration and elimination of ROS [83], [84]. The mRNA expression levels of *Nrf*-1 and *Nrf*-2 are significantly decreased in ATGL-/- mice compared to wild type mice. Contrary to ATGL-/- mice, CM-Plin5 mice exhibit significantly increased mRNA expression levels of *Nrf*-1 and *Nrf*-2. In contrast, ATGL-ATko mice exhibit no difference in the mRNA expression level of *Nrf*-1 and *Nrf*-2 compared to wild type mice. Unlike the mRNA expression level of *Nrf*-2, the protein expression level is significantly increased in ATGL-/- mice, suggesting, that Nrf-2 is regulated post-transcriptionally. Taken together, results indicate that impaired mitochondrial respiration as present in cardiac muscle of ATGL-/- mice or CM-Plin5 mice leads to increased ROS which may induces *Nrf*-1 and *Nrf*-2 expression to protect cardiomyocytes from ROS-mediated protein oxidation and cellular damage.

Two further PPARα-regulated genes include the hypoxic inducible factor (Hif) 1α and succinyl-CoA:3-ketoacid-coenzyme A transferase (Oxct) 1. Hif-1α [85] has emerged as a key regulator of the molecular hypoxic response which influences pathways of metabolic adaption, erythropoiesis, angiogenesis and vascular tone, cell growth and differentiation, survival and apoptosis [86]. Oxct-1 is a mitochondrial matrix enzyme which plays a central

role in extra hepatic ketone body catabolism [87]. The mRNA experssion levels of *Hif*-1α and *Oxct*-1 are significantly decreased in ATGL-/- mice, whereas ATGL-ATko mice exhibit no difference in expression levels compared to control mice leading to the assumption that changes in *Hif-1α* and *Oxct-1* originate from cardiac dysfunction and not from impaired FA supply from adipose tissue. The heart has a marked metabolic flexibility and is capable of utilizing FA, glucose, ketone bodies, lactate and amino acids as energy fuel albeit the adult heart primarily relies on FA followed by glucose oxidation to generate ATP. Pyruvate generated by glycolysis enter the mitochondria via the decarboxylation of pyruvate to acetyl-CoA in a reaction catalyzed by pyruvate dehydrogenase (PDH) complex. In case of prolonged exercise and the utilization of FA as oxidative fuel, PDH complex is inactivated by pyruvate dehydrogenase kinase (PDK) phosphorylation [88]. PDK exists in four isoforms, whereas Pdk-4 is primarily expressed in the heart and skeletal muscle [89]. The mRNA expression level of *Pdk*-4 is significantly decreased in both, ATGL-/- mice and ATGL-ATko mice, whereas CM-Plin5 mice exhibit no difference in *Pdk*-4 expression level compared to control mice. These results suggest that the expression of *Pdk*-4 is regulated by exogenous FA which makes sense in a physiological context as fasting leads to an increased FA supply to the heart and consequently increased FA versus glucose oxidation.

The PPARγ coactivator 1α (PGC-1α) [90], plays a critical role in the dynamic regulation of cellular energy metabolism, including mitochondrial biogenesis and oxidation, hepatic gluconeogenesis, and skeletal muscle glucose uptake [91]–[93]. The mRNA expression level of *Pgc*-1α is significantly increased in ATGL-ATko mice, whereas CM-Plin5 mice exhibit no significant difference compared to control mice suggesting that PGC-1a expression is also under regulation of exogenous FA supply which awaits further clarification.

Taken together, the present master study establishes a cell culture model to investigate the functional role of Plin5 in cardiac lipid and energy metabolism. Furthermore, results extend our knowledge on the role of adipose tissue lipolysis and endogenous TG catabolism in the regulation of energy metabolism in the heart.

7 ABBREVIATION

ADRP	adipose differentiation-related protein	HSL	hormone sensitive lipase
AMPK	adenosine monophosphate activated kinase	kDa	kilodalton
APS	ammonium persulphate	ko	knock out
ARE	antioxidant respiratory element	LCFA	long-chain fatty acid
AT	adipose tissue	LB-Medium	lysogeny broth medium
ATGL	adipose triglyceride lipase	LD	lipid droplet
ATP	adenosine-5`-triphosphate	LSDP5	lipid storage droplet protein 5
BCA	bicinchoninic acid	MG	monoacylglycerol
bp	base pairs	MGL	monoglycerol lipase
BSA	bovine serum albumin	MLDP	myocardial lipid droplet protein
cAMP	cyclic adenosine monophosphate	mRNA	messenger RNA
CAPS	N-cyclohexyl-3-aminopropanesulfonic acid	NADH	nicotinamide adenine dinucleotide
CD36	cluster of differentiation 36	NEB	New England Biolabs
cDNA	complementary DNA	NRF	nuclear respiratory factor
CE	cholesterol ester	OXCT	Succinyl-CoA:3-ketoacid-coenzyme A transferase
CGI-58	comparative gene identification 58	OXPAT	Oxidative PAT
Ci	curie	OXPHOS	oxidative phosphorylation
CoA	coenzyme A	PAT	Perilipin adipophilin tail-interacting protein of 47kDa
CPT-1	carnitine palmitoyltransferase 1	PBS	phosphate buffered saline
ddH_2O	distilled, deionized water	PCR	polymerase chain reaction
DEPC	diethyldicarbonate	PDH	pyruvate dehydrogenase

DG	diacylglycerol	PDK	pyruvate dehydrogenase kinase
DMEM	dulbeccos modified Eagles medium	PDVF-membrane	polyvinylidenfluoride membrane
DMSO	dimethyl sulfoxide	PGC	Peroxisome proliferator-activated receptor γ coactivator
DTT	dithithreitol	PKA	protein kinase A
EDTA	ethylendiamine tetraacetic acid	Plin	perilipin
ER	endoplasmatic reticulum	PPAR	peroxisome proliferator-activated receptor
FA	fatty acid	PPRE	PPAR regulatory element
FACS	fatty acyl-CoA synthetase	P/S	penicillin / Streptomycin
$FADH_2$	flavin adenine dinucleotide	qRT-PCR	quantitative real time PCR
FAO	fatty acid oxidation	ROS	reactive oxygen species
FAT	fatty acid translocase	RXR	retinoid X receptor
FATP1	fatty acid transporter protein 1	SDS	sodium dodecyl sulfate
FCS	fetal calf serum	TAE	Tis-acetate-EDTA
FFA	free fatty acid	TCA	tricarboxylic acid cycle
GAPDH	glycerinealdehyde 3-phosphate dehydrogenase	TG	triacylglycerol
HDAC	histone deacetylates	TIP47	tail-interacting protein of 47kDa
HIF	hypoxic inducible factor	TLC	thin layer chromatography
HIS-tag	poly-histidine tag	TST	Tris-buffered saline supplemented with Tween 20

8 REFERENCES

[1] B. N. Finck, “The PPAR regulatory system in cardiac physiology and disease.,” *Cardiovasc. Res.*, vol. 73, no. 2, pp. 269–77, Jan. 2007.

[2] P. a Crawford and J. E. Schaffer, “Metabolic stress in the myocardium: adaptations of gene expression.,” *J. Mol. Cell. Cardiol.*, vol. 55, pp. 130–8, Feb. 2013.

[3] J. a Madrazo and D. P. Kelly, “The PPAR trio: regulators of myocardial energy metabolism in health and disease.,” *J. Mol. Cell. Cardiol.*, vol. 44, no. 6, pp. 968–75, Jun. 2008.

[4] J. M. Huss and D. P. Kelly, “Nuclear receptor signaling and cardiac energetics.,” *Circ. Res.*, vol. 95, no. 6, pp. 568–78, Sep. 2004.

[5] H. Cd, M. R. El-maghrabis, E. Amrill, E. Lopezs, P. A. Grimaldill, and P. Valrose, “Cloning of a Rat Adipocyte Membrane Protein Implicated in Binding or Transport of Long-chain Fatty Acids That Is Induced during Preadipocyte Differentiation,” vol. 268, no. 24, pp. 17665–17668, 1993.

[6] B. N. Finck and D. P. Kelly, “Peroxisome proliferator-activated receptor ?? coactivator-1 (PGC-1) regulatory cascade in cardiac physiology and disease,” *Circulation*, vol. 115, pp. 2540–2548, 2007.

[7] G. Lopaschuk and J. Ussher, “Myocardial fatty acid metabolism in health and disease,” *Physiol. …*, pp. 207–258, 2010.

[8] A. R. Wende and E. D. Abel, “NIH Public Access,” vol. 1801, no. 3, pp. 311–319, 2011.

[9] R. T. Brookheart, C. I. Michel, and J. E. Schaffer, “NIH Public Access,” vol. 10, no. 1, pp. 9–12, 2010.

[10] G. Concepts, “General Concepts,” *Diabetes*, pp. 1727–1733, 2002.

[11] R. Harmancey, C. R. Wilson, and H. Taegtmeyer, “Adaptation and maladaptation of the heart in obesity,” *Hypertension*, vol. 52, pp. 181–187, 2008.

[12] G. P. Aurigemma, G. De Simone, and T. P. Fitzgibbons, “Cardiac remodeling in obesity,” *Circ. Cardiovasc. Imaging*, vol. 6, pp. 142–152, 2013.

[13] P. K. Mazumder, B. T. O. Neill, M. W. Roberts, J. Buchanan, U. J. Yun, R. C. Cooksey, S. Boudina, and E. D. Abel, “Oxidation in Insulin-Resistant ob / ob Mouse Hearts,” vol. 53, no. September, 2004.

[14] J. Buchanan, P. K. Mazumder, P. Hu, G. Chakrabarti, M. W. Roberts, J. Y. Ui, R. C. Cooksey, S. E. Litwin, and E. D. Abel, “Reduced cardiac efficiency and altered substrate metabolism precedes the onset of hyperglycemia and contractile dysfunction in two mouse models of insulin resistance and obesity,” *Endocrinology*, vol. 146, no. January, pp. 5341–5349, 2005.

[15] N. M. Borradaile, X. Han, J. D. Harp, S. E. Gale, D. S. Ory, and J. E. Schaffer, “Disruption of endoplasmic reticulum structure and integrity in lipotoxic cell death.,” *J. Lipid Res.*, vol. 47, no. August, pp. 2726–2737, 2006.

[16] H. Bugger and E. D. Abel, “Molecular mechanisms for myocardial mitochondrial dysfunction in the metabolic syndrome.,” *Clin. Sci. (Lond).*, vol. 114, pp. 195–210, 2008.

[17] S. Boudina, S. Sena, H. Theobald, X. Sheng, J. J. Wright, X. X. Hu, S. Aziz, J. I. Johnson, H. Bugger, V. G. Zaha, and E. D. Abel, “Mitochondrial Energetics in the Heart in Obesity-Related,” *Diabetes*, vol. 56, no. October, pp. 2457–2466, 2007.

[18] S. Boudina, S. Sena, B. T. O’Neill, P. Tathireddy, M. E. Young, and E. D. Abel, “Reduced mitochondrial oxidative capacity and increased mitochondrial uncoupling impair myocardial energetics in obesity,” *Circulation*, vol. 112, pp. 2686–2695, 2005.

[19] J. H. Moffitt, B. a. Fielding, R. Evershed, R. Berstan, J. M. Currie, and a. Clark, "Adverse physicochemical properties of tripalmitin in beta cells lead to morphological changes and lipotoxicity in vitro," *Diabetologia*, vol. 48, pp. 1819–1829, 2005.

[20] R. Zechner, R. Zimmermann, T. O. Eichmann, S. D. Kohlwein, G. Haemmerle, A. Lass, and F. Madeo, "FAT SIGNALS - Lipases and lipolysis in lipid metabolism and signaling," *Cell Metab.*, vol. 15, no. 3, pp. 279–291, 2012.

[21] R. Zimmermann, J. G. Strauss, G. Haemmerle, G. Schoiswohl, R. Birner-Gruenberger, M. Riederer, A. Lass, G. Neuberger, F. Eisenhaber, A. Hermetter, and R. Zechner, "Fat mobilization in adipose tissue is promoted by adipose triglyceride lipase.," *Science*, vol. 306, no. 2004, pp. 1383–1386, 2004.

[22] J. a. Villena, S. Roy, E. Sarkadi-Nagy, K. H. Kim, and S. S. Hei, "Desnutrin, an adipocyte gene encoding a novel patatin domain-containing protein, is induced by fasting and glucocorticoids: Ectopic expression of desnutrin increases triglyceride hydrolysis," *J. Biol. Chem.*, vol. 279, no. 45, pp. 47066–47075, 2004.

[23] "Lipoprotein lipase and hormone-sensitive lipase activities in adipose tissue.," *Nutr. Rev.*, vol. 37, no. 2, pp. 151–152, 1979.

[24] H. Lee, S. Bahn, and J. Shin, "Progress in Lipid Research," ... *Lipid Res.*, vol. 50, pp. 14–27, 2005.

[25] M. Ahmadian, M. J. Abbott, T. Tang, C. S. S. Hudak, Y. Kim, M. Bruss, M. K. Hellerstein, H.-Y. Lee, V. T. Samuel, G. I. Shulman, Y. Wang, R. E. Duncan, C. Kang, and H. S. Sul, "Desnutrin/ATGL is regulated by AMPK and is required for a brown adipose phenotype.," *Cell Metab.*, vol. 13, no. 6, pp. 739–48, Jun. 2011.

[26] W. Yin, J. Mu, and M. J. Birnbaum, "Role of AMP-activated Protein Kinase in Cyclic AMP-dependent Lipolysis in 3T3-L1 Adipocytes," *J. Biol. Chem.*, vol. 278, no. 44, pp. 43074–43080, 2003.

[27] M. P. Gaidhu, S. Fediuc, N. M. Anthony, M. So, M. Mirpourian, R. L. S. Perry, and R. B. Ceddia, "Prolonged AICAR-induced AMP-kinase activation promotes energy dissipation in white adipocytes: novel mechanisms integrating HSL and ATGL.," *J. Lipid Res.*, vol. 50, pp. 704–715, 2009.

[28] M. Daval, F. Diot-Dupuy, R. Bazin, I. Hainault, B. Viollet, S. Vaulont, E. Hajduch, P. Ferré, and F. Foufelle, "Anti-lipolytic action of AMP-activated protein kinase in rodent adipocytes," *J. Biol. Chem.*, vol. 280, no. 26, pp. 25250–25257, 2005.

[29] J. Watzlawik, L. Skora, D. Frense, C. Griesinger, M. Zweckstetter, W. J. Schulz-Schaeffer, and M. L. Kramer, "Prion protein helix1 promotes aggregation but is not converted into β-sheet," *J. Biol. Chem.*, vol. 281, no. 24, pp. 30242–30250, 2006.

[30] P. Chakrabarti, T. English, S. Karki, L. Qiang, R. Tao, J. Kim, Z. Luo, S. R. Farmer, and K. V Kandror, "SIRT1 controls lipolysis in adipocytes via FOXO1-mediated expression of ATGL.," *J. Lipid Res.*, vol. 52, pp. 1693–1701, 2011.

[31] A. Lass, R. Zimmermann, G. Haemmerle, M. Riederer, G. Schoiswohl, M. Schweiger, P. Kienesberger, J. G. Strauss, G. Gorkiewicz, and R. Zechner, "Adipose triglyceride lipase-mediated lipolysis of cellular fat stores is activated by CGI-58 and defective in Chanarin-Dorfman Syndrome.," *Cell Metab.*, vol. 3, no. 5, pp. 309–19, May 2006.

[32] A. Manuscript, "NIH Public Access," *Changes*, vol. 29, no. 3, pp. 997–1003, 2012.

[33] P. Strålfors and P. Belfrage, "Phosphorylation of hormone-sensitive lipase by cyclic AMP-dependent protein kinase.," *J. Biol. Chem.*, vol. 258, pp. 15146–15152, 1983.

[34] W.-J. Shen, S. Patel, H. Miyoshi, A. S. Greenberg, and F. B. Kraemer, "Functional interaction of hormone-sensitive lipase and perilipin in lipolysis.," *J. Lipid Res.*, vol. 50, pp. 2306–2313, 2009.

[35] H. Miyoshi, J. W. Perfield, S. C. Souza, W. J. Shen, H. H. Zhang, Z. S. Stancheva, F. B. Kraemer, M. S. Obin, and A. S. Greenberg, "Control of adipose triglyceride lipase action by serine 517 of perilipin A globally regulates protein kinase a-stimulated lipolysis in adipocytes," *J. Biol. Chem.*, vol. 282, no. 2, pp. 996–1002, 2007.

[36] H. Wang, L. Hu, K. Dalen, H. Dorward, A. Marcinkiewicz, D. Russell, D. Gong, C. Londos, T. Yamaguchi, C. Holm, M. a. Rizzo, D. Brasaemle, and C. Sztalryd, "Activation of hormone-sensitive lipase requires two steps, protein phosphorylation and binding to the PAT-1 domain of lipid droplet coat proteins," *J. Biol. Chem.*, vol. 284, no. 46, pp. 32116–32125, 2009.

[37] Y. Lee, H. Hirose, M. Ohneda, J. H. Johnson, J. D. McGarry, and R. H. Unger, "Beta-cell lipotoxicity in the pathogenesis of non-insulin-dependent diabetes mellitus of obese rats: impairment in adipocyte-beta-cell relationships.," *Proc. Natl. Acad. Sci. U. S. A.*, vol. 91, no. November, pp. 10878–10882, 1994.

[38] Y. T. Zhou, P. Grayburn, a Karim, M. Shimabukuro, M. Higa, D. Baetens, L. Orci, and R. H. Unger, "Lipotoxic heart disease in obese rats: implications for human obesity.," *Proc. Natl. Acad. Sci. U. S. A.*, vol. 97, pp. 1784–1789, 2000.

[39] S. Park, Y. Cho, H. Kim, T. Higashimori, C. Danton, M. Lee, A. Dey, B. Rothermel, Y. Kim, A. Kalinowski, K. S. Russell, and J. K. Kim, "Unraveling the Temporal Pattern of Diet-Induced Insulin in C57BL / 6 Mice," *Heart*, vol. 54, no. December, 2005.

[40] H. Yagyu, G. Chen, M. Yokoyama, K. Hirata, A. Augustus, Y. Kako, T. Seo, Y. Hu, E. P. Lutz, M. Merkel, A. Bensadoun, S. Homma, and I. J. Goldberg, "Lipoprotein lipase (LpL) on the surface of cardiomyocytes increases lipid uptake and produces a cardiomyopathy," *J. Clin. Invest.*, vol. 111, no. 3, pp. 419–426, 2003.

[41] H. C. Chiu, A. Kovacs, D. a. Ford, F. F. Hsu, R. Garcia, P. Herrero, J. E. Saffitz, and J. E. Schaffer, "A novel mouse model of lipotoxic cardiomyopathy," *J. Clin. Invest.*, vol. 107, no. 7, pp. 813–822, 2001.

[42] J. Egans, "Control of Endogenous Phosphorylation Protein Kinase Substrate in Adipocytes Stimulation * of the Major CAMP-dependent by Insulin and," *Regulation*, vol. 265, no. 31, pp. 18769–18775, 1990.

[43] A. S. Greenberg, J. J. Egan, S. a. Wek, N. B. Garty, E. J. Blanchette-Mackie, and C. Londos, "Perilipin, a major hormonally regulated adipocyte-specific phosphoprotein associated with the periphery of lipid storage droplets," *J. Biol. Chem.*, vol. 266, no. 17, pp. 11341–11346, 1991.

[44] a S. Greenberg, J. J. Egan, S. a Wek, M. C. Moos, C. Londos, and a R. Kimmel, "Isolation of cDNAs for perilipins A and B: sequence and expression of lipid droplet-associated proteins of adipocytes.," *Proc. Natl. Acad. Sci. U. S. A.*, vol. 90, no. December, pp. 12035–12039, 1993.

[45] S. Miura, J. W. Gan, J. Brzostowski, M. J. Parisi, C. J. Schultz, C. Londos, B. Oliver, and A. R. Kimmel, "Functional conservation for lipid storage droplet association among perilipin, ADRP, and TIP47 (PAT)-related proteins in mammals, Drosophila, and Dictyostelium," *J. Biol. Chem.*, vol. 277, no. 35, pp. 32253–32257, 2002.

[46] N. E. Wolins, J. R. Skinner, M. J. Schoenfish, A. Tzekov, K. G. Bensch, and P. E. Bickel, "Adipocyte protein S3-12 coats nascent lipid droplets," *J. Biol. Chem.*, vol. 278, pp. 37713–37721, 2003.

[47] T. Yamaguchi, S. Matsushita, K. Motojima, F. Hirose, and T. Osumi, "MLDP, a novel PAT family protein localized to lipid droplets and enriched in the heart, is regulated by peroxisome proliferator-activated receptor??," *J. Biol. Chem.*, vol. 281, no. 20, pp. 14232–14240, 2006.

[48] N. E. Wolins, B. K. Quaynor, J. R. Skinner, A. Tzekov, M. a. Croce, M. C. Gropler, V. Varma, A. Yao-Borengasser, N. Rasouli, P. a. Kern, B. N. Finck, and P. E. Bickel, "OXPAT/PAT-1 is a PPAR-induced lipid droplet protein that promotes fatty acid utilization," *Diabetes*, vol. 55, no. December, pp. 3418–3428, 2006.

[49] K. T. Dalen, T. Dahl, E. Holter, B. Arntsen, C. Londos, C. Sztalryd, and H. I. Nebb, "LSDP5 is a PAT protein specifically expressed in fatty acid oxidizing tissues.," *Biochim. Biophys. Acta*, vol. 1771, no. 2, pp. 210–27, Feb. 2007.

[50] D. L. Brasaemle, "Thematic review series: adipocyte biology. The perilipin family of structural lipid droplet proteins: stabilization of lipid droplets and control of lipolysis.," *J. Lipid Res.*, vol. 48, pp. 2547–2559, 2007.

[51] A. Paul, L. Chan, and P. E. Bickel, "NIH Public Access," vol. 10, no. 6, pp. 461–466, 2010.

[52] N. E. Wolins, B. K. Quaynor, J. R. Skinner, M. J. Schoenfish, A. Tzekov, and P. E. Bickel, “S3-12, adipophilin, and TIP47 package lipid in adipocytes,” *J. Biol. Chem.*, vol. 280, pp. 19146–19155, 2005.

[53] K. Kuramoto, T. Okamura, T. Yamaguchi, T. Y. Nakamura, S. Wakabayashi, H. Morinaga, M. Nomura, T. Yanase, K. Otsu, N. Usuda, S. Matsumura, K. Inoue, T. Fushiki, Y. Kojima, T. Hashimoto, F. Sakai, F. Hirose, and T. Osumi, “Perilipin 5, a lipid droplet-binding protein, protects heart from oxidative burden by sequestering fatty acid from excessive oxidation.,” *J. Biol. Chem.*, vol. 287, no. 28, pp. 23852–63, Jul. 2012.

[54] A. R. Kimmel and C. Sztalryd, “Perilipin 5, a lipid droplet protein adapted to mitochondrial energy utilization.,” *Curr. Opin. Lipidol.*, vol. 25, no. 2, pp. 110–7, Apr. 2014.

[55] B. Desvergne and W. Wahli, “Peroxisome proliferator-activated receptors: Nuclear control of metabolism,” *Endocr. Rev.*, vol. 20, no. January, pp. 649–688, 1999.

[56] C. Bindesbøll, O. Berg, B. Arntsen, H. I. Nebb, and K. T. Dalen, “Fatty acids regulate perilipin5 in muscle by activating PPARδ.,” *J. Lipid Res.*, vol. 54, pp. 1949–63, 2013.

[57] T. R. Koves, L. M. Sparks, J. P. Kovalik, M. Mosedale, R. Arumugam, K. L. Debalsi, K. Everingham, L. Thorne, E. Phielix, R. C. Meex, C. L. Kien, M. K. C. Hesselink, P. Schrauwen, and D. M. Muoio, “PPARγ coactivator-1α contributes to exercise-induced regulation of intramuscular lipid droplet programming in mice and humans.,” *J. Lipid Res.*, vol. 54, pp. 522–34, 2013.

[58] J. B. Lockridge, M. L. Sailors, D. J. Durgan, O. Egbejimi, W. J. Jeong, M. S. Bray, W. C. Stanley, and M. E. Young, “Bioinformatic profiling of the transcriptional response of adult rat cardiomyocytes to distinct fatty acids.,” *J. Lipid Res.*, vol. 49, pp. 1395–1408, 2008.

[59] S. S. Lee, T. Pineau, J. Drago, E. J. Lee, J. W. Owens, D. L. Kroetz, P. M. Fernandez-Salguero, H. Westphal, and F. J. Gonzalez, “Targeted disruption of the alpha isoform of the peroxisome proliferator-activated receptor gene in mice results in abolishment of the pleiotropic effects of peroxisome proliferators.,” *Mol. Cell. Biol.*, vol. 15, no. 6, pp. 3012–3022, 1995.

[60] K. T. Dalen, K. Schoonjans, S. M. Ulven, M. S. Weedon-Fekjaer, T. G. Bentzen, H. Koutnikova, J. Auwerx, and H. I. Nebb, “Adipose Tissue Expression of the Lipid Droplet Associating Proteins S3-12 and Perilipin Is Controlled by Peroxisome Proliferator-Activated Receptor gamma,” *Diabetes*, vol. 53, no. 4, pp. 1243–1252, 2004.

[61] H. Li, Y. Song, L. J. Zhang, Y. Gu, F. F. Li, S. Y. Pan, L. N. Jiang, F. Liu, J. Ye, and Q. Li, “LSDP5 enhances triglyceride storage in hepatocytes by influencing lipolysis and fatty acid ??-oxidation of lipid droplets,” *PLoS One*, vol. 7, no. 6, 2012.

[62] H. Wang, U. Sreenivasan, D.-W. Gong, K. a O’Connell, E. R. Dabkowski, P. a Hecker, N. Ionica, M. Konig, A. Mahurkar, Y. Sun, W. C. Stanley, and C. Sztalryd, “Cardiomyocyte-specific perilipin 5 overexpression leads to myocardial steatosis and modest cardiac dysfunction.,” *J. Lipid Res.*, vol. 54, no. 4, pp. 953–65, Apr. 2013.

[63] H. Wang, M. Bell, U. Sreenivasan, U. Sreenevasan, H. Hu, J. Liu, K. Dalen, C. Londos, T. Yamaguchi, M. a Rizzo, R. Coleman, D. Gong, D. Brasaemle, and C. Sztalryd, “Unique regulation of adipose triglyceride lipase (ATGL) by perilipin 5, a lipid droplet-associated protein.,” *J. Biol. Chem.*, vol. 286, no. 18, pp. 15707–15, May 2011.

[64] J. G. Granneman, H. P. H. Moore, E. P. Mottillo, and Z. Zhu, “Functional interactions between Mldp (LSDP5) and Abhd5 in the control of intracellular lipid accumulation,” *J. Biol. Chem.*, vol. 284, no. 5, pp. 3049–3057, 2009.

[65] J. G. Granneman, H.-P. H. Moore, E. P. Mottillo, Z. Zhu, and L. Zhou, “Interactions of perilipin-5 (Plin5) with adipose triglyceride lipase.,” *J. Biol. Chem.*, vol. 286, no. 7, pp. 5126–35, Feb. 2011.

[66] V. Subramanian, A. Rotlienberg, C. Gomez, A. W. Cohen, A. Garcia, S. Bhattacharyya, L. Shapiro, G. Dolios, R. Wang, M. P. Lisanti, and D. L. Brasaemle, “Perilipin A mediates the reversible binding of CGI-58 to lipid droplets in 3T3-L1 adipocytes,” *J. Biol. Chem.*, vol. 279, no. 40, pp. 42062–42071, 2004.

[67] T. Yamaguchi, N. Omatsu, S. Matsushita, and T. Osumi, “CGI-58 interacts with perilipin and is localized to lipid droplets: Possible involvement of CGI-58 mislocalization in Chanarin-Dorfman syndrome,” *J. Biol. Chem.*, vol. 279, no. 29, pp. 30490–30497, 2004.

[68] J. G. Granneman, H. P. H. Moore, R. Krishnamoorthy, and M. Rathod, "Perilipin controls lipolysis by regulating the interactions of AB-hydrolase containing 5 (Abhd5) and adipose triglyceride lipase (Atgl)," *J. Biol. Chem.*, vol. 284, no. 50, pp. 34538–34544, 2009.

[69] R. E. K. Macpherson, R. Vandenboom, B. D. Roy, and S. J. Peters, "Skeletal muscle PLIN3 and PLIN5 are serine phosphorylated at rest and following lipolysis during adrenergic or contractile stimulation.," *Physiol. Rep.*, vol. 1, p. e00084, 2013.

[70] R. R. Mason, R. Mokhtar, M. Matzaris, A. Selathurai, G. M. Kowalski, N. Mokbel, P. J. Meikle, C. R. Bruce, and M. J. Watt, "PLIN5 deletion remodels intracellular lipid composition and causes insulin resistance in muscle," *Mol. Metab.*, vol. 3, no. 6, pp. 652–663, 2014.

[71] N. M. Pollak, D. Jaeger, and J. B. Chem, "Metabolism : The interplay of protein kinase A and perilipin 5 regulates cardiac lipolysis," 2014.

[72] J. N. Feige, L. Gelman, L. Michalik, B. Desvergne, and W. Wahli, "From molecular action to physiological outputs: peroxisome proliferator-activated receptors are nuclear receptors at the crossroads of key cellular functions.," *Prog. Lipid Res.*, vol. 45, no. 2, pp. 120–59, Mar. 2006.

[73] H. Koprowski, "~ m," vol. 52, pp. 53–59, 2000.

[74] M. Hill and N. W. Iaa, "Characteristics of a Human Cell Line Transformed by D N A from Human Adenovirus Type 5," no. 2977.

[75] M. Pagano, S. Naviglio, a Spina, E. Chiosi, G. Castoria, M. Romano, a Sorrentino, F. Illiano, and G. Illiano, "Differentiation of H9c2 cardiomyoblasts: The role of adenylate cyclase system.," *J. Cell. Physiol.*, vol. 198, no. 3, pp. 408–16, Mar. 2004.

[76] G. Haemmerle, A. Lass, R. Zimmermann, G. Gorkiewicz, C. Meyer, J. Rozman, G. Heldmaier, R. Maier, C. Theussl, S. Eder, D. Kratky, E. F. Wagner, M. Klingenspor, G. Hoefler, and R. Zechner, "Defective lipolysis and altered energy metabolism in mice lacking adipose triglyceride lipase.," *Science*, vol. 312, no. 5774, pp. 734–7, May 2006.

[77] A. Subramaniams, W. K. Jones, J. Gulick, and J. Neumannli, "Tissue-specific Regulation of the a-Myosin Heavy Chain Gene Promoter in Transgenic Mice *," vol. 266, no. 36, pp. 24613–24620, 1991.

[78] P. C. Kienesberger, T. Pulinilkunnil, M. M. Y. Sung, J. Nagendran, G. Haemmerle, E. E. Kershaw, M. E. Young, P. E. Light, G. Y. Oudit, R. Zechner, and J. R. B. Dyck, "Myocardial ATGL overexpression decreases the reliance on fatty acid oxidation and protects against pressure overload-induced cardiac dysfunction.," *Mol. Cell. Biol.*, vol. 32, no. 4, pp. 740–50, Feb. 2012.

[79] N. Mayer, M. Schweiger, M. Romauch, G. F. Grabner, O. Thomas, E. Fuchs, J. Ivkovic, C. Heier, I. Mrak, A. Lass, G. Höfler, C. Fledelius, R. Zechner, and R. Zimmermann, "Europe PMC Funders Group Development of small molecule inhibitors targeting adipose triglyceride lipase," vol. 9, no. 12, pp. 1–13, 2014.

[80] N. M. Pollak, M. Schweiger, D. Jaeger, D. Kolb, M. Kumari, R. Schreiber, S. Kolleritsch, P. Markolin, G. F. Grabner, C. Heier, K. a Zierler, T. Rülicke, R. Zimmermann, A. Lass, R. Zechner, and G. Haemmerle, "Cardiac-specific overexpression of perilipin 5 provokes severe cardiac steatosis via the formation of a lipolytic barrier.," *J. Lipid Res.*, vol. 54, no. 4, pp. 1092–102, Apr. 2013.

[81] M. J. Evans and C. Scarpullas, "Interaction of Nuclear Factors with Multiple Sites in the Somatic Cytochrome c Promoter," *J Biol Chem*, vol. 264, no. 20, pp. 14361–8, 1989.

[82] J. V Virbasius and R. C. Scarpulla, "Transcriptional activation through ETS domain binding sites in the cytochrome c oxidase subunit IV gene.," *Mol. Cell. Biol.*, vol. 11, no. 11, pp. 5631–5638, 1991.

[83] M. J. Evans and R. C. Scarpulla, "NRF-1: A trans-activator of nuclear-encoded respiratory genes in animal cells," *Genes Dev.*, vol. 4, pp. 1023–1034, 1990.

[84] C. M. Chau, M. J. Evans, and R. C. Scarpulla, “Nuclear respiratory factor 1 activation sites in genes encoding the gamma-subunit of ATP synthase, eukaryotic initiation factor 2 alpha, and tyrosine aminotransferase. Specific interaction of purified NRF-1 with multiple target genes.,” *J. Biol. Chem.*, vol. 267, pp. 6999–7006, 1992.

[85] G. L. Semenza and G. L. Wang, “A nuclear factor induced by hypoxia via de novo protein synthesis binds to the human erythropoietin gene enhancer at a site required for transcriptional activation.,” *Mol. Cell. Biol.*, vol. 12, no. 12, pp. 5447–5454, 1992.

[86] E. Poon, A. L. Harris, and M. Ashcroft, “Targeting the hypoxia-inducible factor (HIF) pathway in cancer.,” *Expert Rev. Mol. Med.*, vol. 11, no. August, p. e26, 2009.

[87] S. Kassovska-Bratinova, T. Fukao, X. Q. Song, a M. Duncan, H. S. Chen, M. F. Robert, C. Pérez-Cerdá, M. Ugarte, C. Chartrand, S. Vobecky, N. Kondo, and G. a Mitchell, “Succinyl CoA: 3-oxoacid CoA transferase (SCOT): human cDNA cloning, human chromosomal mapping to 5p13, and mutation detection in a SCOT-deficient patient.,” *Am. J. Hum. Genet.*, vol. 59, pp. 519–528, 1996.

[88] H. Pilegaard and P. Darrell Neufer, “Transcriptional regulation of pyruvate dehydrogenase kinase 4 in skeletal muscle during and after exercise,” *Proc. Nutr. Soc.*, vol. 63, no. 02, pp. 221–226, Mar. 2007.

[89] M. M. Bowker-Kinley, W. I. Davis, P. Wu, R. a Harris, and K. M. Popov, “Evidence for existence of tissue-specific regulation of the mammalian pyruvate dehydrogenase complex.,” *Biochem. J.*, vol. 329 (Pt 1, pp. 191–196, 1998.

[90] P. Puigserver, Z. Wu, C. W. Park, R. Graves, M. Wright, and B. M. Spiegelman, “A cold-inducible coactivator of nuclear receptors linked to adaptive thermogenesis,” *Cell*, vol. 92, pp. 829–839, 1998.

[91] L. F. Michael, Z. Wu, R. B. Cheatham, P. Puigserver, G. Adelmant, J. J. Lehman, D. P. Kelly, and B. M. Spiegelman, “Restoration of insulin-sensitive glucose transporter (GLUT4) gene expression in muscle cells by the transcriptional coactivator PGC-1.,” *Proc. Natl. Acad. Sci. U. S. A.*, vol. 98, pp. 3820–3825, 2001.

[92] J. C. Yoon, P. Puigserver, G. Chen, J. Donovan, Z. Wu, J. Rhee, G. Adelmant, J. Stafford, C. R. Kahn, D. K. Granner, C. B. Newgard, and B. M. Spiegelman, “Control of hepatic gluconeogenesis through the transcriptional coactivator PGC-1.,” *Nature*, vol. 413, pp. 131–138, 2001.

[93] J. Rhee, Y. Inoue, J. C. Yoon, P. Puigserver, M. Fan, F. J. Gonzalez, and B. M. Spiegelman, “Regulation of hepatic fasting response by PPARgamma coactivator-1alpha (PGC-1): requirement for hepatocyte nuclear factor 4alpha in gluconeogenesis.,” *Proc. Natl. Acad. Sci. U. S. A.*, vol. 100, pp. 4012–4017, 2003.